

PHOTOGRAMMETRIC INVESTIGATION INTO LOW- RESOLUTION DIGITAL CAMERA SYSTEMS

XIAOPENG LI

June 1999



TECHNICAL REPORT
NO. 200

**PHOTOGRAMMETRIC INVESTIGATION
INTO LOW-RESOLUTION DIGITAL
CAMERA SYSTEMS**

Xiaopeng Li

Department of Geodesy and Geomatics Engineering
University of New Brunswick
P.O. Box 4400
Fredericton, N.B.
Canada
E3B 5A3

June 1999

© Xiaopeng Li, 1999

PREFACE

In order to make our extensive series of technical reports more readily available, we have scanned the old master copies and produced electronic versions in Portable Document Format. The quality of the images varies depending on the quality of the originals. The images have not been converted to searchable text.

PREFACE

This technical report is an unedited reproduction of a dissertation submitted in partial fulfillment of the requirements for the degree of Doctor of Philosophy in the Department of Geodesy and Geomatics Engineering, April 1999. The research was supervised by Dr. Wolfgang Faig, and funding was provided by the Natural Sciences and Engineering Research Council of Canada and the University of New Brunswick.

As with any copyrighted material, permission to reprint or quote extensively from this report must be received from the author. The citation to this work should appear as follows:

Li, Xiaopeng (1999). *Photogrammetric Investigation into Low-Resolution Digital Camera Systems*. Ph.D. dissertation, Department of Geodesy and Geomatics Engineering Technical Report No. 200, University of New Brunswick, Fredericton, New Brunswick, Canada, 180 pp.

ABSTRACT

Digital cameras are becoming the mainstream data acquisition tools in photogrammetry and remote sensing, although not originally and specifically designed for these purposes. In order to fully exploit the technical advances in digital camera and other related technologies, it is necessary to study their metric performances. Usually, a calibration can be carried out to determine and compensate for the systematic errors of camera systems aiming at improving the metric performances of the camera systems. However, no thorough investigation of the metric characteristics of low-resolution digital camera systems has been conducted so far. In addition, the calibration models currently in use were developed for film-based cameras and, thus, cannot properly accommodate certain imperfections of camera systems.

This dissertation describes research into the metric performances of low-resolution digital camera systems from both the theoretical and practical aspects. The concepts, working principles, advantages and disadvantages of digital cameras are discussed. The characteristics of an ideal digital imaging device and possible geometric and radiometric error sources of digital camera systems are studied in detail. After a discussion of the current calibration methods, a modified calibration model named MFFEM (Multiple-Frame Finite Element Method) is proposed, verified and compared with other models through simulation and a practical case. The metric performances and the accuracy potentials of three typical low-resolution digital camera systems are investigated by conducting a series of well-designed projects. Based on that, the metric applications of such camera systems and the related issues are also touched upon. A software package UNBDCSC (UNB Digital Camera System

Calibration) was developed and used for data processing, with the MFFEM function being its main feature.

The research findings illustrate that low-resolution digital camera systems can be used for metric purposes with low- or medium accuracy requirements when proper calibration and certain imaging configurations are utilized. The proposed model can compensate for the systematic errors of digital camera systems as effectively as other well-proven models and is advantageous under certain circumstances. Future works lie in the refinement of the software package, combination of geometric and radiometric calibration, and more studies on Finite Element Modeling.

TABLE OF CONTENTS

ABSTRACT	ii
TABLE OF CONTENTS	iv
LIST OF TABLES	viii
LIST OF FIGURES	xi
ACKNOWLEDGMENTS	xiii
CHAPTER 1. INTRODUCTION	1
1.1 Digital Imaging and Digital Camera Systems	1
1.2 Motivation and Scope of the Research	2
1.3 Outline of the Dissertation	5
1.4 Contributions	6
CHAPTER 2. LOW-RESOLUTION DIGITAL CAMERA SYSTEMS	8
2.1 Digital Cameras	8
2.1.1 Definition	8
2.1.2 Advantages and Disadvantages over Film-based Cameras	10
2.1.3 Operational Principles	13
2.2 Digital Camera Systems	14
2.3 Resolution of Digital Camera Systems	16
2.3.1 General Considerations	16
2.3.2 Geometric Resolution	17
2.3.3 Radiometric Resolution	19
CHAPTER 3. ERROR SOURCES OF DIGITAL CAMERA SYSTEMS	21
3.1 An Ideal Digital Imaging System	21
3.1.1 Geometric Considerations	21
3.1.2 Radiometric Considerations	23
3.2 Geometric Distortions	24
3.2.1 Lens Distortion	25
3.2.2 Sensor Plane Deformation	25
3.2.2.1 In-plane Displacement	26
3.2.2.2 Out-of-plane Displacement	26
3.2.3 Interior Orientation Stability	27
3.2.4 Influence of Zoom Lenses	28
3.2.4.1 Variation of Principal Point	29
3.2.4.2 Variation of Lens Distortion	30

3.3 Radiometric Degradation	30
3.3.1 Non-linearity	30
3.3.2 Dark Current Noise	31
3.3.3 Blooming	32
3.3.4 Malfunction of Certain Sensor Elements	32
CHAPTER 4. CALIBRATION OF DIGITAL CAMERA SYSTEMS	34
4.1 Objectives and General Principles of Camera System Calibration . . .	35
4.2 Modeling and Compensation Schemes of Geometric System Errors . . .	37
4.2.1 Mathematical Modeling of Geometric Errors	37
4.2.1.1 Physical Models	38
4.2.1.2 Algebraic Models	40
4.2.1.3 Hybrid Models	44
4.3 Geometric Calibration	45
4.3.1 Methods of Calibration	46
4.3.1.1 Individual Methods	47
4.3.1.2 Combined Methods	50
4.4 Radiometric Calibration	55
4.4.1 'Cap-on Method'	56
4.4.2 'Uniform Grey Page and Grey Step Card Method'	57
4.4.3 Different Clock Rate Method	57
CHAPTER 5. CAMERA SYSTEM CALIBRATION WITH FINITE ELEMENT	
METHOD (FEM)	60
5.1 Introduction	60
5.2 General Nature of the Finite Element Method (FEM)	61
5.2.1 Definition and Characteristics of the FEM	61
5.2.2 Main Idea and Procedure of the FEM	62
5.2.3 Mathematical Expression of the FEM	64
5.2.4 Finite Elements and Shape Functions	64
5.2.4.1 Triangular Elements	66
5.2.4.2 Rectangular Elements	67
5.3 Camera System Calibration with the FEM	69
5.3.1 Basic Principle of the FEM Camera System Calibration	70
5.3.2 Multiple-Frame Finite Element Method (MFFEM)	74
5.3.3 Simplified MFFEM	77
5.4 Empirical Studies of the FEM by a Modeled Case	78
5.4.1 Main Idea of the Studies	79
5.4.2 Model Design	79
5.4.3 Fictitious Camera and Photogrammetric Configuration	81
5.4.4 Data Processing Schemes	84
5.4.5 Results and Analysis	85

CHAPTER 6. PHOTOGRAMMETRIC APPLICATIONS OF LOW-RESOLUTION DIGITAL CAMERA SYSTEMS	94
6.1 Introduction	94
6.2 Practical Considerations Associated with Metric Applications	95
6.2.1 Targeting and Illumination	96
6.2.2 Photogrammetric Network Configuration	97
6.2.3 Camera System Calibration	99
6.2.4 Time and Cost Considerations	100
6.3 Application Areas of Low-Resolution Digital Camera Systems	104
6.3.1 Digital Close-Range Photogrammetry	104
6.3.2 General Application Requirements	106
6.3.3 Existing and Possible Application Areas	106
CHAPTER 7. PRACTICAL STUDIES OF LOW-RESOLUTION DIGITAL CAMERA SYSTEMS	107
7.1 Introduction	107
7.2 Digital Camera Systems Studied	108
7.3 Data Processing Methods and Calibration Tests	109
7.3.1 Self-Calibrating Bundle Adjustment Method I -- UNBASC2	110
7.3.2 Self-Calibrating Bundle Adjustment Method II -- GEBAT	111
7.3.3 Direct Linear Transformation (DLT) Method	112
7.3.4 Finite Element Method (FEM)	113
7.4 Practical Projects and Results	113
7.4.1 Three-Dimensional (3D) Test Plate Calibration Project	114
7.4.1.1 Test Plate	114
7.4.1.2 Imaging configuration	115
7.4.1.3 Image measurement	115
7.4.1.4 Calibration Results	116
7.4.2 Architectural Dimensional Inspection	122
7.4.2.1 Architectural Test-field	123
7.4.2.2 Photogrammetric Configuration	124
7.4.2.3 Accuracy Preanalysis	125
7.4.2.4 Data Reduction Schemes	126
7.4.2.5 Results and Analysis	127
7.4.3 Lightweight Structure Deformation Monitoring	134
7.4.3.1 Model Preparation	134
7.4.3.2 Cameras Utilized	135
7.4.3.3 Photogrammetric Configuration and Image Acquisition	135
7.4.3.4 Image Mensuration	137

7.4.3.5 Results and Analysis	137
CHAPTER 8. CONCLUSIONS AND RECOMMENDATIONS	140
REFERENCES	145
APPENDIX I A SURVEY OF LOW-RESOLUTION DIGITAL CAMERAS ...	154
I.1 Geometric Resolution	154
I.2 Lens System	154
I.3 Light Sensitivity	155
I.4 Storage	156
I.5 Interface and Software	156
I.6 Control	157
I.7 Viewfinder and Other Features	158
APPENDIX II LENS DISTORTION OF DIGITAL CAMERAS	169
II.1 Radial Lens Distortion	169
II.2 Decentering Lens Distortion	171
II.3 Variation of Radial Lens Distortion	172
II.4 Variation of Decentering Lens Distortion	174
APPENDIX III DEFINITIONS OF COMMON TERMS OF GEOMETRIC CAMERA CALIBRATION	176
APPENDIX IV PARTIAL DERIVATIVES OF THE MODIFIED COLLINEARITY EQUATIONS	178

LIST OF TABLES

Table 2.1	Digital Camera Types	12
Table 2.2	Digital Cameras vs. Film Cameras	12
Table 4.1	Common Physical Models used for Digital Camera Calibration Projects	41
Table 5.1	Basic Types of Finite Elements	65
Table 5.2	Number of the Unknowns, Dimensions of Matrices, and Vectors of the MFEM	77
Table 5.3	Exterior Orientation Parameters of the Five Camera Stations	82
Table 5.4	Image Deformation Recovering Capability of the FEM	86
Table 5.5.1	Results of the FEM with Triangular Elements	86
Table 5.5.2	Results of the FEM with Triangular Elements (with 1 μm random errors in image coordinate observations)	87
Table 5.5.3	Results of the FEM with Triangular Elements (with 5 μm random errors in image coordinate observations)	87
Table 5.5.4	Results of the FEM with Triangular Elements (with 10 μm random errors in image coordinate observations)	87
Table 5.6.1	Results of the FEM with Rectangular Elements	88
Table 5.6.2	Results of the FEM with Rectangular Elements (with 1 μm random errors in image coordinate observations)	88
Table 5.6.3	Results of the FEM with Rectangular Elements (with 5 μm random errors in image coordinate observations)	88
Table 5.6.4	Results of the FEM with Rectangular Elements (with 10 μm random errors in image coordinate observations)	88
Table 5.7	Influence of Imaging Configuration upon the Mean Object Accuracy	90
Table 5.8	Mean Object Space Accuracy of the DLT Method	91

Table 5.9	Mean Object Space Accuracy of the UNBASC2 Method	92
Table 6.1	Speed and Accuracy of Some Digital Close-Range Photogrammetric Tasks.	103
Table 7.1	Main Features of the three Low-resolution Digital Cameras Studied	109
Table 7.2	Calibration Tests with UNBASC2	111
Table 7.3	Calibration Tests with DLT	112
Table 7.4	Calibration Tests with FEM	113
Table 7.5.1	Calibration Results of the Fujix DS-100 Camera System by using UNBASC2	116
Table 7.5.2	Calibration Results of the Fujix DS-100 Camera System by using GEBAT	116
Table 7.5.3	Calibration Results of the Fujix DS-100 Camera System by using DLT. .	116
Table 7.6.1	Calibration Results of three Camera Systems by using DLT.	117
Table 7.6.2	Calibration Results of three Camera Systems by using UNBASC2	118
Table 7.7	Calibration Results of three Camera Systems by using FEM	119
Table 7.8	Comparison of Different Data Processing Methods	120
Table 7.9	Accuracy Preanalysis of the Wooden Building Project	126
Table 7.10	Influence of Different Control Configurations	127
Table 7.11	Config III vs. Config I and II (two-exposure vs. one exposure)	128
Table 7.12	R.M.S. Differences of Object Coordinates between Config I and II.	128
Table 7.13.1	Comparison of the Interior Orientation Parameters between Config I and II (Kodak DC-40 Digital Camera System)	129
Table 7.13.2	Comparison of the Interior Orientation Parameters between Config I and II (Kodak DC-50 Digital Camera System)	130

Table 7.13.3 Comparison of the Interior Orientation Parameters between Config I and II (Fujix DS-100 Digital Camera System)	130
Table 7.14.1 Calibration Results for the Kodak DC-40 Digital Camera System	131
Table 7.14.2 Calibration Results for the Kodak DC-50 Digital Camera System.	132
Table 7.14.3 Calibration Results for the Fujix DS-100 Digital Camera System	132
Table 7.15 Integration Test of Multi-Cameras	133
Table 7.16.1 RMS Values of the Image Coordinates	138
Table 7.16.2 RMS Values of the Object Space Coordinates based on the Check Points	138
Table I.1 Common Low-resolution Digital Cameras and Their Main Features . . .	159

LIST OF FIGURES

Figure 2.1	Relationship among the Common Camera Systems	11
Figure 2.2	Digital Camera Components and Digital Imaging Process	15
Figure 3.1	A Pinhole Camera Concept	23
Figure 3.2	Variation of Principal Point with Zooming when Optical Axis is not Perpendicular to the Image Plane	29
Figure 3.3	General Response Function of a Set of Pixels	31
Figure 4.1	General Procedure of Combined Calibration Methods	52
Figure 4.2	Error Sources and Calibration Methods of Digital Camera Systems	58
Figure 5.1	Discretization of a 2D Continuous Structure	62
Figure 5.2	General Procedure of the FEM	63
Figure 5.3	A Triangular Element	67
Figure 5.4	A Rectangular Element	68
Figure 5.5	Projection Compensation for Radial Lens Distortion	73
Figure 5.6	Projection Compensation for Sensor Plane Unflatness	73
Figure 5.7	Projection Compensation for the Combined Effects	74
Figure 5.8	Model Designed for the FEM Studies	80
Figure 5.9	Model Points Distribution	80
Figure 5.10	Image Points Distribution of one Image	81
Figure 5.11	Modeled DPD Surface and Contour Lines based on Radial Lens Distortion	82

Figure 5.12	Modeled DPD Surface and Contour Lines based on Decentering Lens Distortion	83
Figure 5.13	Modeled DPD Surface and Contour Lines based on Sensor Plane Unflatness	83
Figure 5.14	Five-Station Convergent Imaging Configuration	84
Figure 5.15	Discretization of Image Plane.	85
Figure 7.1	Three Low-Resolution Consumer Digital Cameras Studied	108
Figure 7.2	Three-Dimensional Test Plate	114
Figure 7.3	Three-Station Convergent Imaging Configuration	115
Figure 7.4	Accuracy Comparison of Three Camera Systems by using Different Data Processing Methods	117
Figure 7.5	DPD Surfaces Modeled by the FEM	120
Figure 7.6	Wooden Building Test Field and Point Distribution	123
Figure 7.7	Photogrammetric Configuration of the Wooden Building Project	124
Figure 7.8	The Light Weight Roof Model	135
Figure 7.9	Imaging Configuration of the Roof Model	136
Figure 7.10	Deformation of the Roof Model	138
Figure II.1	Radial Lens Distortion of a Digital Camera	169
Figure II.2	Gaussian Radial Distortion at Various Image Scales for a 25mm Fujinon Lens Fitted to a Pulnix CCD Camera	170
Figure II.3	Decentering Distortion for a 25mm Fujinon Lens Fitted to a Pulnix CCD Camera	172

ACKNOWLEDGMENTS

It is with sincere pleasure that I extend my gratitude and appreciation to many persons without whom this dissertation would not have been possible.

The principal debt is owed to Prof. Wolfgang Faig, my supervisor, for his progressive guidance, constant encouragement, and never-ending patience. I am truly grateful to Prof. Faig and the University of New Brunswick for the financial assistance throughout my study and research at the university.

I wish to express my sincere thanks to other members of my supervisory board, Prof. David J. Coleman and Prof. Eugene Derenyi, for their invaluable instruction and advice.

I gratefully acknowledge the criticism and constructive recommendations from the members of my reading committee.

Finally, thanks are expressed to my wife, Ms. Huili Wang, for her love and understanding, and my beloved daughter, Mengting Li and son, Andy Li, who enlighten my life.

CHAPTER 1

INTRODUCTION

1.1 Digital Imaging and Digital Camera Systems

Digital imaging can be considered as one of the most exciting technologies that emerged during the twentieth century, as it greatly facilitates information communication and utilization. The significance of digital imaging is fully illustrated by an application: Mars' exploration, as current science and technology still cannot retrieve the probe sent to study samples of the rock and surface of the planet. It is only the digital imaging device onboard the vehicle *Rover* that landed on Mars which transmits close-up digital images of the planet and, thus, lets the scientists on Earth see the scenes and guide the vehicle's movement (Eastman Kodak Company, 1997).

A digital camera system consists of computer hardware/software, one or more digital cameras and probably certain peripheral devices, such as a card reader. A digital camera is a standalone digital-imaging device composed of a general-purpose camera body and a solid-state sensor, which can provide a direct digital image signal compatible for further computer processing. Nowadays, digital cameras are making major inroads into various areas once dominated by film cameras. This is mainly due to the continuous advancement in semiconductor and microelectronics technologies and the practical advantages of digital cameras, such as instant gratification and low running cost. Although still in their infancy, digital cameras have a brilliant future due to their improved performances, richer features and falling prices. Among various groups of digital cameras, low-resolution digital cameras

(typically with 640 x 480 pixels) are more popular than others as consumer products because of their ready availability, low cost and ease of use. As a result, low-resolution digital cameras are finding more and more applications in many general business areas, such as photojournalism, desktop and network publishing, real estate brokering and the graphic arts industry.

1.2 Motivation and Scope of the Research

Photogrammetry is essentially an information extraction technology whereby quantitative information, such as shapes, positions, volume etc. of various objects or phenomena can be derived from their photographs or images. Although not specifically designed for photogrammetric purposes, digital cameras do possess many practical advantages over their traditional film-based counterparts and, thus, present themselves as powerful and promising digital image acquisition tools in photogrammetry. Therefore, their advent does not escape the photogrammetrists' attention, especially at a time when the photogrammetric technology is evolving from analogue and analytical eras to a digital era at an ever-increasing pace. Using a digital camera as an image acquisition tool in a measuring system avoids the intermediate step of scanning, and also raises the possibility of real-time or near real-time applications.

When applied to photogrammetric projects, the unknown and possibly unstable metric quality of digital camera systems has a direct influence upon the final accuracy of the photogrammetric results. However, digital camera studies in photogrammetry are focused on the medium- or mainly high resolution models, such as the Rollei Chip Back (2048x 2048

pixels) (Godding and Woytowicz, 1995), Kodak DCS-200 (1500x1000 pixels) (Fraser and Shortis, 1995; Peipe, 1995; Peipe and Schneider, 1995), Kodak DCS-420 (1500x1000 pixels) (Beyer, 1995), DCS-460 (3060x2036 pixels) (Peipe, 1995; Beyer, 1995), Kodak Hawkeye M1(1280x1020 pixels) (Edmundson et al., 1991), Videk Megaplus(1320 x 1035 pixels) (Bösemann et al., 1990). Relative object-space accuracies of 1:40,000 to 1:180,000 were achieved by using these cameras, which are comparable to the results of small- and medium format film-based metric cameras. Unfortunately, their high prices (US\$8,000 or more in 1998 prices) largely negate their high level performances, which is especially true when the budget access is very limited. Although the prices of digital cameras keep falling due to the reduced manufacturing costs and the increasing demands, it is not realistic to expect the price to have a significant drop in the very near future. In contrast, more and more off-the-shelf, low-resolution digital cameras are appearing on the market at an affordable price. Furthermore, not all applications have the stringent accuracy requirements, and medium- or even low accuracy may suffice for such applications.

On the other hand, reviews (Li and Faig, 1996, 1997) of related publications indicate that metric characteristics of such a group of digital camera systems have not yet been investigated in detail even in the photogrammetric field, mainly due to the limited image format and inferior image quality of such cameras. As non-metric 35-mm film cameras have found their applications for various measurement jobs, low-resolution digital camera systems should also find their own position in the metric environment.

As an electronic imaging system with optical components, a digital camera, no matter whether low or high the resolution, suffers from certain systematic defects, such as lens distortion, sensor plane deformation, and electronic transfer errors, which degrade the metric

fidelties of the resultant images. In addition, other factors such as image compression/decompression and image displaying devices also influence the system's performance. To make the resulting images metrically useful, these systematic errors have to be determined, modeled and compensated for, which usually can be implemented by a system calibration. It was also found from the above-mentioned review that digital image data acquired by digital cameras are usually reduced with existing algorithms and software developed for film-based cameras (Chen and Schenk, 1992; Curry et al., 1986; Fraser and Shortis, 1995; Heipke et al., 1992; Peipe, 1995; Peipe and Schneider, 1995; Stefanidis et al., 1990). Although relatively satisfying accuracies are reported when using these data reduction techniques, it is claimed that the cameras have not reached their theoretical expectations (Fraser and Shortis, 1995) due to the fact that certain systematic defects of the digital camera systems are different from those of the film-based counterparts. This impedes the full exploitation of the accuracy potential of such digital camera systems. The selection of low-resolution digital cameras further emphasizes the need for complete modeling of systematic errors of the whole system. Thus, an improved systematic error compensation scheme for digital camera systems is imperative.

FEM (Finite Element Method), a widely adopted numerical analysis approach for various engineering environments, was applied for camera calibration purposes by Munjy (1982, 1986a, b) as an alternative calibration method. However, not very much research has been conducted after that primary research, except for three publications (Lichti 1996; Lichti and Chapman, 1995, 1997). The advent of the digital cameras inspires the necessity of further investigation of this method.

The above reasons prompted the research presented in this dissertation. Thus, the scope

of the research is mainly to investigate and evaluate the metric performances and the accuracy potentials of low-resolution digital camera systems for photogrammetric purposes. Both theoretical and practical aspects are investigated, with emphasis on the geometric calibration. Different calibration schemes and different projects were designed and implemented for evaluation purposes. The application potentials of such camera systems and the related issues are also discussed in this dissertation.

1.3 Outline of the Dissertation

The dissertation is organized as follows:

Chapter 1 mainly explains the objectives and scope of the research.

Chapter 2 introduces the concepts and working principles of digital camera systems.

Chapter 3 describes the characteristics of the ideal digital camera systems and, based on that, possible error sources are analyzed.

Error modeling schemes, common calibration methods, their advantages and disadvantages are the main topic of the Chapter 4.

In Chapter 5, a modified version – Multiple Frame Finite Element Method (MFFEM) is proposed and related issues addressed after a brief review of the Finite Element Method and its application principles for camera calibrations.

Photogrammetric applications of low-resolution digital camera systems and some related issues are investigated in Chapter 6.

Chapter 7 is primarily concerned with practical metric performance evaluation of low-resolution digital camera systems. Three different camera systems were investigated under

test environment by using the existing self-calibration software and the newly developed package. An outdoor project and several indoor projects were carried out for this purpose. Project design, data acquisition, data processing, evaluation criteria, results and analyses are described in detail.

Conclusions from the research and recommendations for further studies are presented in Chapter 8.

1.4 Contributions

The principal contribution of this research lies at bridging the gap between the low-resolution and high-resolution digital camera systems, which is neglected or, at best, only touched upon by other researchers. Furthermore, the research findings are expected to be useful for improving the accuracy of high-resolution digital cameras, because both share certain similarities such as the structure of the lens system and sensor plane. In detail, based on the theoretical and practical studies conducted in the research, the unique contributions are summarized as follows:

- A thorough study of low-resolution digital camera systems is conducted from the photogrammetric point of view, which includes working principles, metric characteristics, error sources, systematic error modeling and compensation. This research facilitates the exploitation of the accuracy potential of the camera system and, thus, might further open new applications for low-resolution digital camera systems.
- The metric performances of three different types of low-resolution digital camera systems are investigated by using different systematic error compensation models during

the calibration. Different projects are designed and implemented to fulfill the investigation. The metric application potentials of such groups of digital camera systems are also studied based on the test findings.

- A modified camera calibration scheme MFFEM is proposed and verified through a simulation and a practical case, which is compared with other schemes. Some related issues such as element shape and size, shape functions, algorithm reliability are also discussed.
- A software package UNBDCSC (UNB Digital Camera System Calibration) is developed and tested by using the popular computer language MATLAB. The developed package can also be used for film-based cameras when using the proper option. Results of the data reduction, e.g. lens distortion curves, sensor contour lines, can be easily displayed and understood.

CHAPTER 2

LOW-RESOLUTION DIGITAL CAMERA SYSTEMS

The use of digital cameras continues to grow at an ever increasing rate in many general business fields due to improved performance and reduced prices. Digital cameras range in price from about US\$200 to over US\$40,000 (1998 prices), and there are models to suit most users. New models are pushed into the market frequently and old models updated and improved. In 1996, approximately 1.7 million digital cameras were shipped worldwide, and according to the International Data Corporation, this number may reach 8.4 million in 2001 (Curtin, 1998). Many photo-related companies have presented their own digital cameras to the market, and it is the customers who benefit from the competition between these companies. Most digital cameras currently available on the market are inexpensive, low-resolution consumer products. Although not specifically designed for photogrammetric purposes, digital cameras are proving themselves as a powerful image acquisition tool for photogrammetric systems, especially in close-range applications.

2.1 Digital Cameras

2.1.1 Definition

Unlike a conventional film camera which provides a continuous analog image, a digital camera is an electronic imaging device which outputs digital image signals by using binary numbers (0s and 1s) through on/off impulses which can be directly processed by a digital computer. It usually uses a general purpose camera body and lenses but records the image on solid-state sensors.

The substitution of solid-state sensors for the film makes the digital image output convenient and, this in turn facilitates the subsequent image processing and information extraction. Digital cameras therefore have become a suitable type of data acquisition tool for photogrammetric systems, especially in close-range situations. However, to realize the direct digital output, an on-board analog-to-digital (A/D) conversion is necessary. Due to the probably unstable, partially or completely unknown interior orientation as well as the lack of image frame reference marks, a digital camera can be considered as a non-metric camera from a photogrammetric standpoint.

Solid-state cameras, CCD (Charge Coupled Device) cameras, CID (Charge Injection Device) cameras, CMOS (Complementary Metal Oxide Semiconductor) cameras, still video cameras and digital cameras appear frequently in the literature in photogrammetry, computer vision and other imaging related professions. In fact, they are based on different, interrelated concepts. All of these cameras are essentially electronic imaging devices in contrast to the conventional film-based counterparts. However, the *solid-state camera* is a very comprehensive terminology which in fact encompasses all the cameras mentioned above, because a solid-state camera uses a solid-state sensor as the imaging medium to detect the light. *CCD cameras* and *CID cameras* are two main types of the most commonly found solid-state cameras which employ charge coupled devices (CCDs) or charge injection devices (CIDs) as the imagers, respectively. Standard CCD- and CID cameras, nevertheless, usually do not have on-board image data storage and A/D conversion capability. As a result, a host computer has to be connected to the cameras for the image storage and processing via a frame grabber. *Digital cameras* refer to cameras being capable of delivering digital image signals. Due to the fact that most digital cameras available nowadays are in the form of *still*

video cameras which are equipped with on-board storage and A/D conversion chips, i.e. the digital interface to a computer, digital cameras and still video cameras are often used, alternatively, at present. While more than ninety percent of the digital cameras employ the long-popular CCDs as the imaging sensors, *CMOS cameras* that use complementary metal oxide semiconductor as sensor are emerging. The lower constructional effect and, thus, lower manufacturing cost of the CMOS sensors than the CCD counterparts is the main impetus of the appearance of such cameras (Curtin, 1998; Lake, 1995b). Fig. 2.1 illustrates the relationship of common camera systems.

Digital cameras can also be grouped into three main categories, namely, low-resolution, medium-resolution and high-resolution digital cameras, based on the sensor element number of the sensor chips or the pixel count of the resultant images (see Table 2.1). Although not very accurate as discussed in the subsequent section, this classification scheme is widely adopted in imaging industry and even in photogrammetry. In the author's view, the classification itself does not have a great significance as it just approximately groups a variety of digital cameras into several categories. Nevertheless, it is worthwhile to study the metric characteristics of the cameras at the low end of the digital camera spectrum due to their increasing popularity. This forms the main topic of this dissertation.

2.1.2 Advantages and Disadvantages over Film-based Cameras

While sharing certain similarities, a digital camera differs from a film-based one in many aspects mainly due to the substitution of the silicon-based sensor. Table 2.2 summarizes the principal differences between the two imaging systems.

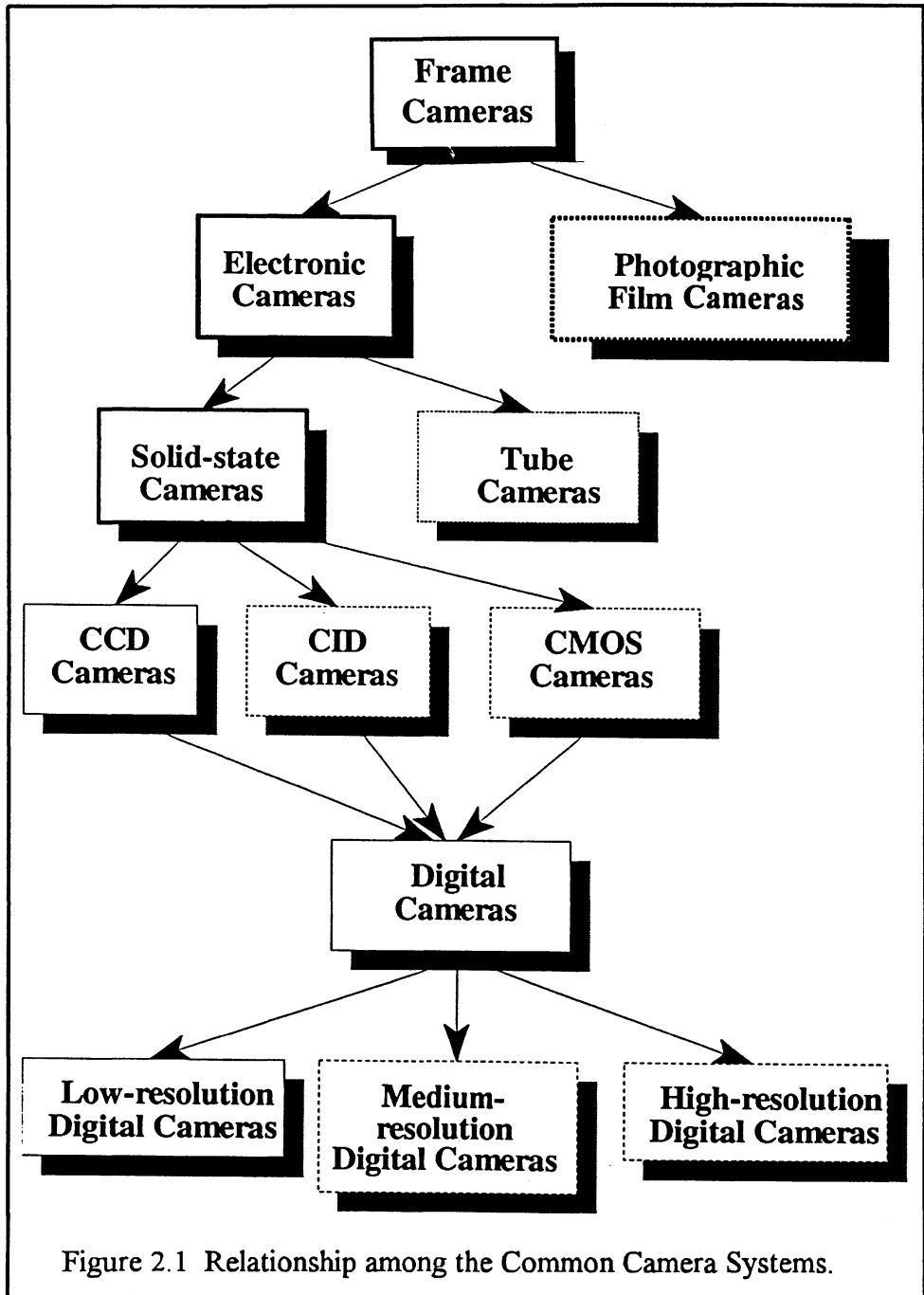


Figure 2.1 Relationship among the Common Camera Systems.

Table 2.1 Digital Camera Types.

Type	General Descriptions
Low-resolution digital cameras	<ul style="list-style-type: none"> • less than 1 million pixels, • also known as sub-megapixel digital camera, • small and inexpensive, • point-and-shoot model.
Medium-resolution digital cameras	<ul style="list-style-type: none"> • more than 1 million and less than 2 million pixels, • also known as megapixel digital camera, • more advanced features (e.g. through-the-lens viewfinder, override of manual control), • positioned between the point-and-shoot and the 35-mm SLR (Single-Lens Reflex) models.
High-resolution digital cameras	<ul style="list-style-type: none"> • more than 2 million pixels, • also known as multi-megapixel digital camera, • based on the SLR model but designed specifically for digital photography, • many accessories are available

Table 2.2 Digital Cameras vs. Film Cameras.

Comparison Items	Digital Cameras	Film Cameras
Imaging medium	solid-state sensors (e.g., CCD, CID, CMOS etc.)	silver halide film
Image resolution	usually lower than that of film cameras	high resolution
Imaging storage	magnetic or solid-state media	films, slides, prints etc.
Image output	softcopy imagery	hardcopy imagery
Image manipulation and processing	digital image processing with 'digital darkroom'	chemical processing in photoshop or laboratory
Image delivery	computer network, e-mail	fax, mail

It can be seen that the principal advantage of digital cameras over the traditional film camera is the computer compatible output because of the on-board A/D conversion. The corollary advantages are:

- no film development;

- no scanning (extra distortion may possibly be introduced through the scanning process);
- no chemical waste;
- image data can be readily stored, processed, and manipulated;
- lower operating costs (no film and no unwanted shots);
- image can be easily circulated through Internet or e-mail;
- less turn-around time.

However, every coin has two sides. Digital cameras also have some drawbacks, such as higher prices, inferior image quality, small field-of-view. Although the price and quality gap is narrowing gradually, this gap will not disappear in the foreseeable future.

2.1.3 Operational Principles

A natural object can be represented as an assembly of continuously varying shades and colours, whereas a digital image is an array of discrete points of grey levels rather than continuously varying tones. The imaging process with a digital camera can thus be divided into two separate phases. In Phase I, the digital camera works identical to a film camera because the front ends of both cameras are almost the same. The lenses, aperture and shutter receive and focus the light coming from the object. The differences occur in Phase II where the focussed light reaches the imaging medium to create an image. For a conventional film camera, silver-halide film particles react to the light chemically to form a latent image that has to be developed and fixed to make it visible and stable through the subsequent steps. On the contrary, the solid-state sensor (usually CCD) used as the imager in the digital camera reacts to light electrically. A CCD is a semiconductor with photoelectric sensor elements

arranged in one- or two-dimensions. When exposed to light, each individual sensor element will create an electronic impulse, with the magnitude being proportional to the brightness of the incident light. Through an A/D conversion inside the camera, the analog electric signal will be further converted into a series of digital codes which can be stored on a built-in or a removable storage device. Once the image is in digital form, it can be processed by a computer, transferred from one computer to another or transmitted electronically. Figure 2.2 depicts the main components and the working principles of a digital camera.

2.2 Digital Camera Systems

The adoption of digital cameras facilitates the evolution of photogrammetry from analogue and analytical eras to the digital era. However, no matter how powerful a digital camera is, it is only part of the imaging system. To apply a digital camera for any metric purpose, certain computer hardware and software are necessary for supporting the applications of such cameras and, thus, a digital camera system is formed.

A computer, certain peripheral hardware and some general purpose software are needed to transfer, store, process and display the images taken by the digital cameras. In addition, to derive metric information from the resulting digital images, certain specialized software, such as FotoG-FMS™ and Photomodeler™, has to be installed in the computer. The purpose of including such software in the systems is for image mensuration, image orientation and photogrammetric adjustment.

Although more than one digital camera can be used for a system, a typical digital camera system consists of a low-resolution digital camera and a laptop or desktop computer with

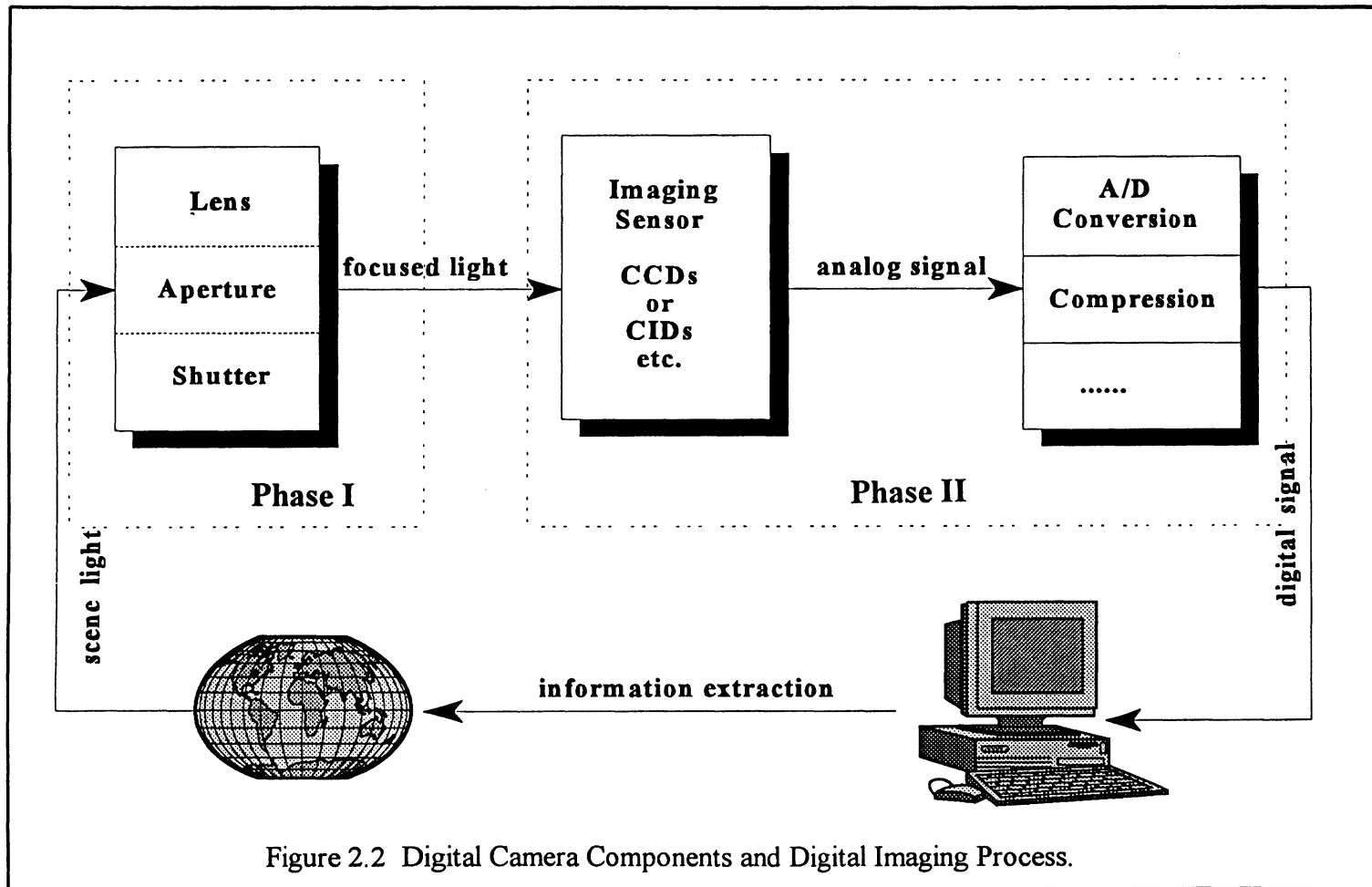


Figure 2.2 Digital Camera Components and Digital Imaging Process.

corresponding software, which serves as a powerful measuring system for many metric applications. More about such kind of systems, their advantages over other measuring systems and their applications are discussed in Chapter 6.

2.3 Resolution of Digital Camera Systems

Digital imagery provides the basic input for digital photogrammetry, with image quality playing an important role in data evaluation. Other characteristics of the imagery such as detectability and recognizability have to be considered with the resolution when evaluating and measuring the quality and usefulness of the imagery used for remote sensing and earth resource observation purpose (Rosenberg, 1971). From the metric standpoint, image resolution (geometric and radiometric) is the main factor defining image quality which is dependent upon the nature of the object imaged, the lens characteristics, imaging medium, imaging process and other factors of the camera systems.

2.3.1 General Considerations

Resolution is a commonly used terminology related to many input/output devices, such as cameras, scanners, printers and monitors. In the context of this dissertation, the resolution is mainly related to digital cameras -- a special kind of imaging device. Generally speaking, resolution of any imaging device can be defined as its capability to represent detail in the original scene. Due to the fact that a digital camera system usually consists of many interconnected components as discussed in the previous sections, and the imaging process

is influenced by many factors, the resolution of the whole system, therefore, is quite a complicated function of the following components and their interactions:

- camera lens types and quality (e.g., focal length, materials);
- imaging medium (e.g., solid-state sensors, sensitivity);
- scene or object (e.g., contrast, movement, distance from camera);
- imaging process (e.g., illumination, camera setting);
- image transformation (A/D conversion, compression/decompression) and displaying.

Usually, resolution can be classified into two primary parts, geometric resolution and radiometric resolution. The quality of a digital camera system can, thus, be evaluated by the geometric resolution and radiometric resolution of the images it delivers.

2.3.2 Geometric Resolution

Geometric resolution, or spatial resolution dealing with geometric or spatial characteristics, is the measure of the degree of fineness of the detail that the imaging system can resolve. As a human operator cannot discriminate more than 50 gray shades (Baxes, 1994), the geometric resolution plays a much more important role than the radiometric one for photogrammetric applications based on the hardcopy imagery. In digital photogrammetry, on the other hand, radiometric resolution is also one of the important quality indexes of the digital system because the image is usually processed by computer. However, as most modern digital cameras can provide the images very close to the radiometric quality of 24-bit color, the geometric resolution serves as the most dominant demarcation of various digital cameras. Strictly speaking, the measurement of a digital image's spatial resolution is related to two distinct measurements (Baxes, 1994):

- spatial density: a measure of the number of pixels in the image;
- optical resolution: a measure of the capability of how well the entire imaging system can resolve the spatial details of an original scene. This relates to the quality of the imaging system's optics, sensor element and electronics.

A reasonable evaluation for the total geometric resolution of a film-based imaging system is given by Warner et al.(1996) as following:

$$\frac{1}{R_T} = \frac{1}{R_L} + \frac{1}{R_F} + \frac{1}{R_{IM}} \quad (2.1)$$

where R_T , R_L , R_F and R_{IM} are the total resolution of the system, lens resolution, film resolution, and image movement resolution, respectively. This relationship also holds true for a digital counterpart with the exception of the substitution of R_{CCD} for R_F , which is the resolution of the CCD sensor onboard the digital camera.

As discussed before, the heart of most digital cameras is the CCD, a solid-state chip consisting of thousands of tiny light-sensitive elements. The geometric quality of the resulting images of a digital camera is directly related to the performance of the CCD inside the camera which, in turn, depends on the number and the size of the sensor elements. Although, many other factors have certain contributions, such as the lens quality, imaging process, the signal conversion and transmission and the original scene itself. If other factors are the same, the spatial resolution of a digital camera primarily depends on the spatial resolution of the solid-state sensors defined as the ratio of the pixel size to sensor format size (Fraser and Shortis, 1995) or simply as the number of the sensor elements. It is true, therefore, that a digital camera with fewer and smaller CCD sensor elements can deliver a partial image of equivalent or even better geometric quality than a digital camera with more

and bigger sensor elements. The more and the smaller the sensor elements on the CCD chip, the more and finer are the pixels of the output image, and the higher is the spatial resolution of the image. Nevertheless, as most of the current digital cameras have approximately the same pixel size of roughly 10 μm , many advertisements and publications in the digital imaging industry and in photogrammetry directly classify the digital cameras into different categories of resolution, such as low resolution, medium resolution and high resolution, solely based on the number of the CCD sensor elements (Bösemann et al., 1990; Godding and Woytowicz, 1995; Peipe, 1995; Peipe and Schneider, 1995). It can be easily seen from the above discussion that this classification represent only a simplified situation. The following figures give some standards of comparison concerning of the simplified geometric resolution of different imaging devices or media (Curtin, 1998):

- The human eye has a resolution equivalent to 120 million pixels.
- A 35-mm slide has a resolution equivalent to 20 million pixels.
- Most low-end digital cameras have resolutions between 300, 000 and 500, 000 pixels.
- Some of the most expensive professional digital cameras have resolutions of about 6 million pixels.

2.3.3 Radiometric Resolution

Each pixel of a digital image represents the intensity of the spatial location in the original scene, with radiometric resolution determine how well the captured image can represent the original brightness and color. Therefore, radiometric resolution can further be broken into brightness resolution and color resolution.

“Brightness resolution” describes how well the digital pixel’s brightness can represent the brightness of the original scene while “color resolution” deals with the degree of color

fidelity of the digital image. Radiometric resolution is represented as 'bit number' and is generally fixed for a particular digital camera. As stated previously, almost all the low-resolution digital cameras nowadays have a radiometric resolution of 24 bits, with 8-bit brightness resolution (256 grey scale) for each of the three primary colours (red, green and blue), although 30-bit cameras are becoming available. In spite of the fact that colour has taken on increased importance in recent years for the general imaging market (Berger, 1998) and in remote sensing, it is the brightness resolution that has to be taken into consideration for close range photogrammetric applications. This is because that digital photogrammetric measurements are based on the grey values of the pixels.

More detail about low-resolution digital cameras can be found in Appendix I, where a survey of low-resolution digital cameras is presented. It can be seen from the above discussion that digital camera technologies are advancing at an amazing speed with the support from the related rapidly developing technologies and the ever-increasing demands of the consumer market. As a result, cameras with better quality and more features will be available at a lower street price in the future. Being a relatively small profession, photogrammetry cannot affect a big change in the digital camera market. Therefore, more research on the metric applications of the available digital camera systems should be conducted in the photogrammetric field to meet the challenge, especially those consisting of low-resolution digital cameras, due to the price attraction.

CHAPTER 3

ERROR SOURCES OF DIGITAL CAMERA SYSTEMS

A photograph obtained with a film-based camera suffers from certain deformations due to many interrelated factors, such as the quality of lens and film, processing of the film, printing and storage of the photograph as well as external influences, such as atmospheric refraction (Faig, 1976a). In the past several decades, much research has been devoted to investigate the sources and the effects of image deformation in order to model and compensate for their influences for the purpose of deriving accurate metric information from the deformed photographs. The introduction of digital cameras brings many practical benefits and also some new types of image deformations, which necessitates the study of various sources of image deformation for digital camera systems.

3.1 An Ideal Digital Imaging System

In digital photogrammetry, digital images are processed with a computer based on both geometric and radiometric information of the images. Generally, digital images contain information whereby the geometric characteristics of the imaged object are represented by 2D arrays in the domain area, and the radiometric properties are reflected in the range of the digital images. Consequently, an ideal digital imaging system should faithfully conserve both geometric and radiometric qualities of the original scene.

3.1.1 Geometric Considerations

For aerial photographs, light rays emitted from objects on the ground have to pass quite

a long way to reach the camera. Aside from the camera quality, refraction, air turbulence, etc. also influence the locations of the image points. However, low-resolution digital cameras are primarily applied to close-range situations due to their limited resolution and sensor format size. Therefore, the above factors can be neglected when low-resolution digital cameras are considered.

The pinhole camera model is widely used to represent the geometry of an ideal camera, free from distortion. It simply models a rigid body transformation followed by a perspective transformation (Melen and Balchen,1994). Therefore, an ideal imaging geometry should have the following properties (Faig, 1976a):

- projection center is a point;
- light propagates according to geometric optics (straight rays);
- imaging media is a plane that is perpendicular to the optical axis of the system.

In addition, the sensor elements should be sized and distributed uniformly for solid-state sensors. Figure 3.1 illustrates this concept. Under the ideal case, the following relationship exists between the object coordinates of a 3D point and the image coordinates of the imaged point on the image positive:

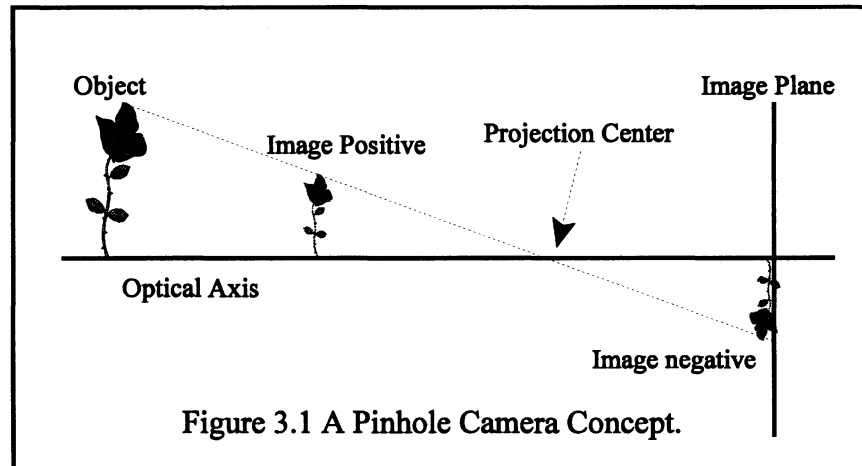
$$\begin{bmatrix} x_{ij} \\ y_{ij} \\ -c_i \end{bmatrix} = \lambda_j \begin{bmatrix} m_{11} & m_{12} & m_{13} \\ m_{21} & m_{22} & m_{23} \\ m_{31} & m_{32} & m_{33} \end{bmatrix} \begin{bmatrix} X_j - X_i^c \\ Y_j - Y_i^c \\ Z_j - Z_i^c \end{bmatrix} \quad (3.1)$$

where x_{ij} , y_{ij} denote image coordinates; λ_j refers to the scale factor for point j ; m_{11} to m_{33} are nine elements of the rotation matrix between object space and image space coordinate

systems; X_j, Y_j, Z_j and X_i^c, Y_i^c, Z_i^c are the object coordinates of the point j and of the i th perspective center, respectively. As all image points are located in the same image plane at a distance c_i (principal distance) from the perspective center, the following well-known collinearity equations can be derived from equation (3.1):

$$\begin{aligned} x_{ij} &= -c_i \frac{m_{11}(X_j - X_i^c) + m_{12}(Y_j - Y_i^c) + m_{13}(Z_j - Z_i^c)}{m_{31}(X_j - X_i^c) + m_{32}(Y_j - Y_i^c) + m_{33}(Z_j - Z_i^c)} \\ y_{ij} &= -c_i \frac{m_{21}(X_j - X_i^c) + m_{22}(Y_j - Y_i^c) + m_{23}(Z_j - Z_i^c)}{m_{31}(X_j - X_i^c) + m_{32}(Y_j - Y_i^c) + m_{33}(Z_j - Z_i^c)} \end{aligned} \quad (3.2)$$

This set of equations is the mathematical expression of ideal imaging geometry in which the object point, the perspective center and the image point lie on a straight line, which provides the basic mathematical framework for analytical and digital photogrammetry.



3.1.2 Radiometric Considerations

A digital image is a numerical record of a natural scene with continually varying levels of shades and colors, which is generated by a digital camera system through a series of steps, such as light sensing, signal processing and transmission, analog-to-digital (A/D) conversion

and image compression/decompression. The quality of the sensor and the complicated imaging process definitely affect the radiometric characteristics of the final output images. An ideal digital camera system is capable of conserving the radiometry of the original scene. The following criteria should be met by an ideal system for photogrammetric applications (El-Hakim et al, 1989; Shortis and Beyer, 1996):

- uniform and wide spectral sensitivity;
- low noise;
- no blemishes;
- no blooming;
- high charge collection and transfer efficiency;
- stable system performance.

3.2 Geometric Distortions

Digital camera systems suffer from imperfections in both geometric and radiometric aspects, which means that the generated images are deformed in certain ways. Image deformation can thus be understood as any metrical difference between the original scene and the final image from which measurements are taken (Ziemann, 1971). The deformation may be due to imperfect system structure such as physical movements of the imaging medium, improper support of the imaging medium by the camera platen, and/or to electronic inaccuracies for cases in which the image is obtained from solid-state sensors (Mcglone et al., 1989). El-Hakim et al. (1989) pointed out that geometric distortion of a digital image is caused by many sources of errors, such as lens distortion, non-perpendicularity of optical axis and image plane, non-perpendicularity of the image axes, location and non-alignment of

sensor elements, and the exact size of the elements. The combined effects of such errors cause the image points on the digital image to be distorted from their ideal locations, which in turn makes the final extracted information metrically inaccurate.

3.2.1 Lens Distortion

Unlike a geometrically perfect imaging system, no matter how small a perspective center is, it still consists of an infinite number of points. Most digital cameras have a compound lens system composed of several lens elements with different refractive indices rather than a single lens in order to decrease chromatic- and spherical lens aberrations. Again, these lenses are not perfect and the assembly of the overall system is not error-free. Errors such as imperfect components, polishing, centering of individual elements and assembling, all have adverse influences on the imaging geometry. As a result, the incident ray of light is distorted from the theoretical direction after it travels through the lens system and before reaching the solid-state imaging sensors. Generally, lens distortion can be divided into two main types, radial- and decentring lens distortion according to the causes and their influences, which are discussed in detail in Appendix II.

3.2.2 Sensor Plane Deformation

Concerning the sensor plane aspect, according to Curry et al.(1986), the solid-state cameras have certain advantages when compared to film based cameras, since no film distortion due to film buckling and emulsion is present. However, even without any lens distortion, image points will still be displaced from their ideal positions after photons strike the sensor plane to generate an image because of sensor plane imperfections. Sensor plane

displacement can be resolved into two components, namely, in-plane displacement and out-of-plane displacement (Fraser, 1997a) based on the physical characteristics of the sensor plane geometry.

3.2.2.1 In-plane Displacement

The limitation of sensor manufacture still causes:

- irregular distribution of sensor elements, resulting in non-uniform pixel size when an image is formed;
- non-orthogonality between the row-axis and column-axis of the sensor chips.

The geometric integrity of the layout of the pixel array is typically precise to the 0.1 μm level (Shortis and Beyer, 1996). Nevertheless, for applications pursuing very high accuracies, influences of these errors are still significant compared to 0.01 μm or higher image measuring precision.

In addition to the above geometric shortcomings, electronic effects such as clock synchronization can also cause in-plane distortion of the image for many standard CCD cameras, which is greatly alleviated in digital cameras as both the acquisition and sampling processes are driven by the same clock (Beyer, 1992a; Lichti, 1996).

3.2.2.2 Out-of-plane Displacement

The mathematics of all analytical photogrammetry is based on the assumption that the image points are coplanar (Fryer, 1992), which implies that the sensor plane should ideally be a plane for a digital camera. Again, solid-state sensors are not perfect in this aspect. As

film unflatness in a film based camera, focal plane unflatness in a digital camera caused by either inaccurate manufacturing (e.g. chip bowing or the ‘crinkle’ of thin wafers) or by the parallel motion of a linear sensor which can also lead to systematic image coordinate errors, and certainly limits the accuracy of the final photogrammetric results. Fraser (1997a) pointed out that the induced radial image displacement from the sensor plane unflatness is a function of the incident angle of the imaging ray. For example, at an incidence angle of 45 degree, a departure from planarity of 10 μm will give rise to an image displacement of the same magnitude. Thus, narrow angle lenses of long focal length are much less influenced by out-of-plane deformation than short focal length, wide angle lenses. Unfortunately, many digital cameras employ wide angle lenses to achieve a workable field of view due to the limited format of the solid-state sensors.

In contrast to a 600 μm film unflatness of a typical 35 mm film-based camera Canon AE-1 (Donnelly, 1988), KAF-1600 (14mm x 9 mm) and KAF-1000 (24.6 mm x 24.6 mm) CCD chips used in Kodak professional digital cameras (DCS series) are reported to have unflatness of 1.7 μm and 5 μm , respectively, expressed by the maximum peak-to-valley height difference (Fraser, 1997a), which should also definitely attract the photogrammetrist’s attention if the cameras are to be used for precision work.

3.2.3 Interior Orientation Stability

Unlike metric aerial cameras which are specifically designed for photogrammetric applications, almost all digital cameras are non-metric types. This is because of their completely unknown, or partially unknown and potentially unstable interior orientations

(principal point, principal distance, lens distortion and sensor deformation etc.) (Faig, 1976b). There are very few metric digital cameras, such as the Kodak Megaplug series which were designed for metric purposes. Interior orientation (IO) instability greatly influences the accuracy of photogrammetric triangulation when using digital cameras. Such problem is usually caused by the following factors (Fraser, 1997a):

- movement of the solid-state sensor with respect to the camera body;
- movement of the lenses with respect to the camera body;
- differential movement of lens elements when a compound lens system is adopted.

Under most cases, these errors combine to present the mixed results, which will be more complicated when zoom lenses are incorporated into digital cameras.

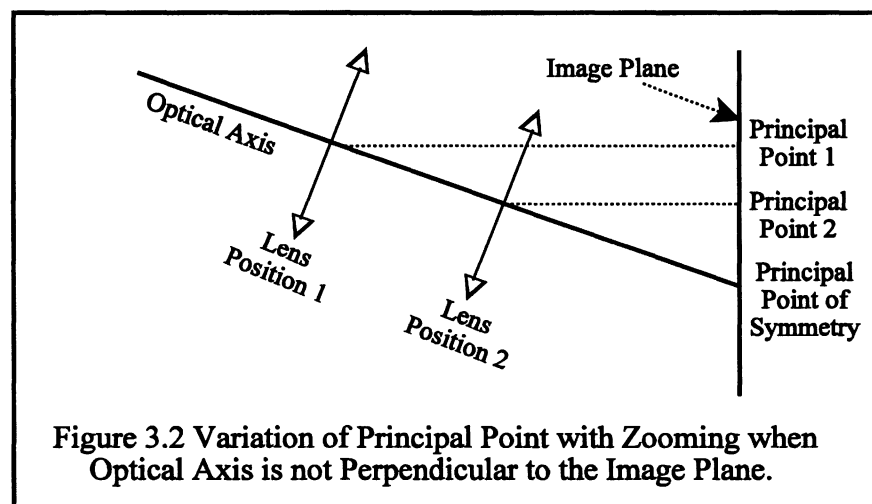
3.2.4 Influence of Zoom Lenses

A zoom lens is the one whose focal length can be changed within a certain range. As stated in Appendix I, about twenty-five percent of low-resolution digital cameras are equipped with zoom lenses, and more and more digital cameras will incorporate zoom lenses as one of the standard features. With the relatively smaller dimensions and the limited resolution of the imaging sensors in low-resolution digital cameras, zoom lenses can enhance their flexibility by providing a certain range of focal length settings and, thus, variable fields of view without having to further physically approach the object. This could make zoom lenses a viable alternative for use in high accuracy digital photogrammetry work (Wiley and Wong, 1990). Imaging with a zoom lens is essentially a dynamic process rather than a static one with a lens of fixed focal length. Zooming is achieved by the rotation and movement of one or more lens elements. While the direct result from the zooming operation is obviously

the variation of the principal distance, variations of the principal point position and lens distortions may be by-products due to the imperfect geometric structure of the system. Therefore, the key to the metric use of such lenses lies in the inherent stability of the camera systems and in the understanding of potential changes of the interior geometry of such cameras.

3.2.4.1 Variation of Principal Point

The principal point (PP) is defined as the foot of the perpendicular from the rear perspective center to the image plane. The cause of variation of the PP mainly lies in the non-perpendicularity of the optical axis with respect to the image plane. Misalignment angles of 0.5 degree have been found for several solid-state cameras (Burner et al., 1990). Figure 3.2 is largely self-explanatory of this concept (exaggerated). Wiley and Wong (1990) noted the significant changes with translation of up to 100 pixels of the PP for some CCD cameras. This is because that such cameras are designed for mass use rather than photogrammetric purposes and are usually mass produced to keep the price affordable.



3.2.4.2 Variation of Lens Distortion

Other factors disturbing image coordinates for zoom lenses are variable lens distortion, which indicates that the distortion patterns derived from infinite focus are not valid throughout the whole focus range. Both radial and decentring lens distortions vary in a predictable manner with lens focusing (Brown, 1971), with the strongest variation occurring at larger image scales (Fraser and Shortis, 1992). Therefore, distortion variation merits consideration in precision close-range photogrammetry using digital cameras with zoom lenses. Sections II.3 and II.4 of Appendix II present a detail discussion of this topic.

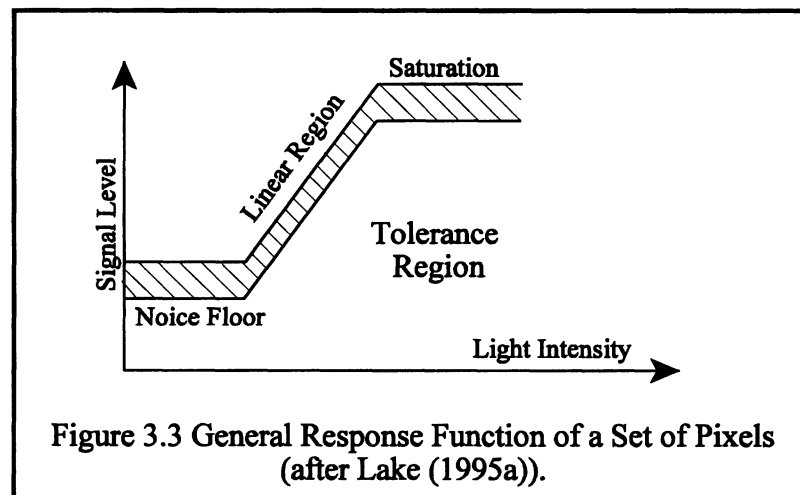
3.3 Radiometric Degradation

After photons strike the solid-state sensors, a series of electric and electronic operations are accomplished, such as charge coupling, charge transfer, A/D conversion and data compression. Faults in the fabrication of the solid-state sensor and/or deficiencies in the technology of CCD, CID lead to radiometric degradation of the image quality. While geometric distortion of a digital camera system causes departure of image points from their ideal positions, radiometric degradation influences the digital numbers(DNs) of certain image pixels and deteriorates the appearance of the image when displayed on a screen. The latter is of main concern when a manual operation is conducted for image mensuration, and the former changes the image coordinates derived from the automatic image measurement.

3.3.1 Non-linearity

During the digital imaging process, the incoming light is converted into discrete DNs, usually in a range of 0 (black) to 255 (white) through an A/D conversion. Ideally, the whole

conversion process should be linear for a certain wavelength region. The effect of non-linearity of the image system is that the resulting DN's of the digital image are not proportional to the original brightness of the natural scene. The reasons for this may be two fold; one is the sensor itself, e.g. photo response is not uniform for each sensor element (Sel); another reason lies in the electronic circuitry through which the signals are amplified and transmitted. PRNU (photo response non uniformity) is the term given to signal variations from Sel to Sel in a sensor, given the same level and wavelength of incident illumination (Shortis and Beyer, 1996). Figure 3.3 illustrates a typical transfer function pattern of a series of Sels, in which each Sel has different PRNU which should lie in a tolerance region.



3.3.2 Dark Current Noise

'Dark current noise' also known as dark noise, is a systematic noise with a fixed pattern, which is essentially the thermal generation of minority carriers, electrons in the case of silicon, in any semi-conductor (Shortis and Beyer, 1996). In total absence of light, the ideal case is that the output DN's of all pixels are zero. However, due to the presence of the dark

current noise, the recorded images have non-zero values. Although these thermally generated electrons can hardly be distinguished from the photon generated ones, a radiometric calibration can greatly eliminate this effect.

3.3.3 Blooming

Blooming is the local overload of an image sensor which is caused when one Sel or group of Sels are charged over their saturation limit and the extra electrons 'overflow' to the surrounding Sels, which makes the DN's of the corresponding pixels incorrect. Blooming is mostly associated with localized high-intensity light sources, such as car headlamp in night viewing (McCaughan and Holeman, 1979), and the response of retro-reflective targets to a light flash in close range digital photogrammetry (Shortis and Beyer, 1996). A CID sensor is less sensitive to this process than a CCD one (Curry et al., 1986). Nevertheless, the inclusion of anti-blooming has greatly alleviated this problem in the current generation of CCD cameras.

3.3.4 Malfunction of Certain Sensor Elements

Malfunction of certain Sels is mainly due to imperfections in sensor manufacturing, which results in systematic effects in the output images. Generally speaking, such malfunction can come in several combinations (Lake, 1995a), namely, single Sel defect, cluster defects, or a row defect, depending on the quality of the sensor. Generally, the more Sels a sensor has, the more defective Sels are encountered. The affected pixels can usually be detected by their abnormal DN's and thus corrections can be applied to them.

In closing this chapter, it is noted that digital imaging is quite a complicated electro-

optical process. Above are just main error sources related to a digital camera system. For photogrammetric applications, image quality is a main concern. Understanding the image formation process and the error sources can help us to avoid some avoidable problem (such as blooming), and also pave a road for calibration in order to exploit the metric potential provided by digital camera systems.

CHAPTER 4

CALIBRATION OF DIGITAL CAMERA SYSTEMS

It is known from the previous discussion that digital imaging is a transformation process from the three-dimensional (3D) real world to the two-dimensional (2D) image space, in which the original scene is represented both geometrically and radiometrically by the resulting digital image. On the other hand, digital photogrammetry is essentially an information extraction technique based on the digital images of the objects or phenomena of interest obtained by a digital camera system or other digital imaging devices (eg. a scanner or frame grabber). Therefore, to make the derived information metrically useful and to exploit the accuracy potential of digital camera systems, the relationship between the real world and the digital images should be maintained as correctly as possible. However, various errors existing in the digital camera systems prevent this. To circumvent this situation, two ways seem possible: one is to further improve the quality of the camera systems physically and to tightly control the imaging process in order to reduce the occurrence probability of the errors, and the other is to determine, model and compensate for the systematic errors mathematically. From the practical point of view, the former may be out of reach for many general applications mainly because the “built-in” quality of the imaging system is controlled by the manufacturers, while the latter alternative is of main concern to photogrammetrists and is referred to as camera system calibration, which forms the main topic of this chapter.

4.1 Objectives and General Principles of Camera System Calibration

Basically, the purpose of camera system calibration is to reconstruct the precise geometry of the bundle of rays that entered the camera at the instant of exposure from the 2D measurements of points on the resulting imagery (Moffitt and Mikhail, 1980). It is traditionally defined as a process of determining the geometric characteristics of the camera system. Practically, however, in the author's opinion, camera system calibration can be comprehensively understood as a process of and compensating for systematic errors of camera system and imaging process, through which the system's characteristics can be determined and the metric performance of the camera system be enhanced. Calibration of film-based cameras, especially non-metric types have been an important topic since the 1970's and many methods and results were published in close-range photogrammetry (Abdel-Aziz, 1975; Brown, 1971; Faig, 1971; Faig et al., 1990; Fryer, 1986, 1989, 1992, 1996, etc.). Consequently, after the introduction of digital cameras, digital camera system calibration is attracting much attention. Many calibration projects have already been carried out, and others are still in progress by different researchers and organizations for different types of digital camera systems.

Theoretically, an ideal digital camera system calibration scheme should calibrate the characteristics of the camera system that affect the geometry and radiometry of the resulting digital images, which includes the following objectives:

- to evaluate the performance of the lens systems (eg. distortion, resolving power);
- to evaluate the performance of the sensor chips (eg. sensor response, dark current, signal transfer efficiency, sensor element size and distribution, sensor deformation);
- to determine the relationship between the lens and sensor system (eg. alignment of the

- lens with respect to the sensor plane, principal point offsets and principal distance);
- to investigate the behaviour of the image transmission, compression/decompression;
 - to investigate the stability of the camera system (eg. variation of interior geometric configuration, temperature influence).

A review of the current research in digital camera system calibration (Li and Faig, 1997, 1998) indicates that most calibration research concentrates on the cameras' geometric aspects while only very few radiometric studies were implemented in the photogrammetric area. Furthermore, many digital camera system calibration projects simply applied the widely used methods developed for film-based cameras. The reasons for this situation are firstly, the optical part of a digital camera is the same (eg. some digital cameras simply substitute the CCD chips for the film without other modifications of the camera bodies) or very similar to the traditional film-based cameras; secondly, the digital imaging process is very complicated and a thorough investigation into a digital camera system is quite difficult. Therefore, it is unrealistic to expect a comprehensive mathematical model to encompass and effectively compensate for all the systematic errors of the digital camera system.

Generally speaking, the main principle underlying most camera system calibration methods is to model and compensate for the systematic errors of the systems based on the relationship between certain precisely known facts (e.g. the relative geometry of a group of object points, the determined grey values of an object or a scene) and the resulting geometrically and radiometrically distorted image. In the following sections, after a brief discussion of error modeling schemes, calibration methods currently used for digital camera systems are studied from both the geometric and radiometric aspects, with the main emphasis being on the geometric calibration techniques.

4.2 Modeling and Compensation Schemes of Geometric System Errors

The success of any precision metric application of a digital camera system is largely dependent upon the determination, modeling and compensation of the systematic errors of the camera systems. While many of radiometric systematic errors can be relatively easily detected and corrected (as discussed in Section 4.4), this section focuses on the geometry part. To better understand the calibration process, some common calibration related terms have to be defined. Appendix III lists the definitions of those terms.

4.2.1 Mathematical Modeling of Geometric Errors

Geometric camera calibration can be conducted based on analytical methods where the physical characteristics of the camera system are described by certain mathematical models, i.e., the systematic errors are modeled by functions of specific parameters. The ideal pinhole camera model described in Chapter 3 is not realistic for a real camera system. From the geometrical point of view, the basic collinearity equations (3.2) related to the pinhole camera model have to be expanded as follows to account for the systematic errors of the camera system by using a number of parameters, i.e. additional or added parameters (APs):

$$\begin{aligned}x_{ij} - x_0 + \Delta x &= -c_x \frac{m_{11}(X_j - X_i^c) + m_{12}(Y_j - Y_i^c) + m_{13}(Z_j - Z_i^c)}{m_{31}(X_j - X_i^c) + m_{32}(Y_j - Y_i^c) + m_{33}(Z_j - Z_i^c)} \\y_{ij} - y_0 + \Delta y &= -c_y \frac{m_{21}(X_j - X_i^c) + m_{22}(Y_j - Y_i^c) + m_{23}(Z_j - Z_i^c)}{m_{31}(X_j - X_i^c) + m_{32}(Y_j - Y_i^c) + m_{33}(Z_j - Z_i^c)}\end{aligned}\tag{4.1}$$

where x_0 , y_0 are the offset components of the principal point from the coordinate origin; Δx and Δy refer to the image coordinate perturbation functions accounting for the departures

from collinearity due to the systematic errors in the camera system. The terms c_x and c_y are the principal distances derived from the image coordinate x_{ij} and y_{ij} , respectively, which in most cases are simplified to one common value c (Fryer, 1992). In the above extended collinearity equations, the calibration terms consist of the principal distance c , the principal point offsets x_0, y_0 , and image coordinate correction functions Δx and Δy . Sometimes, such calibration parameters as x_0, y_0, c and other orientation parameters are implicitly expressed by specific parameters for the sake of simplicity, which leads to the extended Direct Linear Transformation (DLT) model:

$$\begin{aligned} x_{ij} + \Delta x &= \frac{L_1 X_j + L_2 Y_j + L_3 Z_j + L_4}{L_9 X_j + L_{10} Y_j + L_{11} Z_j + 1} \\ y_{ij} + \Delta y &= \frac{L_5 X_j + L_6 Y_j + L_7 Z_j + L_8}{L_9 X_j + L_{10} Y_j + L_{11} Z_j + 1} \end{aligned} \quad (4.2)$$

where L_1 to L_{11} are the DLT parameters for transformation between the machine coordinates (x_{ij}, y_{ij}) and the object coordinates (X_j, Y_j, Z_j) (Abdel-Aziz and Karara, 1971).

As the same physical object or phenomenon can be expressed with different mathematical models of different elements depending on the particular choice, many types of models of camera calibration exist in photogrammetry and in machine vision. These models can be categorized into physical, algebraic and hybrid (Faig and Shih, 1988) differing in the form of the functions $\Delta x, \Delta y$ and the APs involved.

4.2.1.1 Physical Models

The most straightforward way to model any physical system is to determine and describe its physical components and mathematically express the relationship among these

components. Physical models are formed based on the known physical characteristics of the camera system, such as radial and decentring lens distortions, scale change and non-orthogonality of image axes. In fact, this group of models is basically set up to model the causes of image deformations (Faig, 1984), which are being widely used for digital camera calibration due to their main advantage that all the parameters have interpretable physical meanings which are helpful in evaluating the system performance.

The most general form of the image coordinate correction functions Δx and Δy of physical models are given by Fraser (1997a) as:

$$\begin{aligned}\Delta x &= \Delta x_r + \Delta x_d + \Delta x_u + \Delta x_f \\ \Delta y &= \Delta y_r + \Delta y_d + \Delta y_u + \Delta y_f\end{aligned}\tag{4.3}$$

where the subscript r refers to radial lens distortion, d to decentring distortion, u to out-of-plane image deformation effect and f to in-plane image distortion influence. Different forms of the correction functions and different sets of the APs were used by different researchers in their digital camera system calibration projects according to their understanding of the systematic errors and the nature of the systems. Table 4.1 summarizes the physical models for camera system calibration and the physical meanings of the calibration parameters contained in the models, based on the reported projects of digital camera system calibration in photogrammetry and computer vision. It can be seen from this table that most calibration projects carried out by different authors still adopted the familiar model reported in Kenefick et al. (1972) which was developed for the calibration of film-based camera systems. In most cases, eight additional parameters were included in the models, namely, principal distance (one parameter), principal point offsets (two parameters), radial lens distortion (three parameters) and decentring lens distortion (two parameters). In addition, two further

parameters, differential axis scaling and non-orthogonality were added to the above eight-parameter model to account for the in-plane deformation, with the out-of-plane deformation being left open.

While the main advantage of physical models lies at the direct physical interpretation of the APs, the disadvantages are that some systematic errors are not physically known and thus cannot be completely modeled by the above functions of APs. Also, the over-parameterization and correlations among the APs themselves and among the APs and other orientations parameters will sometimes degrade the accuracy of the final photogrammetric results.

4.2.1.2 Algebraic Models

Algebraic models are formed from geometric considerations only, usually with orthogonal or near orthogonal components (Shih, 1989) with their principal strength being low correlation among the parameters and being capable of compensating for unpredicted or unspecified effects. Compared to physical models, algebraic models are established to model the effects of image deformations. The shortcoming of this kind of model lies in that the parameters of the model are not physically interpretable, in other words, they do not possess physical meanings. A typical example of such a model is given by the spherical-harmonics functional model as Equation 4.4 (El-Hakim, 1979) using a general polynomial for possible distortion, which was applied for the calibration of a digital camera system reported by Faig and Li (1997).

$$\begin{aligned}\Delta x &= T\bar{x} \\ \Delta y &= T\bar{y}\end{aligned}\tag{4.4}$$

Table 4.1 Common Physical Models used for Digital Camera System Calibration Projects.

Projects	Model Formats	Physical Meaning of Calibration Parameters
Beyer's project (Beyer, 1992a)	$\Delta x = \Delta x_0 - \frac{\bar{x}}{c} \Delta c - s_x \bar{x} + a\bar{y} + \bar{x}(k_1 r^2 + k_2 r^4 + k_3 r^6)$ $+ p_1(r^2 + 2\bar{x}^2) + 2p_2 \bar{x}\bar{y}$ $\Delta y = \Delta y_0 - \frac{\bar{y}}{c} \Delta c + a\bar{x} + \bar{y}(k_1 r^2 + k_2 r^4 + k_3 r^6)$ $+ 2p_1 \bar{x}\bar{y} + p_2(r^2 + 2\bar{y}^2)$	k_1, k_2, k_3 : coefficients of radial lens distortion; p_1, p_2 : coefficients of decentring lens distortion; s_x : scale factor in x direction; a: shear factor
Burner's project (Burner et al., 1990)	$\Delta x = \Delta s_h \bar{x} + \Delta s_v \Delta \phi \bar{y} + \bar{x}(k_1 r^2 + k_2 r^4 + k_3 r^6)$ $+ p_1(r^2 + 2\bar{x}^2) + 2p_2 \bar{x}\bar{y}$ $\Delta y = \Delta s_v \bar{y} + \bar{y}(k_1 r^2 + k_2 r^4 + k_3 r^6)$ $+ 2p_1 \bar{x}\bar{y} + p_2(r^2 + 2\bar{y}^2)$	$\Delta s_h, \Delta s_v$: differential scale between the horizontal and vertical pixel spacing; $\Delta \phi$: non-perpendicularity of the pixel axes
Edmundson's project (Edmundson et al., 1991)	$\Delta x = \bar{x}(a_1 r^2 + a_2 r^4) + a_3(r^2 + 2\bar{x}^2)$ $+ 2a_4 \bar{x}\bar{y}$ $\Delta y = \bar{y}(a_1 r^2 + a_2 r^4) + 2a_3 \bar{x}\bar{y}$ $+ a_4(r^2 + 2\bar{y}^2)$	a_1, a_2 : coefficients of radial lens distortion; a_3, a_4 : coefficients of decentring lens distortion

(Table 4.1 continued)

Projects	Model Formats	Physical Meaning of Calibration Parameters
Fraser's project (Fraser et al., 1995; Fraser, 1997a)	$\Delta x = -\frac{\bar{x}}{c} \Delta c + \bar{x}(k_1 r^2 + k_2 r^4 + k_3 r^6)$ $+ p_1(r^2 + 2\bar{x}^2) + 2p_2 \bar{x}\bar{y} + b_1 \bar{x} + b_2 \bar{y}$ $\Delta y = -\frac{\bar{y}}{c} \Delta c + \bar{y}(k_1 r^2 + k_2 r^4 + k_3 r^6)$ $+ 2p_1 \bar{x}\bar{y} + p_2(r^2 + 2\bar{y}^2)$	<p>Δc : variation of principal distance; b_1, b_2: coefficients of in - plane distortion, where b_1 accounts for differential scaling between the horizontal and vertical pixel spacing; b_2 is the 'shear' term modeling non - orthogonality between the axes. All other terms have the same meanings as before</p>
Heipke's project (Heipke et al., 1992)	$\Delta x = A_1(r^2 - r_0^2)\bar{x} + A_2(r^4 - r_0^4)\bar{x}$ $+ B_1(\bar{y}^2 + 3\bar{x}^2) + 2B_2 \bar{x}\bar{y}$ $\Delta y = A_1(r^2 - r_0^2)\bar{y} + A_2(r^4 - r_0^4)\bar{y}$ $2B_1 \bar{x}\bar{y} + B_2(\bar{x}^2 + 3\bar{y}^2)$	<p>A_1, A_2, r_0: parameters for radial distortion; B_1, B_2: parameters for decentring distortion</p>
Li and Faig's project (Li and Faig, 1996)	$\Delta x = \bar{x}(k_1 r^2 + k_2 r^4 + k_3 r^6)$ $+ p_1(r^2 + 2\bar{x}^2) + 2p_2 \bar{x}\bar{y} + A\bar{y}$ $\Delta y = \bar{y}(k_1 r^2 + k_2 r^4 + k_3 r^6)$ $+ 2p_1 \bar{x}\bar{y} + p_2(r^2 + 2\bar{y}^2) + B\bar{y}$	<p>k_1, k_2, k_3: coefficients of radial lens distortion; p_1, p_2: coefficients of decentring lens distortion; A, B: coefficients of scale change and non - perpendicularity of coordinate axes;</p>

(Table 4.1 continued)

Projects	Model Formats	Physical Meaning of Calibration Parameters
Lichti and Chapman's project (Lichti and Chapman, 1995; 1997)	$\Delta x = \bar{x}(k_1 r^2 + k_2 r^4 + k_3 r^6) + p_1(r^2 + 2\bar{x}^2) + 2p_2 \bar{x}\bar{y}$ $\Delta y = \bar{y}(k_1 r^2 + k_2 r^4 + k_3 r^6) + 2p_1 \bar{x}\bar{y} + p_2(r^2 + 2\bar{y}^2)$	as before
Peterson's project (Peterson et al., 1993)	$\Delta x = \bar{x}(k_1 r^2 + k_2 r^4) + p_1(r^2 + 2\bar{x}^2) + 2p_2 \bar{x}\bar{y}$ $\Delta y = \bar{y}(k_1 r^2 + k_2 r^4) + 2p_1 \bar{x}\bar{y} + p_2(r^2 + 2\bar{y}^2)$	as before
Wong's project (Wong et al, 1990; Wiley and Wong, 1990)	$\Delta x = \bar{x}(k + l_1 r^2 + l_2 r^4) + [p_1(r^2 + 2\bar{x}^2) + 2p_2 \bar{x}\bar{y}](1 + p_3 r^2)$ $\Delta y = \bar{y}(l_1 r^2 + l_2 r^4) + [2p_1 \bar{x}\bar{y} + p_2(r^2 + 2\bar{y}^2)](1 + p_3 r^2)$	<i>k</i> : scale correct for x - coordinates; <i>l</i> ₁ , <i>l</i> ₂ : coefficients of radial lens distortion; <i>p</i> ₁ , <i>p</i> ₂ , <i>p</i> ₃ : coefficients of decentring lens distortion;
Notes: \bar{x} , \bar{y} : image coordinates with respect to principal point (x_0, y_0); $\bar{x} = x - x_0$, $\bar{y} = y - y_0$; $r = \sqrt{\bar{x}^2 + \bar{y}^2}$, radial distance from principal point to the image point under consideration; Δx_0 , Δy_0 and Δc : variations of interior orientation parameters.		

T is the harmonic function in the form of:

$$T = a_{00} + a_{11} \cos \lambda + b_{11} \sin \lambda + a_{20}r + a_{22}r \cos 2\lambda + b_{22}r \sin 2\lambda + a_{31}r^2 \cos \lambda + b_{31}r^2 \sin \lambda + \dots \quad (4.5)$$

where

$$\lambda = \arctan \frac{\bar{x}}{\bar{y}} \quad (4.6)$$

a_{ij} , b_{ij} are coefficients of the spherical-harmonic function, and \bar{x} , \bar{y} and r were specified as before. Brown (1976) describes a more general algebraic model used for camera calibration as:

$$\begin{aligned} \Delta x &= a_1 \bar{x} + a_2 \bar{y} + a_3 \bar{x}\bar{y} + a_4 \bar{y}^2 + a_5 \bar{x}^2 \bar{y} + a_6 \bar{x}\bar{y}^2 + a_7 \bar{x}^2 \bar{y}^2 \\ &\quad + \frac{x}{c} [a_{13} (\bar{x}^2 - \bar{y}^2) + a_{14} \bar{x}^2 \bar{y}^2 + a_{15} (x^4 - y^4)] \\ &\quad + x [a_{16} (\bar{x}^2 + \bar{y}^2)^2 + a_{17} (\bar{x}^2 + \bar{y}^2)^4 + a_{18} (\bar{x}^2 + \bar{y}^2)^6] \\ \Delta y &= a_8 \bar{x}\bar{y} + a_9 \bar{x}^2 + a_{10} \bar{x}^2 \bar{y} + a_{11} \bar{x}\bar{y}^2 + a_{12} \bar{x}^2 \bar{y}^2 \\ &\quad + \frac{y}{c} [a_{13} (\bar{x}^2 - \bar{y}^2) + a_{14} \bar{x}^2 \bar{y}^2 + a_{15} (x^4 - y^4)] \\ &\quad + y [a_{16} (\bar{x}^2 + \bar{y}^2)^2 + a_{17} (\bar{x}^2 + \bar{y}^2)^4 + a_{18} (\bar{x}^2 + \bar{y}^2)^6] \end{aligned} \quad (4.7)$$

4.2.1.3 Hybrid Models

Hybrid models combine both the physical and algebraic models. Therefore, they are supported by both physical and algebraic aspects. Chen and Schenk (1992) use the following hybrid functions to model image deformation of a CCD based digital camera system, which consist of regular polynomials of radial- and decentring lens distortion and a seventh order polynomial accounting for the rest of the image distortions:

$$\begin{aligned}
\Delta x &= \bar{x}(k_1 r^2 + k_2 r^4 + k_3 r^6) + (1 + p_3 r^2)[p_1(r^2 + 2\bar{x}^2) + 2p_2 \bar{x}\bar{y}] \\
&\quad + m_1 \bar{x} + m_2 \bar{x}^3 + m_3 \bar{x}^5 + m_4 \bar{x}^7 \\
\Delta y &= \bar{y}(k_1 r^2 + k_2 r^4 + k_3 r^6) + (1 + p_3 r^2)[2p_1 \bar{x}\bar{y} + p_2(r^2 + 2\bar{y}^2)]
\end{aligned} \tag{4.8}$$

In addition, the FEM (Finite Element Method) proposed by Munjy (1982) can also be considered as a hybrid model as it possesses the characteristics of both the physical and algebraic models. However, it differs from above models in that no corrections are to be applied to the image coordinate measurements. Instead, variations of the principal distance are incorporated into the basic functional model to model image deformations. Chapter 5 is devoted to a detailed discussion of this topic.

4.3 Geometric Calibration

The objective of geometric calibration is to determine and compensate for the systematic errors that influence the geometric positions of the image points. Generally speaking, in addition to other system influences, a thorough geometric calibration should consist of the investigation from both lens system and sensor plane aspects which should include the determination of :

- principal point (PPP, PPA and PPS);
- (calibrated) principal distance/ camera constant;
- lens distortion (radial and decentering lens distortion);
- sensor plane geometry (sensor element spacing/pixel size, planarity, orthogonality of pixel axes);
- variation of the interior geometry of the camera system, especially with a focusable lens;
- stability of the above calibration parameters.

However, many geometric calibration projects of digital camera systems were performed considering mainly the lens part of the camera (e.g. Chen & Schenk, 1992; Edmundson et al, 1991; Kochi et al, 1995; Paquette et al, 1990, etc.). Few of them deal with the sensor aspect (Curry et al., 1986; Burner et al., 1990). The following sections are designed to discuss the common methods of geometric calibration, their strengths and weaknesses.

4.3.1 Methods of Calibration

Methods of geometric camera system calibration are usually classified into three categories (Faig, 1989), namely,

- pre-/post-calibration: represents the conventional laboratory, test range and stellar calibration. For the calibrated system, calibration parameters remain constant or change according to a determined pattern during the subsequent evaluation. The typical characteristic of such a calibration method is that the calibration and the evaluation are separate processes.
- on-the-job calibration: calibration and evaluation are either combined into one process or carried out sequentially in which calibration parameters are treated as unknowns. Additional object-space control is required to solve for these parameters.
- self-calibration: these approaches differ from on-the-job methods in that they do not need additional object-space control for the solution of the calibration parameters. They make use of the geometric strength of overlapping images to determine these parameters. Therefore, unlike the on-the-job method which can be implemented either in the case of single-image or of multi-image, self-calibration is only valid when overlapping images are available, and the configuration of the image acquisition has a direct influence upon the final results.

From the author's point of view, all camera calibration approaches can be grouped into two

main types, individual methods and combined methods, according to the recovery situation of the calibration parameters.

4.3.1.1 Individual Methods

In this case, particular calibration parameters describing lens distortion, principal point offset and sensor unflatness are determined separately from each other, based on either empirical or analytical methods with the help of certain special devices, such as a laser beam, collimators or a goniometer. Traditional laboratory approaches belong to this group. However, this type of method can also be thought of as a partial method which derives a subset of calibration parameters (Shortis et al, 1995), e.g. lens distortion parameters, principal point offset, etc.

Principal point location. As discussed in preceding sections, principal points cited by many publications of camera calibration usually refer to one of the PPP, PPA and PPS. Under most cases where the accuracy requirement is not extremely stringent, they are not differentiated. Although the PPP and PPA can be used synonymously, the PPS is usually not located at the same place if the optical axis is not perpendicular to the sensor plane, and the displacement between the PPA and PPS indicates the misalignment between the optical axis and the sensor plane. The PPA for a solid-state camera can be found by using a low power laser beam (Burner et al, 1990). First, the laser beam is aligned normal to the sensor when the lens is removed. Then, with the lens mounted on the camera and approximately focussed at infinity, the centroid of the focussed laser spot on the image locates the PPA. The PPS can be determined in the similar way as used for the PPA except that the laser beam needs to be

aligned with the optical axis of the lens.

Principal distance determination. Principal distance can be determined analytically based on the measurement of the image scale over the central part of the image (near the PPS and corrected for the third- order radial distortion) as a function of the inverse of the object-to-camera distance. A well-controlled target plate can be used for this purpose. The precisely known relative positions of the target points and their recorded images form the foundation of the computation (Burner et al, 1990). Usually, this procedure can be repeated several times with different object-to-camera distances in order to improve the accuracy of the estimated principal distance. Determination of the principal distance by using this method is commonly conducted when the same focus setting of the lens is maintained throughout the calibration. Therefore, the determined principal distance should be independent of the object-to-camera distance and valid at that focus setting, which is suitable for a lens with a fixed focal length. For a zoom lens, however, the situation would be more complicated due to a variable focal length and, thus, a varying principal distance while the lens is refocusing. Theoretically, the above method could be applied to determine the varying principal distance at each focus setting. If the variation of the principal distance displays a systematic trend when compared to focal length, the principal distance at focal lengths other than the ones set during the calibration can be approximately found by an interpolation method (Wiley and Wong, 1995).

Lens distortion evaluation. Unlike principal distance determination, where only the central part of the image field is used to minimize the effect of lens distortion, a large number of object points with known positions covering the whole sensor field should be imaged in

order to effectively evaluate the lens distortion. Coefficients of radial- and decentring lens distortions are acquired based on the differences between the measured image point locations and the predicted or known ones for all the image points covering the image field. A lens is usually calibrated in at least two distinct object distances if lens distortion at any other object distances are to be expected. The 'plumb line method'(Brown, 1971) can also be successfully applied to determine the lens distortion, which is based on the fact that an image of an object space straight line (vertical, horizontal or other orientations) should also be a straight line if no lens distortion is present. Therefore, any departure from the straightness is attributed to lens distortion and forms the base of the distortion calculation. This kind of method is capable of deriving the distortion coefficients independently from all other parameters and can be carried out under operational conditions (Shortis et al, 1995).

The above described individual calibration methods are not especially designed for digital camera systems. They have been widely used for calibrating film-based close-range cameras. However, differences exist in target designing and in the image point location techniques. The image coordinates of the target points which serve as the base of the calibration can be determined with the strategies outlined in the following sections.

Sensor evaluation. The Sel spacing or pixel size can either be precisely measured directly with a microscope with a ruled stage (Curry et al., 1986) or determined by a Moirè technique (Lenz, 1989). Burner et al. (1990) designed a reticule method to determine the horizontal and vertical pixel spacing and angle of non-perpendicularity of the pixel axes based on an affine transformation from a known image. A surface gauge can be used for direct sensor topography measurement. Fraser (1997a) reported a similar measurement by

using a flatness interferometer plus a Wyko phase-shifting interferometer. After the determination of the unflatness and the affinity of the sensor chip, corrections can be applied to the image coordinate observations to compensate for these effects.

The main strength of the individual methods is the relative independence of the calibration parameters which makes the results more reliable. The calibrated values derived from the individual methods could be incorporated into the combined methods to decouple the possible correlations among the calibration parameters and other parameters. As lenses and sensor can be evaluated individually, calibration of a number of different sensors with the same lenses, or of same sensor with different lenses raises the possibility to test the stability of the lens distortion parameters and of the affine scale and orthogonality parameters, respectively (Shortis et al., 1995). However, individual methods have the weakness of high time consumption and the requirement for certain special devices. In addition, the camera systems have to be disassembled for the calibration and under most cases, system calibration is separated from data evaluation. Thus, for some digital camera systems, the variation of their internal geometry may sometimes make the calibration results meaningless if the variation is unpredictable.

4.3.1.2 Combined Methods

These methods are being widely used to determine the principal point offset, principal distance, lens distortion parameters, even part of the sensor information (orthogonality and affinity) at the same time based on the relationship between a well-controlled test-field composed of an array of precisely coordinated targets and its distorted image. Such methods can also determine the calibration parameters with confidence or with a reasonable degree

of independence if the data acquisition network is strong. Figure 4.1 describes the general procedure of the combined methods as image taking, image mensuration and photogrammetric adjustment. Calibration parameters can either be derived based on single- or multi-frame resection if enough satisfactory object-space control information is available, or can be recovered together with the exterior orientation parameters and object coordinates simultaneously from the photogrammetric bundle adjustment. Traditional on-the-job and self-calibration can be thought of as special cases of combined methods differing in the control requirement. Essentially, these methods are based on the mathematical modeling of the systematic errors of camera systems as described in Section 4.2.1. There exist a variety of approaches in the combined method group depending on the systematic error modeling schemes, single- or multi-frame images, control requirement. Due to the fact that the lens system used in digital cameras is not very different from that of conventional film-based cameras, many existing well-established methods were adopted for the geometric calibration of digital camera systems without any significant modifications. Satisfying results have been reported by different authors (Bösemann et al., 1990; El-Habrouk et al., 1996).

The remainder of this section is designed to describe the above stated procedures and related issues involved in the combined calibration.

Image acquisition. It is a well known fact that the imaging configuration has a direct influence upon the recovery of the calibration parameters and the reconstruction of the 3D object. In detail, an ideal photogrammetric network should have the following characteristics for a successful camera calibration and object reconstruction:

- highly convergent images;
- a large range of depth-of-field;

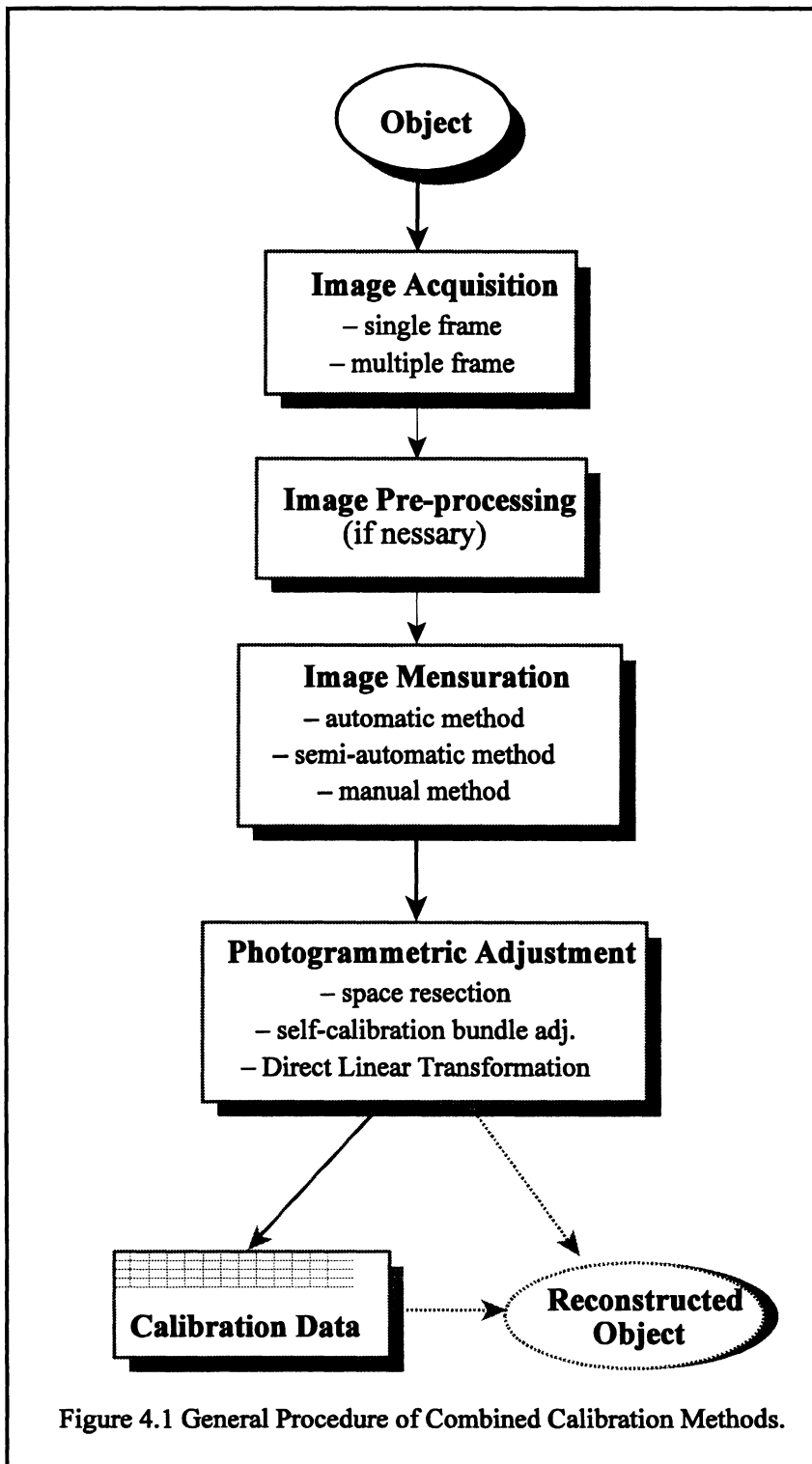


Figure 4.1 General Procedure of Combined Calibration Methods.

- a variety of camera rotation angles;
- an appropriate amount of well designed and distributed target points (with or without precisely known positions).

These goals can be fulfilled to a large extent in many cases. Practically, the test-field is imaged from more than two camera stations resulting in a multi-station convergent image block (El-Habrouk et al., 1996; Heipke et al., 1992; Peipe, 1995). Usually, more than one image with varying rotation angles is taken from each camera station, which makes the calibration process highly redundant and is beneficial for the reliability of the results. Vösselmann and Förstner (1988) rotated the camera around its axis by 90 degrees to take other images at the same camera location, which ensures that the difference between the pixel size in row and column directions would be more precisely determined during the subsequent photogrammetric adjustment. The image scale can be selected in such a way that the images of the test-field occupy most of the format of the sensor. It is also known that targeting and illumination of the test-field are important for the image quality. Most test-fields are targeted by appropriately sized black circles against a white background (Heipke et al., 1992; Lee and Faig, 1996), while some are equipped with light emitting diodes (LEDs) (Kochi et al., 1995) or retro reflective targets. More detail about the imaging configuration and targeting will be presented in Chapter 6.

Image mensuration. The precise image position of target points always plays an important role for any photogrammetric project. Various automatic or semiautomatic schemes or manual operations are employed to locate the digital image points. Under the appropriate targeting and illumination, the recorded images display a high contrast.

Therefore, the imaged targets can be easily identified from the background with subpixel accuracy by using simple thresholding and weighted centroid detection algorithms (Edmundson et al., 1991; Chen and Schenk, 1992; Shortis et al., 1995; Stefanidis et al., 1990). Some of the more complex image location strategies, e.g. least-squares matching (Heipke et al., 1992; Vösselmann and Förstner, 1988) can be employed to improve the accuracy. For certain digital images with much noise, the manual method is necessary to determine the image positions in order to avoid the failure of the automatic detection approach (El-Habrouk et al., 1996; Faig et al., 1996). After the image location, the image coordinates have to be transformed from pixel units to metric units which serve as the basic input to the subsequent photogrammetric adjustment. Usually, the transformation is based on the Sel spacing /pixel size specified by the manufacturer or on the calibrated value from the described individual method. However, it is also possible to treat the pixel size as a free or weighted observation quantity in the photogrammetric adjustment if precise object space scale information is available, and the data acquisition configuration is geometrically strong.

Photogrammetric adjustment. Various self-calibrating bundle adjustments based on the expanded collinearity equations are the most often used methods which can easily accommodate the calibration parameters into the functional model. To eliminate the constraints imposed by the control information, self-calibration methods with minimal constraint (Vösselmann and Förstner, 1988) or free-network adjustment (Bösemann et al., 1990) are preferred. Chen and Schenk (1992), and Faig and Li (1997) also applied the Direct Linear Transformation (DLT) as the functional models with the inclusion of certain calibration parameters. After the photogrammetric adjustment, the calibration parameters

and the corresponding accuracy information are provided, by which the performance of the camera system can be evaluated through a series of statistical tests. Usually, the RMS (Root-Mean-Square) values of image coordinate residuals and of object space intersection parallax serve as quality indicators of the camera calibration and object reconstruction.

The advantages of the combined methods are their easy availability and parameter completeness as well as the combination of camera system calibration and data evaluation. The main drawback is that the calibration parameters are severely influenced by the imaging configuration and the existence of the correlations between the calibration parameters themselves and other adjustment parameters (e.g. the object coordinates). The correlation may cause adjustment divergency or distort the calibration results in that the derived parameters are not accurately representative of their actual effects. In addition, for certain applications (Burner, 1995), these methods are excluded due to the physical limitations of the environment which make the appropriate data acquisition configuration impossible.

4.4 Radiometric Calibration

Radiometric calibration is conducted to investigate the radiometric characteristics of digital camera systems, i.e. 'how well' the recorded grey values by the system can preserve the natural brightness. It has been proven that increased radiometric precision improves the precision of target location in digital images (Trinder, 1989) and, thus, enhances the performance of the digital camera systems. It is the author's view that the geometric and radiometric calibration should not be carried out separately for an ideal digital camera calibration, as they are interconnected. However, in practice they are conducted separately

for the sake of simplicity. A complete calibration of all aspects of a digital data acquisition and processing system is extremely complex as radiometric and geometric degradation and environmental parameters such as humidity and temperature all affect the performances of the system (El-Hakim et al., 1989). On the other hand, in a majority of close-range and machine vision applications, the geometry of the sensor is of paramount importance to maintain metric accuracy and the radiometry is often a secondary issue (Shortis and Beyer, 1996), which is especially true for low-resolution digital cameras due to their limited geometric resolution. This is why there are very few publications (Curry et al., 1986; Stefanidis et al., 1990) available about radiometric calibration of digital cameras in the photogrammetric field. Generally, the radiometric calibration can be performed in the laboratory to study certain aspects of the radiometric characteristics of the digital cameras.

4.4.1 ‘Cap-on Method’

This is a very simple method used to determine the ‘dark current noise’: a systematic system noise. With the lens cap on, an absence-of-light situation is imitated and the recorded output grey levels should have theoretical values of zero. Any differences from zero can be considered as the ‘dark current noise’ for that imaging condition. Based on the recorded values, a mask can be generated and used for subtraction from the subsequent images to counteract the influence of the ‘dark current noise’, which can effectively make the digital images largely free of the dark signals. It is worth noting that some digital cameras cannot function properly when the cap is kept on. In such cases, alternative methods have to be devised, for example, a uniform black background could be imaged to mimic the no-light situation.

4.4.2 ‘Uniform Grey Page and Grey Step Card Method’

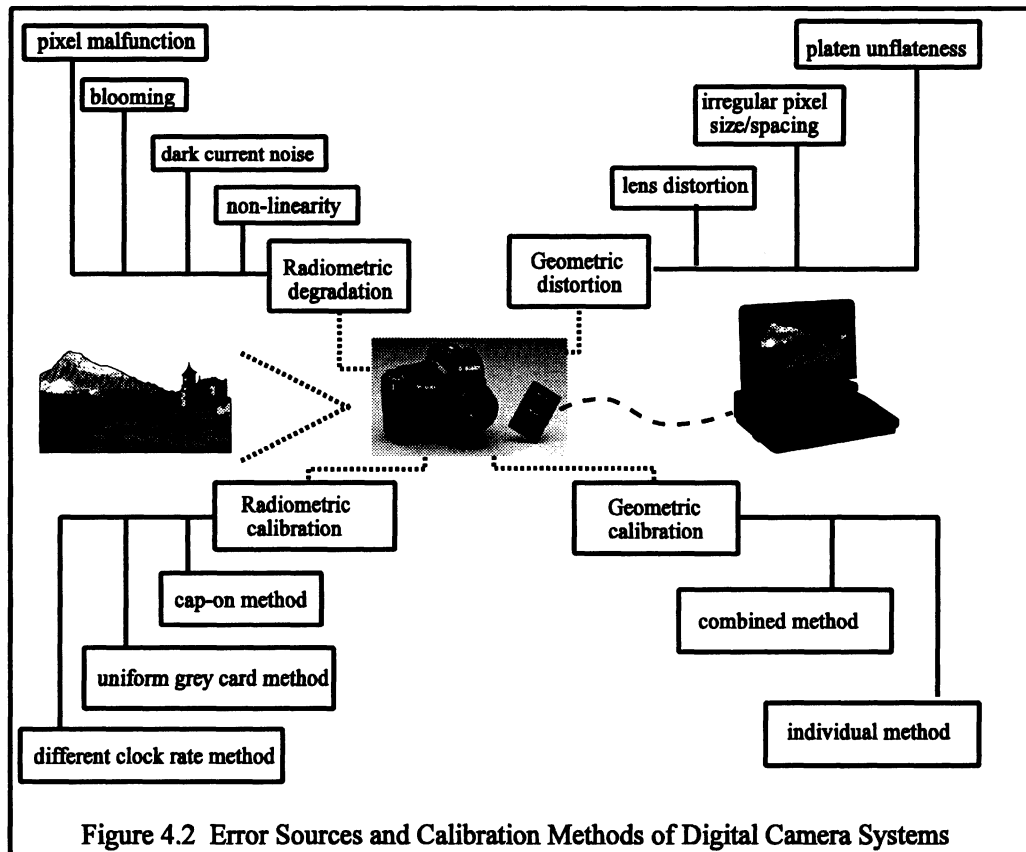
The function of all elements in the sensor and the sensor response linearity can be evaluated by using a uniform grey page and a grey step card, respectively. The precisely known grey value of the uniform page and intensity steps of the grey card serve as appropriate calibration references. The malfunction effect can be easily detected from the recorded abnormal grey values of the uniform grey page, and the corresponding pixels are discarded during subsequent image processing. On the other hand, from the taken image of the grey step card, the average intensity of a small region (eg. 3 x 3 pixels) in the centre of each density step is determined. The resulting average intensity plot thus shows the sensor linearity.

4.4.3 Different Clock Rate Method

Different pixel clock rates are used during the image taking for the same reference object. This approach can evaluate the level of certain random image noises, such as variation during A/D conversion, electron leakage etc. After comparing the recorded digital images for different clock rates, the effect of random noise can be checked. The best clock rate is determined and adopted for the subsequent applications in order to minimize the random influences. While this method was used for the radiometric calibration for standard CCD cameras (Curry et al., 1986), it is rarely applied to calibrate low-resolution digital cameras, as the pixel clock rate is usually fixed.

It is worth noting that the above radiometric calibration strategies are all approximate. Due to the fact that digital imaging is quite a complicated process whereby the radiometric errors of digital camera systems are interlaced, it is difficult to study them individually. By repeating the calibration at certain periods under different imaging conditions, e.g. different

lighting, different temperatures, and different camera speeds, while taking digital images of the same scene, the calibration results would be more reasonable and reliable. Radiometric stability of the imaging system can also be demonstrated by using this method.



It can be seen from the above discussion that calibration is necessary for digital camera systems to be applied for metric purposes. A variety of calibration methods exist, differing in the mathematical models, devices, designs and emphasis. Figure 4.2 depicts these common methods used for digital camera calibration. Each approach determines and models certain characteristics of the camera systems and thus has its strengths and weaknesses. So far, no calibration can provide a complete picture of the system performance by its own. It is worth

noting that above discussion is mainly focussed on the digital cameras, as they are the core parts of the whole systems. Although not explicitly, adverse influences from other parts of the camera systems, such as image compression/decompression and displaying screen deformation are also accounted in the system calibration models. This is because that all the influences are reflected in the final images on which the calibration is based.

CHAPTER 5

CAMERA SYSTEM CALIBRATION WITH FINITE ELEMENT METHOD (FEM)

As discussed in the previous chapter, the currently used methods for geometric calibration of digital camera systems are based on the assumption of symmetry and are not designed for digital camera systems. Therefore, the characteristics of digital camera systems cannot be fully considered during the calibration process, especially on the camera sensor chip side. In this chapter, a modified finite element method (FEM), namely the multiple-frame finite element method (MFFEM) is presented and discussed from both theoretical and practical aspects. The effectiveness of systematic error modeling and compensation is studied from both the theoretical and practical aspects.

5.1 Introduction

The effectiveness of any camera system calibration largely depends on the modeling and compensation of the systematic errors of the systems and the imaging process. Various systematic errors are modeled as perturbation to the image coordinates which are taken into consideration in the extended photogrammetric projection equations. All of the analytical calibration methods discussed so far have a common assumption of validity of the adopted mathematical models throughout the whole image space, independent of the type of the models (physical, algebraic or hybrid). Thus, the closeness of the assumption to reality dictates the calibration accuracy that can be achieved by using such kinds of calibration models. On the other hand, local image deformation such as sensor unflatness and other

irregular image distortion cannot be effectively modeled by such methods. A logical extension of this theory is to divide the image plane domain into sub-domains or finite elements and then to model the systematic errors over the image domain in a piecewise fashion, element by element, thereby eliminating the assumption of symmetry (Munja, 1986a, b) and also raising the possibility to better model local image deformations such as sensor unflatness, non-symmetric deformation, etc. This serves as the general principle underlying camera system calibration by the FEM.

5.2 General Nature of the Finite Element Method (FEM)

The FEM emerged in 1950's as a quick and accurate numerical solution of large and complex structural analysis inspired by the availability of high-speed digital computers. It has gained increasing importance almost everywhere in engineering and related areas. Nowadays, the FEM is predominately used to perform computer-based analyses of static, dynamic or thermal behavior of physical systems, structures and components, from the human body to the wings of an airplane (Baran, 1988).

5.2.1 Definition and Characteristics of the FEM

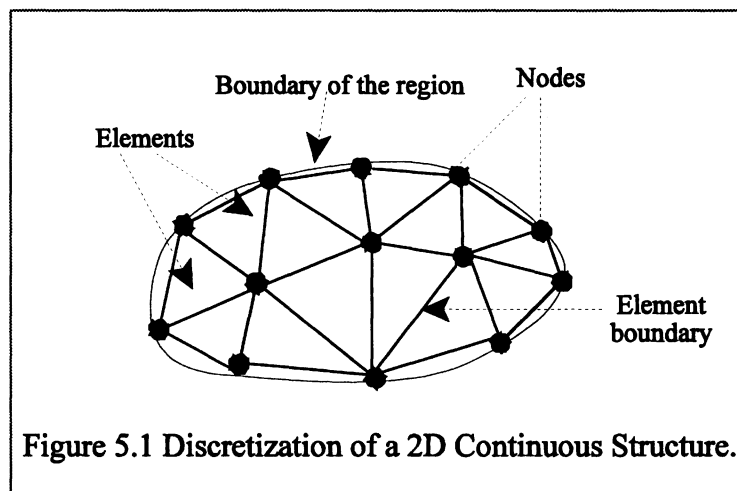
The FEM can be generally defined as a group of numerical methods of analyzing a structural system represented as an assemblage of a finite number of discrete elements interconnected by a series of nodal points. The favorable characteristics of the FEM are summarized by Ural (1973) as:

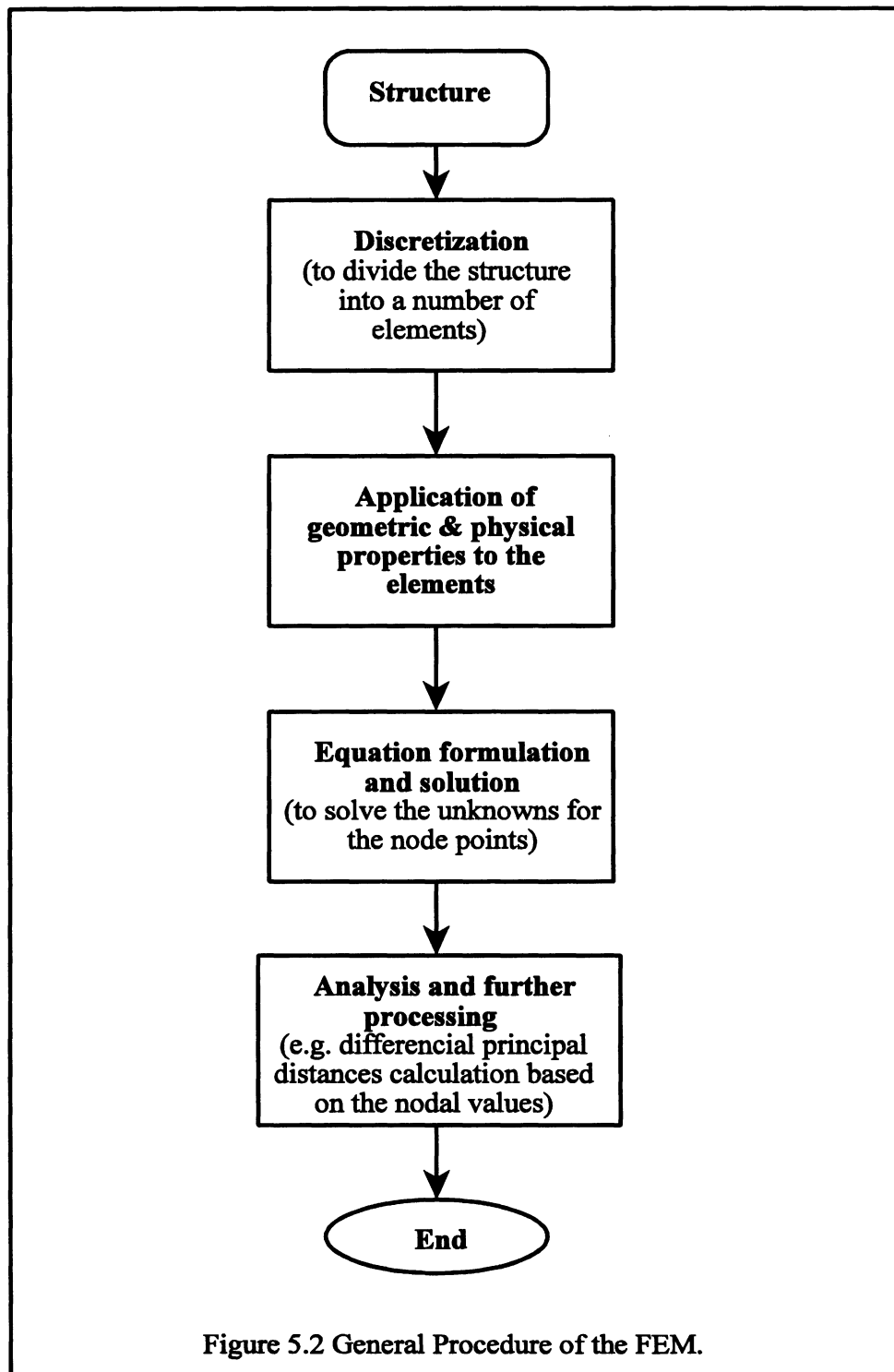
- the idealization of continuous complex geometric forms by a set of interconnected finite

- elements with known behavioral characteristics;
- the analysis of the elements instead of a complete structural system;
- the simplicity in superimposing the element solutions to develop the total results of the system;
- the adaptability of matrix formulation to the digital computers; and
- the generality of the approach for applications to the engineering field beyond structural analysis.

5.2.2 Main Idea and Procedure of the FEM

The basic idea behind the FEM is to divide the structure into a mesh of discrete elements (see Figure 5.1) and to create equations for each element to express its behavior in order to approximate the behavior of the whole structure. Therefore, the general procedures of the FEM include the discretization of the structure, property application to each element, equation formulation and solution, analysis, and further processing. Figure 5.2 depicts the steps involved in a typical FEM.





5.2.3 Mathematical Expression of the FEM

The final objective of the FEM is to find a function f which minimizes a given expression. The minimizing property leads to a differential equation for f (the Euler equation), where an exact solution is impossible due to the complexity of the problem. Therefore, a certain approximation is imperative. A trial solution is achieved by a solution f_m of linear form (Strang and Fix, 1973):

$$f_m = \sum_{r=1}^M c_r \phi_r \quad (5.1)$$

where ϕ_r are selected linearly independent functions existing over the domain of the structure and its boundary and, c_r are unknowns to be estimated by a system of M discrete algebraic equations which the digital computer can handle rather than by a differential equation. Unlike in the Rayleigh-Ritz method, where the function f is given by an expression valid throughout the whole domain thus leading to simultaneous equations in which no banding occurs and a fully occupied coefficient matrix (Munjy, 1986a), the FEM works in piecewise fashion. An individual function f is defined for each element such that the nodal parameters influence only adjacent elements and, thus, a sparse and usually banded matrix of coefficients is found (Zienkiewicz, 1989). With the different form of trial functions, different physical phenomena can be modeled. For camera system calibration applications, above trial functions f are described by shape functions that will be defined in the following sections.

5.2.4 Finite Elements and Shape Functions

The accuracy and effectiveness of the FEM will usually depend on the type and number of elements used in the mesh generation (Ural, 1973). The decision on the types of the

elements to be selected is influenced by the geometry and nature of the structure. Theoretically, any geometric shape can be adopted for this purpose. Some mainframe computer finite element programs have sixty or more element types in their element library (Baran, 1988). Due to mathematical and practical constraints, only a few basic types are frequently used by most structural analyses. Table 5.1 lists the commonly used element types for different dimensional problems. As mentioned in the next section, the photogrammetric applications of the FEM are usually 2D problems, therefore, the triangular and rectangular elements are discussed in more detail due to their wide acceptance in FEM applications.

Table 5.1 Basic Types of Finite Elements.

Element Type	Element shape
One-dimensional beam element	linear or curved line element
Two-dimensional plate element	triangle, quadrilateral
Three-dimensional solid element	tetrahedra, hexahedral, rectangular prism

After the division of the structure into a mesh of finite elements, the FEM requires the assumption of a general trial function or shape function as a function of the unknown nodal values, e.g. nodal displacements. For camera system calibration purposes, a shape function is the mathematical model describing the behavior of an entity or structure subjected to a phenomenon such as plate bending under stress or point displacement due to imaging distortions (Lichti, 1996). A shape function can be expressed in various simple forms, such as polynomials and trigonometric functions. Generally speaking, in any acceptable numerical formulation, the approximate solution must converge to the final solution. For the FEM applications, the solution for the whole structure should tend towards the true solution as the

element size decreases. In order to achieve this goal, the shape function selected for each element must meet the following three conditions (Desai and Abel, 1972):

- must be continuous within the element, and the modeled behavior must be compatible between the adjacent elements;
- must include the rigid body displacement of the element;
- must include the constant strain state of the element.

A polynomial is the most common form of shape function due to two reasons: first, the mathematics of polynomials are easy to handle when formulating the desired equations for various elements in performing digital computation; secondly, a polynomial of arbitrary order permits a recognizable approximation to the truth. The general polynomial form of a 2D shape function is:

$$f(x,y) = a_1 + a_2x + a_3y + a_4x^2 + a_5xy + a_6y^2 + \dots + a_my^n \quad (5.2)$$

where

$$m = \sum_{i=1}^{n+1} i \quad (5.3)$$

By truncating the above infinite polynomial at a specific order, we can vary the degree of the approximation according to the element type and the image distortion pattern.

5.2.4.1 Triangular Elements

Triangular elements are the most basic and simplest type in the 2D domain because of their capability of defining boundaries with relative ease, and the comparatively simple shape function. A triangular element as shown in Figure 5.3 has three nodes, and each node has two DOF (degree of freedom). Most frequently, the linear function

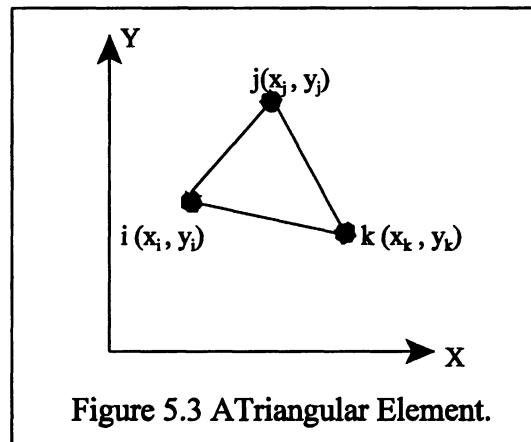
$$f(x,y) = a_1 + a_2x + a_3y \quad (5.4)$$

is used as the shape function for triangular elements, which is linear inside the element and

continuous across each edge. Equation (5.4) can also be written as:

$$f(x,y) = l_1f_i + l_2f_j + l_3f_k \quad (5.5)$$

where f_i, f_j and f_k are functional values (i.e. principal distances for camera system calibration) at the nodal points; l_1, l_2 and l_3 are nodal position $(x, y)_i$ related coefficients.



If necessary, higher order shape functions (e.g. Equation (5.6)) than the above linear function can also be used to describe the behavior of the triangular element more accurately. However, more nodal points are required to evaluate the unknown coefficients of the functions. For example, a shape function of :

$$f(x,y) = a_1 + a_2x + a_3y + a_4x^2 + a_5xy + a_6y^2 \quad (5.6)$$

requires three more nodes than those indicated in Figure 5.3. The additional nodes can be selected at the midpoint of each side of the triangle.

5.2.4.2 Rectangular Elements

As depicted in Figure 5.4, a rectangular element has four nodes and, thus, eight DOF.

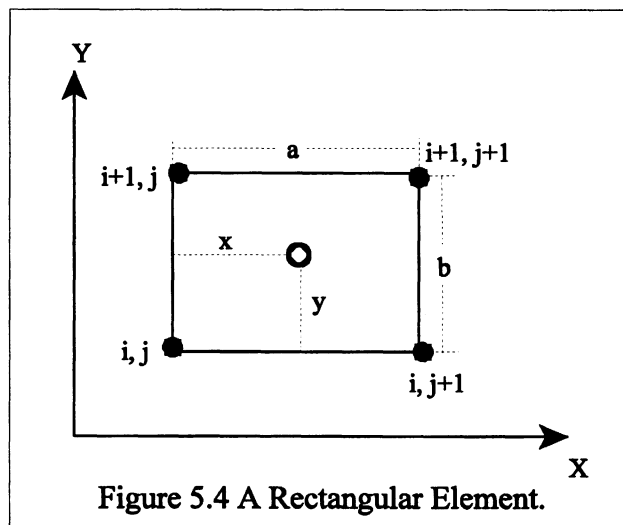
While triangular elements are better at approximating a curved boundary, rectangular elements have advantages in the interior as there are fewer of them and higher order functions can be easily used (Strang and Fix, 1973). As linear functions for rectangular elements will be discontinuous across the boundaries, the simplest shape function is a piecewise bi-linear function:

$$f(x,y) = a_1 + a_2x + a_3y + a_4xy \quad (5.7)$$

which guarantees the continuity along the boundaries of the elements. If written in terms of nodal values of the function, Equation (5.7) takes the following form:

$$f(x,y) = \begin{bmatrix} 1 - \frac{y}{b} & \frac{y}{b} \end{bmatrix} \begin{bmatrix} f_{i,j} & f_{i+1,j} \\ f_{i,j+1} & f_{i+1,j+1} \end{bmatrix} \begin{bmatrix} 1 - \frac{x}{a} \\ \frac{x}{a} \end{bmatrix} \quad (5.8)$$

where a and b are the size of the grid in the x and y directions (see Figure 5.4), respectively; and x and y are the local coordinates with origin at point (i, j) .



It can be seen that both the linear and bilinear polynomials satisfy the three conditions listed above to guarantee the solution convergence, which is due to the inclusion of the constant and linear terms in the polynomials. Similar to the triangular element method, higher order polynomials such as bi-cubic or bi-quadratic polynomials can also be used as shape functions for the rectangular method if necessary.

5.3 Camera System Calibration with the FEM

Although the FEM was originally developed for structural analysis which is still the major application, the general nature of the methods has also raised the possibility for successful applications in other fields of engineering. Therefore, it is not surprising that the FEM has also found some applications in geomatics, e.g. digital terrain model (Ebner et al., 1980), deformation monitoring and analysis (Szostak-Chrzanowski, 1988; Li, 1990), and camera calibration (Munjy, 1982, 1986a, b; Lichti, 1996; Lichti and Chapman 1995, 1997). The utilization of the FEM for camera system calibration was proposed by Munjy (1982) in his Ph.D. dissertation. In addition to Munjy's primary publications, the author is aware of only several other reported publications (Lichti, 1996; Lichti and Chapman, 1995, 1997) on this topic, which indicates that this topic has not been widely treated for camera system calibration. The limited applications of FEM for camera system calibration are probably due to the relatively extensive calculation and insignificant accuracy improvement over the traditional methods. Although Munjy (1982) claimed that better results were achieved with the FEM, Lichti (1996), Lichti and Chapman (1995) stated no obvious accuracy improvement by using this method, but rather consider it an alternative method to other

analytical calibration methods. Nevertheless, the advent of digital camera systems creates interest in the FEM topic, mainly due to the small format of the imaging sensor and the out-of-plane deformations not modeled by other analytical methods.

5.3.1 Basic Principle of the FEM Camera System Calibration

Any application of the FEM is an attempt to obtain information about the 'whole' by understanding its 'parts'(Desai and Abel, 1972). Thus, application of the FEM for camera system calibration is based on its general nature known as 'going from parts to whole'. In more detail, an image is divided into a number of elements, and image deformation caused by various systematic errors of the camera system and imaging process is analyzed and modeled by a piecewise fashion. The backbone of the FEM camera system calibration is the fact that the image deformation occurring at a certain image point is equivalent to a proportional change of the principal distance at that location. In other words, image deformation can be compensated for by adaptation of appropriate principal distances. This idea is shown in Figures 5.5 to 5.7 where the two main categories of image deformation, namely those caused by radial lens distortion (Figure 5.5) and sensor plane unflatness (Figure 5.6) are modeled by the proportional change of principal distances. Figure 5.7 illustrates the combined effect of these two cases. In these figures, image displacements dr or dr' caused by lens distortion or/and sensor plane unflatness can be modeled by the equivalent variation of the principal distance Δc in order for the distorted image point a' to be corrected to its theoretical position a'' .

Essentially, the idea of projection compensation of image deformation is not new in

photogrammetry. For example, radial distortion compensation was achieved for some plotters by changing the principal distance (Wolf, 1974). Furthermore, this has been used in the process of differential rectification where relief displacements are corrected by adopting different projection distances according to the terrain heights set up by a Digital Terrain Model (DTM). However, application of projection compensation for the camera system calibration was proposed by Munjy (1982) and not much research was found after the primary investigation. The essence of the application of the FEM to camera system calibration is a surface-modeling problem based on a certain number of data points. The domain is the 2D image area and the surface is spanned over the domain with the differential principal distances (DPDs) being the range. Any point on the surface is located by its 3D Cartesian coordinates $(x, y, c)_j$, where the x_j and y_j are the image coordinates and c_j the DPD of the image point j . Therefore, the traditional analytical camera system calibration can be considered as a special case where the surface is modeled as a plane parallel to the image plane and only one uniform principal distance is used for the whole domain. On the other hand, for the FEM counterpart, the surface is modeled as an assembly of a number of patches with each patch being described by local shape functions. It can be seen that the key to the successful application of the FEM to camera system calibration lies in accurate surface modeling, because the image deformation information is modeled by the DPDs that are derived from the modeled surface. Therefore, the following issues have to be dealt with in the FEM camera system calibration:

- discretization of the image domain into a series of elements, where different numbers and types of elements can be adopted depending on the accuracy requirements and the image deformation pattern;

- data point selection, where a certain number of control points can be used for this purpose;
- surface modeling in a piecewise manner using different shape functions;

To implement the FEM to camera system calibration, the original functional models discussed in Chapter 4 have to be further expanded to accommodate the DPDs. The following modified collinearity equations can be written for this purpose:

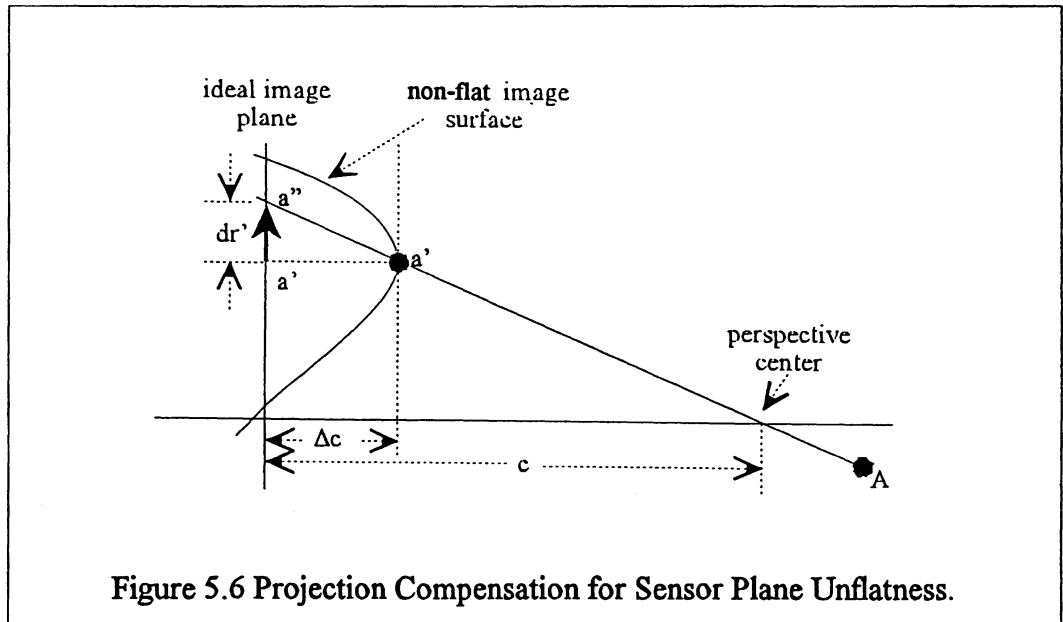
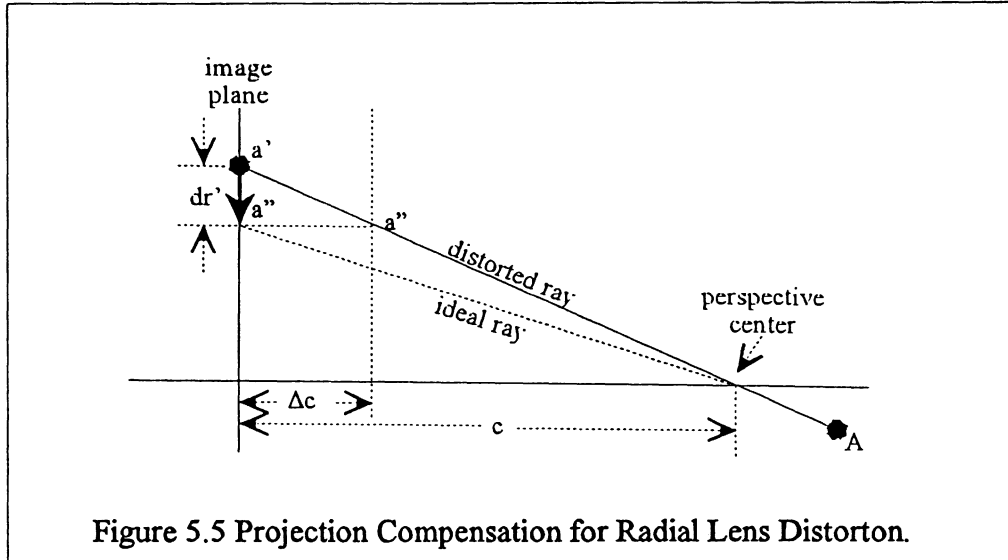
$$\begin{aligned} x_{ij} - x_{oi} &= -c_{ij} \frac{m_{11}(X_j - X_i^c) + m_{12}(Y_j - Y_i^c) + m_{13}(Z_j - Z_i^c)}{m_{31}(X_j - X_i^c) + m_{32}(Y_j - Y_i^c) + m_{33}(Z_j - Z_i^c)} \\ y_{ij} - y_{oi} &= -c_{ij} \frac{m_{21}(X_j - X_i^c) + m_{22}(Y_j - Y_i^c) + m_{23}(Z_j - Z_i^c)}{m_{31}(X_j - X_i^c) + m_{32}(Y_j - Y_i^c) + m_{33}(Z_j - Z_i^c)} \end{aligned} \quad (5.9)$$

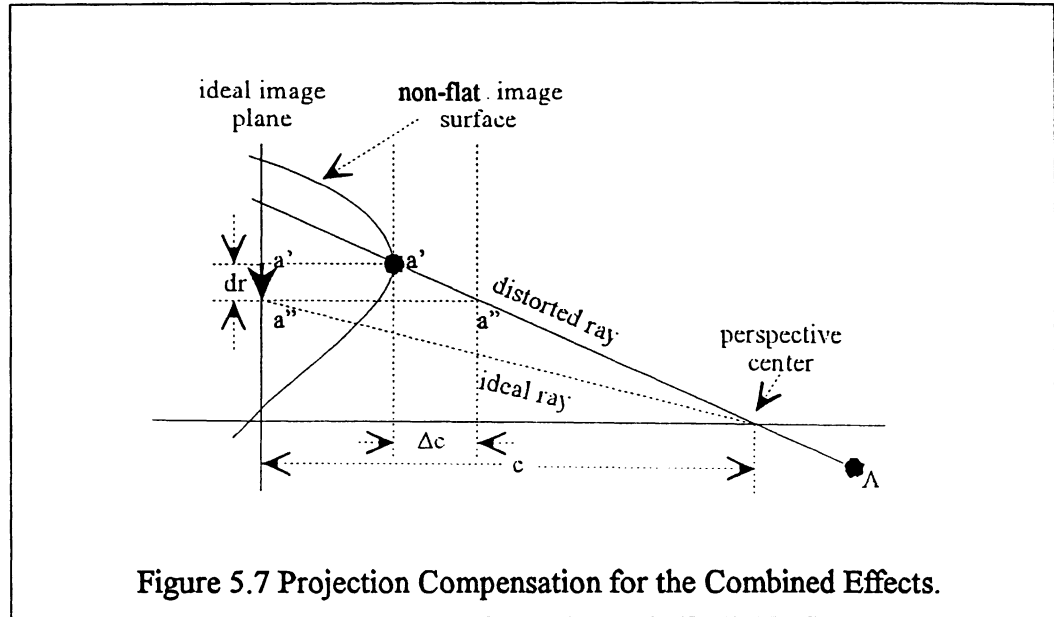
where x_{ij} and y_{ij} are observed image coordinates of point j on the i^{th} image; c_{ij} refers to the DPD at the j^{th} point of the i^{th} image; x_{oi} and y_{oi} are image coordinates of the principal point on the i^{th} image; X_j, Y_j and Z_j are object space coordinates of the point j ; X_i^c, Y_i^c and Z_i^c denote object space coordinates of the perspective center of the i^{th} image, m_{11} to m_{33} denote elements of the rotation matrix M_i of the i^{th} image with respect to object space, and M_i is expressed as:

$$M_i = \begin{bmatrix} m_{11} & m_{12} & m_{13} \\ m_{21} & m_{22} & m_{23} \\ m_{31} & m_{32} & m_{33} \end{bmatrix} \quad (5.10)$$

where

$$\begin{aligned} m_{11} &= \cos\varphi\cos\kappa, & m_{12} &= \sin\omega\sin\varphi\cos\kappa + \cos\omega\sin\kappa, \\ m_{13} &= -\cos\omega\sin\varphi\cos\kappa + \sin\omega\sin\kappa, & m_{21} &= -\cos\varphi\sin\kappa, \\ m_{22} &= -\sin\omega\sin\varphi\sin\kappa + \cos\omega\cos\kappa, & m_{23} &= \cos\omega\sin\varphi\sin\kappa + \sin\omega\cos\kappa, \\ m_{31} &= \sin\varphi, & m_{32} &= -\sin\omega\cos\varphi, \\ m_{33} &= \cos\omega\cos\varphi. \end{aligned} \quad (5.11)$$





5.3.2 Multiple-Frame Finite Element Method (MFFEM)

The application of the FEM to camera system calibration discussed by Munjy (1982) is mainly based on the single frame case. The MFFEM presented in this dissertation is essentially a modified photogrammetric bundle adjustment where the differential principal distances (DPDs) are adopted in the functional models for the different image locations instead of one uniform principal distance c , or two DPDs c_x and c_y for the whole image area. These principal distances are subject to the least squares adjustment instead of the image coordinate observations during the adjustment, which means that the image coordinates will not be corrected for compensating for systematic errors, but only for random variations.

To facilitate this, the above functional model can be expressed for the most probable values of the measurements and the parameters involved as:

$$f(\hat{l}, \hat{u}, \hat{u}, \hat{u}) = 0 \quad (5.12)$$

where \hat{l} refers to the image coordinates; \hat{u} is the vector of the exterior orientation parameters $(X^c, Y^c, Z^c, \omega, \phi, \kappa)_i$, plus two interior orientation parameters $(x_o, y_o)_i$; \hat{u} is the vector of the differential principal distances c_{ij} ; \hat{u} is the vector of the object-space coordinates $(X, Y, Z)_j$. Due to the non-linearity of the model, a Taylor Series expansion is used for the linearization. Thus, equation (5.12) can be written as:

$$f(l + v, \dot{u}^o + \delta, \ddot{u}^o + \ddot{\delta}, \ddot{u}^o + \ddot{\delta}) = 0 \quad (5.13)$$

where l is the observation vector of image coordinates; v is the residual vector of image coordinates; $\dot{u}^o, \ddot{u}^o, \ddot{u}^o$ are initial values of the vectors \dot{u} , \ddot{u} and \ddot{u} ; $\delta, \ddot{\delta}, \ddot{\delta}$ are the correction vectors for \dot{u} , \ddot{u} and \ddot{u} .

After the linearization, we have:

$$v = \dot{B}\delta + \ddot{B}\ddot{\delta} + \ddot{B}\ddot{\delta} - e \quad (5.14)$$

where

$$\dot{B} = \frac{\partial f}{\partial \dot{u}} = \left[\frac{\partial f}{\partial X^c} \quad \frac{\partial f}{\partial Y^c} \quad \frac{\partial f}{\partial Z^c} \quad \frac{\partial f}{\partial \omega} \quad \frac{\partial f}{\partial \phi} \quad \frac{\partial f}{\partial \kappa} \quad \frac{\partial f}{\partial x_o} \quad \frac{\partial f}{\partial y_o} \right] \quad (5.15)$$

$$\ddot{B} = \left[\frac{\partial f}{\partial c} \right] \quad (5.16)$$

$$\ddot{B} = \left[\frac{\partial f}{\partial X} \quad \frac{\partial f}{\partial Y} \quad \frac{\partial f}{\partial Z} \right] \quad (5.17)$$

$$e = l - f(\dot{u}^o, \ddot{u}^o, \ddot{u}^o) \quad (5.18)$$

Therefore, the design matrices \dot{B} , \ddot{B} , \ddot{B} are composed of partial derivatives, which are derived in full detail in Appendix IV. Generally, equation (5.14) can be expressed as :

$$v=B\delta-e \quad (5.19)$$

where

$$B=[\dot{B} \quad \ddot{B} \quad \ddot{\ddot{B}}] \quad (5.20)$$

and

$$\delta = [\dot{\delta} \quad \ddot{\delta} \quad \ddot{\ddot{\delta}}]^T \quad (5.21)$$

In order to find the most probable values of the above equations, the least squares principle is applied, which results in the following normal equations:

$$Nd=K \quad (5.22)$$

where

$$N=B^T P B \quad (5.23)$$

and

$$K=B^T P e \quad (5.24)$$

P is the weight matrix of the observations. Under most of the cases when image coordinates are the only type of observations included in the adjustment process, P becomes a unity matrix due to the fact that image coordinates can be considered as independent observations with equal precision. Solution of the normal equations (5.22) leads to estimated corrections of the unknowns. Since higher order terms are neglected during the linearization, iteration is usually necessary to obtain precise results. The number of iterations is dependent upon the degree of closeness between the initial values and the resulting values of the parameters, and also the photogrammetric network configuration.

Without losing generality, let us suppose that there are m images in the photogrammetric network, and n object points appear on each image. Table 5.2 lists the number of the observations and unknowns, the dimensions of the matrices, and vectors involved.

Table 5.2 Number of the Unknowns, Dimensions of Matrices, and Vectors of the MFFEM.

Number of images	m
Number of points	n
Number of observations	2mn (2 for each imaged point, assuming all points are seen all images)
Number of unknowns	8m (6 exterior orientation parameters + 2 interior orientation parameters for each image) + mn (1 principal distance for each imaged point) + 3n (3 object space coordinates for each object point)
Degrees of freedom	2mn - 8m - mn - 3n
Dimensions of the \dot{B} matrix	Row: 2mn, Column: 8m
Dimensions of the \ddot{B} matrix	Row: 2mn, Column: mn
Dimensions of the $\ddot{\ddot{B}}$ matrix	Row: 2mn, Column: 3n
Dimensions of the B matrix	Row: 2mn, Column: 8m + mn + 3n
Dimensions of the N matrix	Row: 8m + mn + 3n, Column: 8m + mn + 3n
Dimensions of the l, v, e vectors	Row: 2mn, Column: 1
Dimensions of the K, δ vectors	Row: 8m + mn + 3n, Column: 1

5.3.3 Simplified MFFEM

Most often, the above general MFFEM is simplified to a two-step process, i.e., resection and intersection, for the sake of computation. In this case, single or multiple frame resection is carried out to determine the orientation parameters (exterior orientation parameters plus basic interior orientation parameters) and the DPDs based on a certain number of control points. Therefore, Equation (5.14) is simplified to:

$$v = \dot{B}\delta + \ddot{B}\ddot{\delta} - e_1 \quad (5.25)$$

After the resection, intersection is conducted to compute the object-space coordinates based on the determined quantities by using equation:

$$v = \ddot{B} \ddot{\delta} - e_2 \quad (5.26)$$

With the adaptation of the DPDs, the final results should be largely free of image deformation. It can be seen, that the simplified two step procedure is quite similar to the traditional resection and intersection approach. However, they differ in the determination and utilization of the principal distances. In the traditional method, one principal distance is used for one image, and the image deformations are compensated for by using the image refinement process or additional parameters. In the FEM, DPDs are determined for each image point which eliminates the additional image correction process.

5.4 Empirical Studies of the FEM by a Modeled Case

The basic principle and related issues of the application of the FEM to camera system calibration were briefly discussed in previous sections. Due to reasons mentioned before, this method has not been widely used for camera system calibration for systematic errors of camera systems. As a result, there are many areas which are worthy of further research for the FEM for camera system calibration. The following items have not been fully investigated in Munji's primary research (Munji, 1982, 1986a and 1986b):

- investigation of the recovering capability of different types of image deformation (radial lens distortion, decentering lens distortion, sensor plane unflatness);
- detailed comparison of triangular elements versus rectangular elements;
- influence of the precision of the image coordinate measurements;

- influence of the photogrammetric configuration upon the FEM;
- application of higher order shape functions.

This section is designed for answering the above questions by an empirical investigation of the application of the FEM to camera system calibration through a series of tests based on the simulation of a multi-station convergent photogrammetric configuration.

5.4.1 Main Idea of the Studies

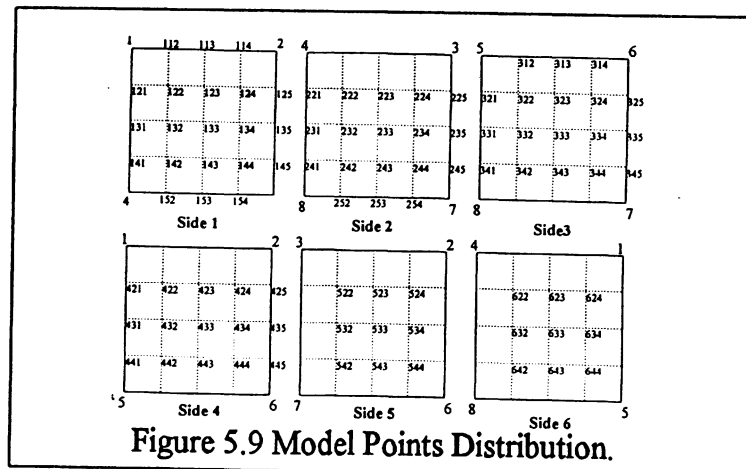
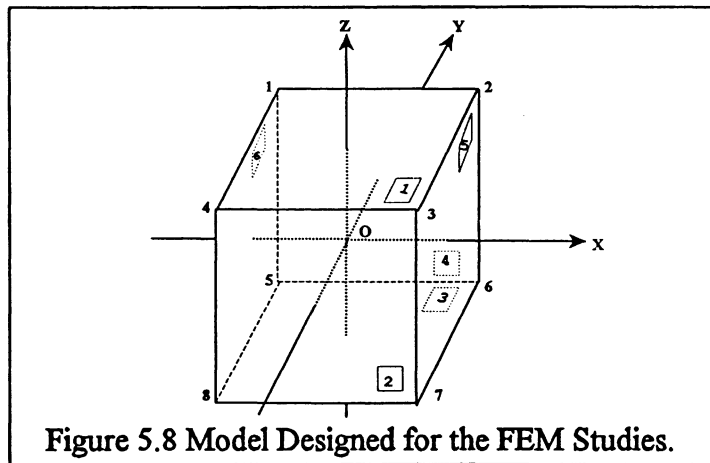
One of the best ways of investigating the efforts of the FEM for camera system calibration is to compare the results of the FEM with true or accurately known values. As these values are difficult to obtain in a practical situation, an alternative way is simulation by using a model and fictitious cameras with known properties. Followings are the details of the main idea of the project:

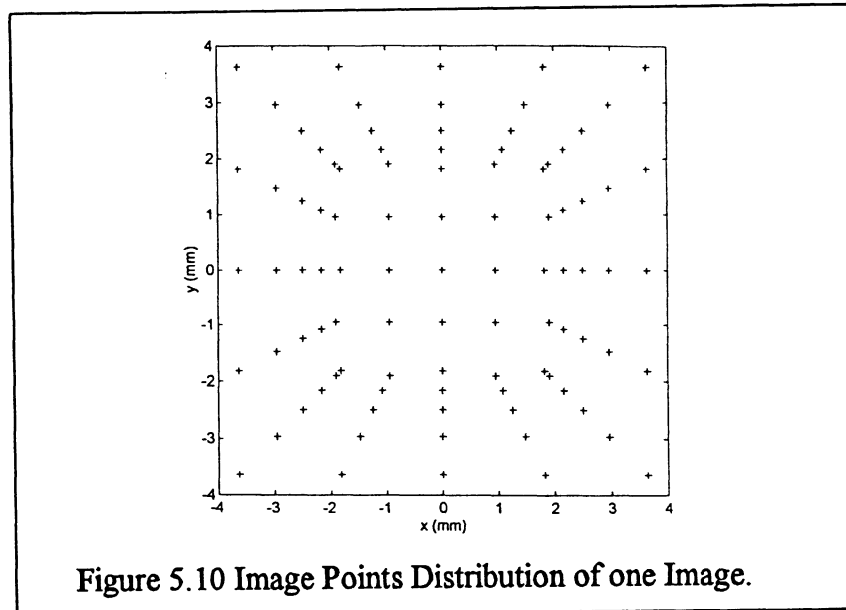
- a model is designed with proper dimensions;
- a photogrammetric configuration composed of a fictitious camera is deployed around the model, in which the locations and attitudes of the cameras are theoretically known;
- image coordinates are obtained by using projection from 3D object space to 2D image space based on the known camera data;
- different image deformation information and different levels of random errors are added to the above image coordinates to investigate the FEM under different considerations.

5.4.2 Model Design

Objects in industrial and engineering environments are mostly 3D types. Considering

this, a transparent cube with the dimension of 1 meter for each edge is designed for the studies (see Figure 5.8). 98 points uniformly distributed on each of the six sides of the cube (Figure 5.9) are used as the control or check points in the photogrammetric data processing. Their relative positions are known from the uniform distribution and the specified cube dimensions. The nature of transparency makes it possible that all the object points can be imaged by the appropriately located cameras. Figure 5.10 presents the image points' distribution taken from one of the camera stations.





5.4.3 Fictitious Camera and Photogrammetric Configuration

As the main topic of this dissertation is about low-resolution digital camera systems, a fictitious camera is designed with the following characteristics of a common digital camera:

- 8 mm nominal focal length;
- 6 mm by 5 mm image format;
- 60 μm maximum radial lens distortion ($k_1 = 7 \times 10^{-3}$, $k_2 = 5 \times 10^{-5}$);
- 10 μm maximum decentering lens distortion ($p_1 = 8 \times 10^{-2}$, $p_2 = 4 \times 10^{-2}$);
- 25 μm maximum random sensor plane unflatness.

Figures 5.11 to 5.13 are the surfaces and DPD contour lines modeled based on the above radial-, and decentering lens distortion, as well as sensor plane unflatness, respectively.

Multi-station convergent imaging configuration is widely used in non-topographic photogrammetric applications as it provides good network strength, more redundancy,

and uniform 3D object coordinate precision. A five-station, convergent imaging configuration is deployed around the model (Figure 5.14). If the center of the model is selected as the origin of the reference object-space coordinates, the camera stations have the following exterior orientation parameters:

Table 5.3 Exterior Orientation Parameters of the Five Camera Stations.

Camera station	Xs (m)	Ys (m)	Zs (m)	ω (°)	ϕ (°)	κ (°)	Camera-to-object distance (m)	Image scale
1	0	-1.60	0	90	0	0	1.60	1:200
2	-1.13	-1.13	0	90	-45	0	1.60	1:200
3	1.13	-1.13	0	90	45	0	1.60	1:200
4	0	-1.13	1.13	45	0	0	1.60	1:200
5	0	-1.13	-1.13	135	0	0	1.60	1:200

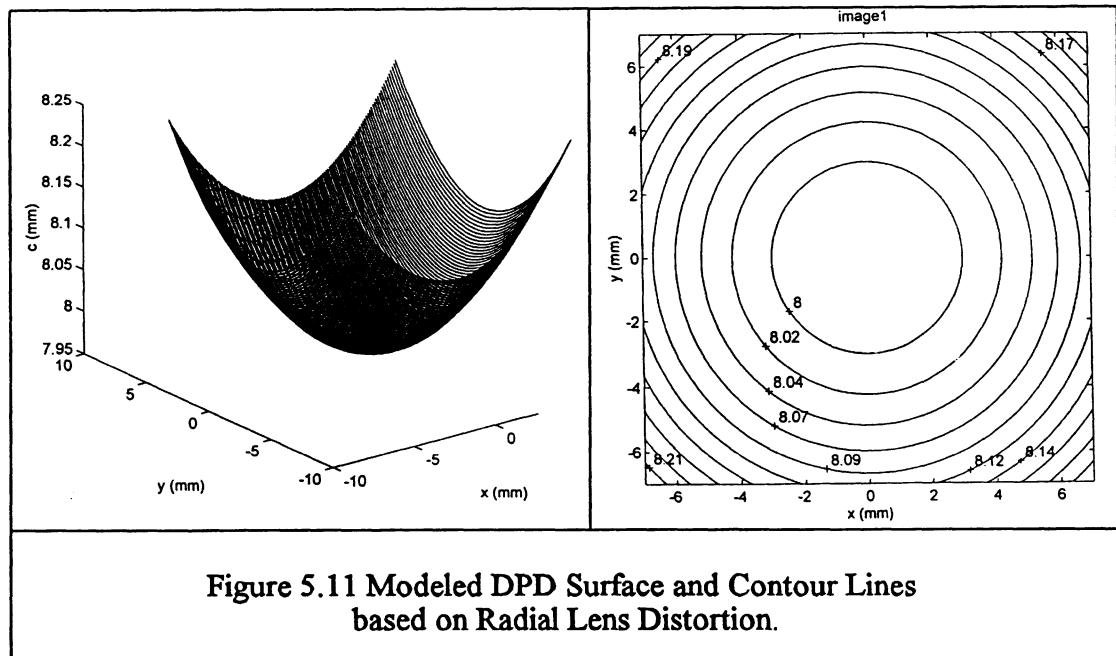


Figure 5.11 Modeled DPD Surface and Contour Lines based on Radial Lens Distortion.

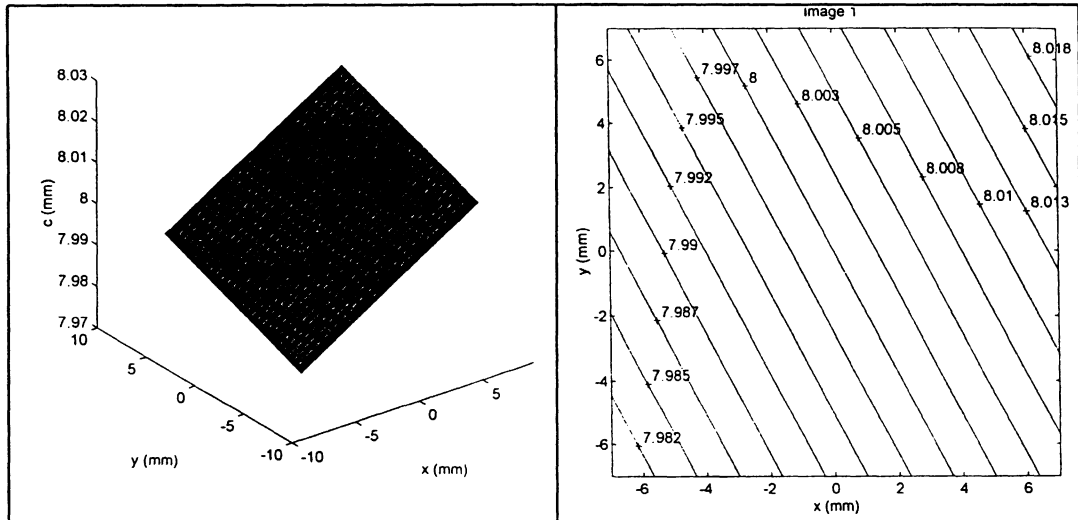


Figure 5.12 Modeled DPD Surface and Contour Lines based on Decentering Lens Distortion.

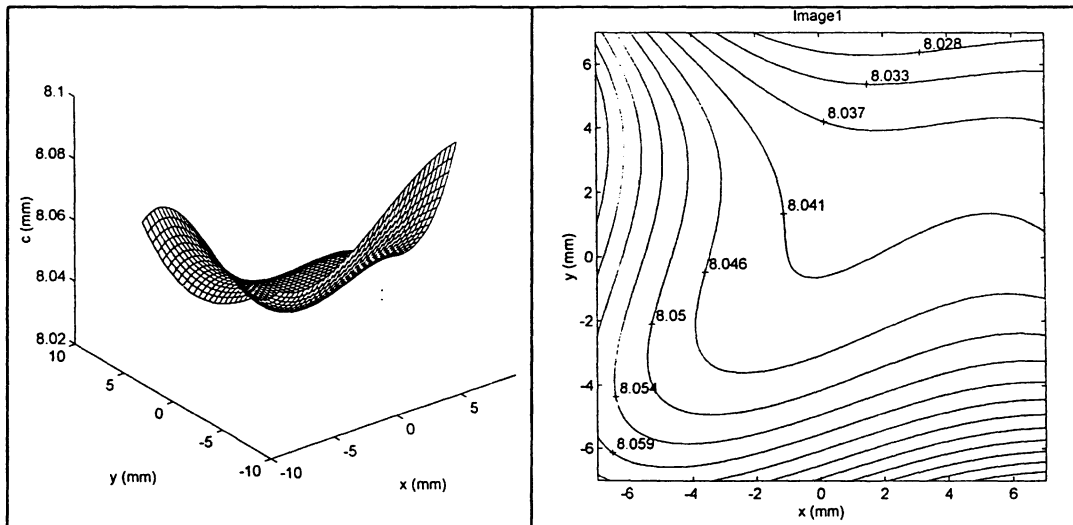
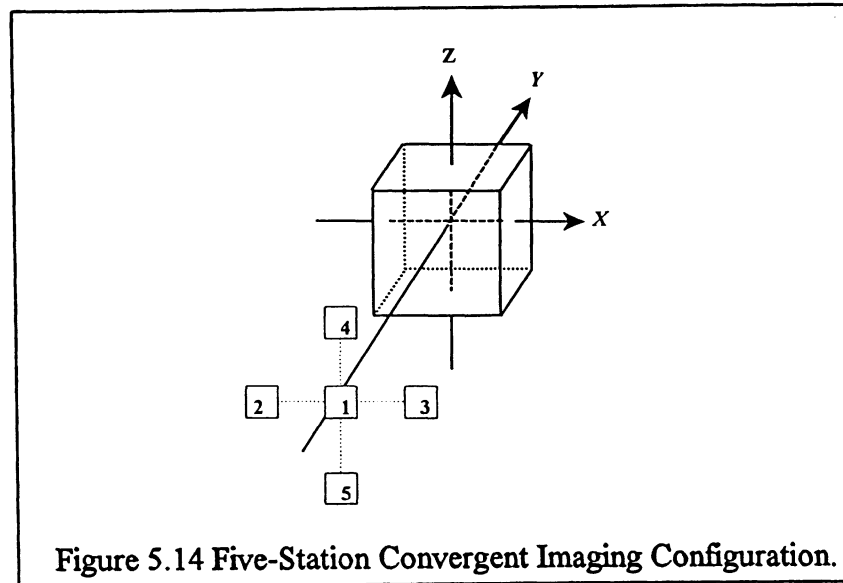


Figure 5.13 Modeled DPD Surface and Contour Lines based on Sensor Plane Unflatness.



5.4.4 Data Processing Schemes

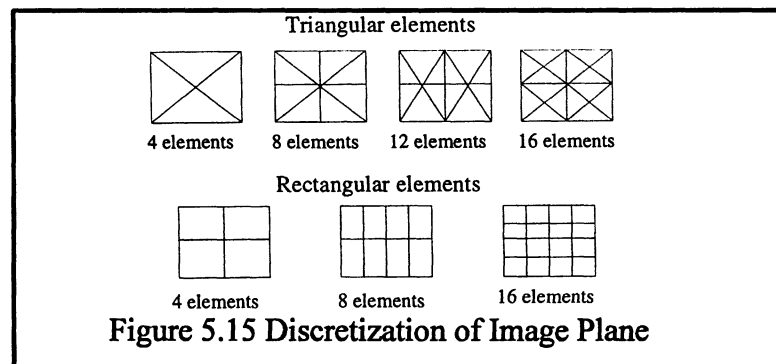
As all the modeled image deformations and imaging configuration data are known, many studies can be carried out about the application of the FEM to camera system calibration by comparing the results with the known facts. To effectively evaluate the performance of the FEM, the data processing schemes were designed for investigating the:

- effect of compensating for radial lens distortion alone;
- effect of compensating for decentering lens distortion alone;
- effect of compensating for sensor plane unflatness alone;
- effect of compensating for combined image perturbations;
- influence of different types of elements (triangular, rectangular), different numbers of elements (see Figure 5.15), different form of shape functions;
- performance of the FEM compared with other well-proven methods (e.g. self-calibrating bundle adjustment, DLT);
- influence of different levels of random errors of image coordinates;

For any comparison, certain standards have to be selected or established as the comparison criteria. As true values are available in the simulated case, the following indicators are used to evaluate the performances of the FEM under different situations:

- accuracy of the DPDs determined based on the differences between the interpolated values and the true values;
- standard deviation of unit weight for the adjustment based on the image coordinate residuals;
- mean object space precision calculated from the standard deviation and the cofactor matrix of the unknowns after the photogrammetric adjustment, which indicates the quality of the adjustment itself and the internal accuracy of the algorithm;
- mean object space accuracy computed from the discrepancies between the adjusted object space coordinates and the true values.

The last two indicators should be very close if the image deformations are successfully compensated for.



5.4.5 Results and Analysis

A software package **UNBDCSC (UNB Digital Camera System Calibration)** was developed by the author and used for data processing. **MATLAB**, a widely accepted computational language with user friendly graphics capabilities, was utilized for the programming. The package has the FEM function which can take different numbers,

different types of finite elements, as well as different shape functions. Results from the data processing based on the schemes designed in the previous section are tabulated in Tables 5.4 to 5.9. Analyses are carried based on the these tabulated results.

Table 5.4 Image Deformation Recovering Capability of the FEM.

	σ_o (μm)	Mean object-space precision (mm)	Mean object-space accuracy (mm)
Radial lens distortion	0.00	0.00	0.00
Decentering lens distortion	0.27	0.03	0.07
Sensor plane unflatness	0.00	0.00	0.00
Combined case	0.27	0.03	0.07

It can be seen from Table 5.4 that radial lens distortion can be completely modeled by DPD surface. Part of the decentering lens distortion (the radial components) can be compensated by using the DPDs, with the tangential part being left unmodeled; Influence of the sensor plane unflatness (uniform or non-uniform) can be completely modeled by the DPD if the mesh is fine enough to model irregular local sensor plane deformation. Above observations lead to the conclusion that the FEM camera system calibration can effectively but not totally compensate for all image deformation.

Table 5.5.1 Results of the FEM with Triangular Elements.

No. of elements	Data points required	DPD accuracy (μm)	Mean precision (mm)	Mean accuracy (mm)	CPU time (seconds)
4	5	21.6	0.26	1.07	502
8	9	12.0	0.16	0.54	412
12	13	9.8	0.17	0.38	405
16	17	8.7	0.15	0.33	410
High 4*	13	1.3	0.05	0.07	367

Note: High 4 – four elements with higher order shape functions than linear shape functions.

Table 5.5.2 Results of the FEM with Triangular Elements

(with 1 μm random errors in image coordinate observations).

No. of elements	Data points required	DPD accuracy (μm)	Mean precision (mm)	Mean accuracy (mm)	CPU time (seconds)
4	5	23.5	0.25	1.13	524
8	9	14.1	0.18	0.61	449
12	13	12.0	0.19	0.45	434
16	17	10.8	0.18	0.40	366
High 4	13	2.2	0.08	0.14	443

Table 5.5.3 Results of the FEM with Triangular Elements

(with 5 μm random errors in image coordinate observations).

No. of elements	Degree of freedom	DPD accuracy (μm)	Mean precision (mm)	Mean accuracy (mm)	CPU time (seconds)
4	5	32.5	0.35	1.42	492
8	9	24.3	0.33	0.95	436
12	13	22.5	0.34	0.80	470
16	17	21.6	0.33	0.75	468
High 4	13	8.5	0.23	0.44	337

Table 5.5.4 Results of the FEM with Triangular Elements

(with 10 μm random errors in image coordinate observations).

No. of elements	Data points required	DPD accuracy (μm)	Mean precision (mm)	Mean accuracy (mm)	CPU time (seconds)
4	5	45.9	0.58	1.87	508
8	9	38.9	0.58	1.43	511
12	13	37.2	0.59	1.28	510
16	17	36.6	0.58	1.24	318
High 4	13	16.9	0.44	0.81	527

Table 5.6.1 Results of the FEM with Rectangular Elements.

No. of elements	Data points required	DPD accuracy (μm)	Mean precision (mm)	Mean accuracy (mm)	CPU time (seconds)
4	9	10.0	0.14	0.47	344
8	15	4.4	0.06	0.19	407
16	25	2.2	0.05	0.12	406
High 4	21	1.4	0.04	0.07	406

**Table 5.6.2 Results of the FEM with Rectangular Elements
(with 1 μm random errors in image coordinate observations).**

No. of elements	Data points required	DPD accuracy (μm)	Mean precision (mm)	Mean accuracy (mm)	CPU time (seconds)
4	9	10.4	0.16	0.48	364
8	15	4.8	0.08	0.22	369
16	25	2.9	0.07	0.16	358
High 4	21	2.5	0.06	0.14	405

**Table 5.6.3 Results of the FEM with Rectangular Elements
(with 5 μm random errors in image coordinate observations).**

No. of elements	Data points required	DPD accuracy (μm)	Mean precision (mm)	Mean accuracy (mm)	CPU time (seconds)
4	9	14.0	0.26	0.64	541
8	15	10.7	0.22	0.46	323
16	25	9.8	0.22	0.44	409
High 4	21	10.0	0.25	0.43	238

**Table 5.6.4 Results of the FEM with Rectangular Elements
(with 10 μm random errors in image coordinate observations).**

No. of elements	Data points required	DPD accuracy (μm)	Mean precision (mm)	Mean accuracy (mm)	CPU time (seconds)
4	9	23.1	0.45	0.96	562
8	15	20.2	0.42	0.82	536
16	25	19.3	0.41	0.80	482
High 4	21	19.8	0.48	0.80	587

Results from Tables 5.5.1 to 5.6.4 show that all the quality indicators were improved with increased number of elements. Accuracy approaches precision when the mesh gets finer, which indicates that better effects of systematic error compensation can be achieved by using a finer mesh. However, this trend becomes less obvious when the level of the random errors contained in the image coordinate observations gets higher.

It is obvious that for the same number of the elements, the rectangular methods usually provided better results than the triangular methods. This is probably due to the more accurate surface modeling over the domain and more data points involved than for the triangular element.

For both the triangular and rectangular element methods, when the number of elements is kept the same, shape functions with higher order can greatly improve the FEM performance compared with the commonly used linear or the bilinear functions. In addition, when the image coordinate precision is not very high, application of higher order shape functions can effectively enhance the FEM performance. This is because the effect of increasing the fineness of the mesh is not very obvious. However, the shortcoming of adaptation of high order shape functions is the requirement of more nodal points which means more control points are needed.

In addition to the above studies around the FEM camera system calibration, influences of the imaging configuration upon the FEM application were also investigated. The performance of the FEM were also compared with two well-proven methods, i.e., self-calibrating bundle adjustment UNBASC2 and the DLT.

Table 5.7 Influence of Imaging Configuration upon the Mean Object Accuracy. (units: mm)

	Config. I				Config. II				Config. III				Config. IV				Config. V				Config. VI			
	σ	σ_y	σ_z	σ_m	σ_x	σ_y	σ_z	σ_m	σ_x	σ_y	σ_z	σ_m	σ_x	σ_y	σ_z	σ_m	σ_x	σ_y	σ_z	σ_m	σ_x	σ_y	σ_z	σ_m
4T	1.2	1.22	1.01	1.16	1.01	1.22	1.22	1.16	0.98	1.17	0.95	1.04	0.95	1.17	0.98	1.04	1.08	1.18	1.08	1.11	1.01	1.1	1.0	1.06
8T	0.6	0.58	0.60	0.59	0.61	0.58	0.59	0.59	0.52	0.56	0.55	0.54	0.57	0.55	0.51	0.54	0.58	0.54	0.57	0.56	0.55	0.5	0.5	0.54
12T	0.4	0.41	0.49	0.45	0.50	0.41	0.42	0.45	0.39	0.40	0.45	0.42	0.46	0.40	0.38	0.42	0.44	0.34	0.43	0.41	0.42	0.3	0.4	0.38
16T	0.3	0.35	0.41	0.38	0.42	0.35	0.37	0.38	0.34	0.35	0.38	0.36	0.40	0.36	0.34	0.37	0.37	0.29	0.36	0.34	0.35	0.2	0.3	0.33
H4T	0.0	0.04	0.13	0.09	0.08	0.08	0.09	0.09	0.11	0.07	0.07	0.09	0.08	0.08	0.09	0.09	0.08	0.05	0.07	0.07	0.09	0.0	0.0	0.07
4R	0.5	0.49	0.51	0.51	0.50	0.52	0.52	0.51	0.44	0.49	0.48	0.47	0.46	0.50	0.46	0.47	0.48	0.47	0.50	0.49	0.46	0.4	0.4	0.47
8R	0.2	0.18	0.21	0.21	0.21	0.19	0.22	0.21	0.21	0.18	0.21	0.20	0.20	0.19	0.22	0.21	0.21	0.18	0.21	0.20	0.20	0.1	0.2	0.20
16R	0.1	0.11	0.12	0.13	0.12	0.13	0.15	0.13	0.14	0.11	0.11	0.12	0.11	0.13	0.13	0.12	0.13	0.11	0.12	0.12	0.12	0.1	0.1	0.12
H4R	0.1	0.08	0.09	0.09	0.13	0.05	0.08	0.09	0.11	0.05	0.07	0.08	0.09	0.07	0.08	0.08	0.10	0.05	0.07	0.08	0.10	0.0	0.0	0.07

Notes:

1. Config. I: imaging configuration with two camera stations S2, S3;
2. Config. II: imaging configuration with two camera stations S4, S5;
3. Config. III: imaging configuration with three camera stations S1, S2, S3;
4. Config. IV: imaging configuration with three camera stations S1, S4, S5;
5. Config. V: imaging configuration with four camera stations S2, S3, S4, S5;
6. Config. VI: imaging configuration with all five camera stations S1, S2, S3, S4, S5;
7. 4T, 8T, 12T, 16T: four, eight, twelve and sixteen triangular elements with linear shape functions, respectively;
8. 4R, 8R, 16R: four, eight and sixteen rectangular elements with bilinear shape functions, respectively;
9. H4T, H4R: four triangular and four rectangular elements with higher order shape functions than above.

Table 5.8 Mean Object Space Accuracy of the DLT Method.

units: mm

	9 control points				14 control points				38 control points				full control			
	11P ¹	12P ²	14P ³	16P ⁴	11P	12P	14P	16P	11P	12P	14P	16P	11P	12P	14P	16P
Error free case ⁵	0.11	0.20	N/R ⁶	N/R	0.10	0.05	0.05	0.00	0.08	0.07	0.02	0.00	0.06	0.05	0.02	0.00
1 μm random errors ⁷	0.12	0.12	N/R	N/R	0.12	0.09	0.06	0.05	0.09	0.08	0.05	0.05	0.10	0.08	0.05	0.05
5 μm random errors ⁸	0.26	0.30	N/R	N/R	0.25	0.23	0.27	0.25	0.21	0.21	0.22	0.21	0.20	0.20	0.21	0.21
10 μm random errors ⁹	0.48	0.67	N/R	N/R	0.46	0.45	0.53	0.53	0.41	0.41	0.45	0.44	0.40	0.40	0.44	0.43
Notes:																
1. 11P: eleven DLT parameters, L_1 to L_{11} ;																
2. 12P: eleven DLT parameters plus one additional parameter (k_1) to model radial lens distortion;																
3. 14P: eleven DLT parameters plus three additional parameter (k_1, k_2, k_3) to model radial lens distortion;																
4. 16P: eleven DLT parameters plus three additional radial lens distortion parameter (k_1, k_2, k_3) and two decentring lens distortion parameters (p_1, p_2);																
5. No random errors were added to the modeled image coordinate observations;																
6. N/R: not reliable;																
7. 1 μm random errors were added to the modeled image coordinates observations;																
8. 5 μm random errors were added to the modeled image coordinates observations;																
9. 10 μm random errors were added to the modeled image coordinates observations;																

Table 5.9 Mean Object Space Accuracy of the UNBASC2 Method.

units: mm

	Less control					Full control				
	Case I ¹	Case II ²	Case III ³	Case IV ⁴	Case V ⁵	Case I	Case II	Case III	Case IV	Case V
Error free case	N/R	0.18	0.04	0.01	0.00	0.30	0.15	0.03	0.00	0.00
1 μ m random errors	0.38	0.19	0.06	0.04	0.04	0.38	0.16	0.06	0.04	0.04
5 μ m random errors	0.57	0.28	0.25	0.23	0.22	0.41	0.30	0.24	0.22	0.21
10 μ m random errors	N/R	0.49	0.42	0.42	0.45	0.53	0.47	0.43	0.43	0.42
<p>Notes:</p> <ol style="list-style-type: none"> 1. Case I: no additional parameters were included; 2. Case II: basic interior orientation parameters were considered; 3. Case III: radial distortion parameters were added as well; 4. Case IV: decentring distortion parameters were added too; 5. Case V: all additional parameters were included (above plus two affinity parameters) 										

Results from above three tables indicate that for certain imaging configurations, the finer the mesh, the better the results of the FEM. When the number, type of the elements and the shape function are the same, the stronger the configuration, the better the performance. This suggests that, as with other analytical calibration methods, the FEM methods are also influenced by the image configuration. When many control points are available, the FEM results do not show any advantages over the DLT and UNBASC2. However, with less control (e.g. less than 9 control points), the FEM calibration does have the better performance, because results of the other two methods are not reliable.

The FEM camera system calibration was discussed in this chapter. Certain useful conclusions are derived based on the studies. This method is exposed further in the Chapter 7 where the performances of three low-resolution digital camera systems are evaluated by FEM methods and the results are compared with other well-established methods.

CHAPTER 6

PHOTOGRAMMETRIC APPLICATIONS OF LOW-RESOLUTION DIGITAL CAMERA SYSTEMS

After many years' evolution, photogrammetry has proven itself to be a non-contact, accurate, reliable and productive measurement technology for a diversity of application areas. The advent of digital cameras has further strengthened this trend and broadened the application base of this technology. In this chapter, issues related to the photogrammetric applications of low-resolution digital camera systems are investigated in order to further study the feasibility of applying such camera systems for metric purposes, especially in industrial and engineering environments.

6.1 Introduction

As a special branch of photogrammetry, close-range photogrammetry has many operational advantages over other traditional close-range measurement tools. It has witnessed an enormous development and has found numerous applications in many measurement related areas. With the advances in computer- and digital technologies, close-range photogrammetry has evolved into a digital era. As a result, digital close-range photogrammetry, also known as videometrics or vision metrology (VM) within the photogrammetric and other measurement related communities (Fraser, 1998), is becoming a firmly established 3D measurement tool with its roots in aircraft-, aerospace-, automobile- and shipbuilding industry and other engineering fields.

Applications of digital close-range photogrammetry in industrial and engineering

environments can be grouped into two domains (Fraser, 1998):

- high accuracy dimensional measurement in industrial and large scale engineering;
- a broad range of low to medium accuracy applications, including such areas as architectural and archaeological recording, process plant documentation, and measurement in support of traffic accident reconstruction and forensics.

Due to their limitations, such as small formats, unknown and variable interior orientations, and low spatial resolution, the accuracy achieved with low-resolution digital camera systems is limited to certain levels. Therefore, it is rare that such cameras find applications in the first domain. In fact, this application domain is being firmly occupied by metric, film-based cameras and some high-resolution digital camera systems. Nevertheless, there exist many opportunities within the second application domain where the low-resolution digital camera systems can be adopted as powerful measuring devices. To fulfill this goal, however, a few key issues associated with the metric applications need to be carefully considered due to the non-metric characteristics of the low-resolution digital camera systems. In the following sections, issues on targeting, network design and calibration aspects are addressed. Finally, actual and potential applications are discussed.

6.2 Practical Considerations Associated with Metric Applications

Although low-resolution digital cameras can be used for on-line real-time or near-real-time photogrammetric systems, they are widely incorporated into single sensor off-line systems due to their onboard storage capabilities and their portability. For such types of

digital camera systems, issues related to targeting, illumination, network design and calibration have to be considered.

6.2.1 Targeting and Illumination

Most photogrammetric applications in industrial and engineering environments require 3D coordinate determinations of a number of discrete targets on the object of interest in the user defined reference systems. Although some natural points on the object can be used as targets, under many circumstances artificial targets are deployed in order to obtain reliable and accurate measurements. For identification and mensuration purposes, targets appearing on the images should be of high contrast against the background. Compared to the conventional black-and-white paper targets, greyish-colored retro-reflective targets are universally used in a host of precise applications. The major advantage of retro-reflective targets is that they can return light very effectively under proper illumination and exposure conditions. The use of such targets can make the resulting images binary or near binary, i.e., the targets can be easily detected from the background and measured either manually or automatically, which greatly facilitates the mensuration. In addition to the material and color of the targets, their size and form also affect the image measurement precision. The target size must be considered together with imaging scale. Beyer (1992b) stated that circular targets with a diameter of six pixels performed well for precise digital image measurements. Furthermore, coded targets are becoming popular as they can remove the requirement to manually identify a selected subset of image points, specially for those points used for the initial determination of the exterior orientation (Fraser, 1997b).

The illumination determines the distribution of the light intensity on the object, which in turn influences the image measuring precision. If the object is targeted with paper targets or the whole object needs to be mapped without any targeting, uniform and steady illumination is very important during the imaging process. Application of retro-reflective targets largely alleviates these requirements. A small, battery powered strobe located at or close to the camera is enough for illumination. The strobe makes the exposure of the targets independent of the ambient light level. For example, the targets can be exposed by the strobe while the object is exposed by the ambient light either bright or totally dark (Johanning, 1996).

6.2.2 Photogrammetric Network Configuration

Two major factors influencing photogrammetric triangulation accuracy are angular measurement resolution of the camera and the photogrammetric network geometry. While the former is limited by the camera structure and the image measuring precision, the latter should be carefully designed in order to exploit the cameras' accuracy potentials. It is not surprising that similar sensors yield 3D measurement accuracies varying by an order of magnitude due to network configuration differences (Fraser, 1996).

Network design problems can be classified into four interconnected stages in accordance with the classification scheme proposed by Grafarend (1974):

- zero-order design (ZOD): the datum problem;
- first-order design (FOD): the configuration problem;
- second-order design (SOD): the weight problem;
- third-order design (TOD): the densification problem.

However, only the FOD needs to be further addressed for photogrammetric projects while the others are either not applicable or are greatly simplified in comparison to geodetic networks (Fraser, 1996).

In close- range measurement applications, photogrammetric triangulation accuracies are usually expressed in terms of relative accuracy in object space, being as a proportion of the principal dimension of the object field. A coarse indicator of the accuracy of triangulation in a convergent, multi-station photogrammetric network is given by Fraser (1992) as:

$$\frac{\sigma_c}{R} = \frac{q}{\sqrt{k}} \frac{\sigma}{r} \quad (6.1)$$

where r : the image dimension; R : the corresponding distance in object space; σ : the image coordinate standard error; q : the design factor expressing the strength of the photogrammetric network configuration; k : the average number of exposures at or near each camera station. Basically, network configuration design should solve the following problems based on the accuracy requirements, object shape and dimension, and the cost consideration:

- (i) type of camera to be used and image mensuration method;
- (ii) number and location of the camera stations;
- (iii) attitude of the cameras (directions of the optical axes, camera roll angles) ;
- (iv) number of images to be taken at each camera station.

r and σ of Equation (6.1) are determined after the step (i); q is determined by steps (ii) and (iii), and k is determined in step (iv). However, for many applications, photogrammetric network configuration design is a knowledge intensive process because of the complexity and the constraints of the environment. Mason (1995) summarized the constraints affecting the configuration of a photogrammetric network as: image scale constraint, resolution

constraint, workplace constraint, depth of field constraint, incidence angle constraint, number and distribution of the image points constraint, field of view constraint, and visibility constraint. Therefore, network design was only implemented by specialist photogrammetrists in the past. Nevertheless, with the integration of the Computer Aided Design (CAD) and expert systems to the photogrammetric network design process, this task can be carried out much easier than before by nonspecialist photogrammetrists, which largely facilitates the wider acceptance of photogrammetric systems by many potential application clients.

One advantage of a digital camera system photogrammetric network is that the configuration can be easily strengthened by taking more images than necessary because the workload will not be increased significantly due to the rapid automatic image mensuration. Stereoscopic imaging configuration is rarely used in industrial and engineering photogrammetry except for certain niche applications such as car body mapping. Instead, multi-image, monoscopic/convergent networks are widely used in a variety of photogrammetric applications. For example, Fraser and Mallison (1992) described the close-range photogrammetric measurement project of a 43 m aircraft structure where the network configuration was designed to comprise 92 camera stations and 1400 targets based on the accuracy requirement of 0.25 mm and various constraints.

6.2.3 Camera System Calibration

In contrast to the widely used film-based metric cameras whose interior orientations are either fixed or known, digital camera systems, especially low-end ones have unstable and unknown interior orientations and possibly suffer from large geometric imperfections.

Theoretical and practical studies in the previous chapters clearly showed that calibration for those camera systems is imperative when they are being used for measurement purposes.

As discussed in Chapter 4, various camera system calibration methods exist with each method having its own advantages and disadvantages. However, the self-calibration category stands out from the others and is being widely used in a host of digital close-range photogrammetric applications. This is mainly because the calibration is incorporated into the photogrammetric bundle adjustment and the up-to-date interior orientation is always recovered during the evaluation. Under this circumstance, the internal geometry of the imaging network is used, and thus no external control information is needed purely for calibration purposes. It is worthy of reiteration that configuration of the imaging network is critical for a successful self-calibration. Other calibration methods can provide similar calibration results, nevertheless, precise control information in object space or certain special devices have to be adopted, which largely excludes them from wide acceptance except for some research of camera structure characterizations or systematic error modeling and compensation algorithm comparisons. When accuracy requirements are not very stringent, pre-and post-calibration (i.e., camera systems are calibrated prior and after the image acquisition phase) can also be considered, in order to facilitate the subsequent data evaluation and to loosen the requirements upon the network configurations.

6.2.4 Time and Cost Considerations

In addition to accuracy concerns, time and cost are two other important factors associated with many measurement tasks.

Implementation of a photogrammetric project mainly involves steps of problem analysis, network design, object preparation and targeting (if necessary), image acquisition, image mensuration, data processing and results presentation. Many industrial and engineering measurement applications require rapid provision of final results with little or no interruption to the manufacturing or assembling processes. On the other hand, the measurement load of such applications is quite heavy, sometimes, hundreds of images with thousands of points are involved in certain projects. The initial impact of digital camera systems on photogrammetry is quick image acquisition, transfer and automatic image mensuration through techniques such as simple centroiding and advanced least squares template matching. The integration of a CAD module with the close-range photogrammetric environment makes the network configuration design and data presentation much easier and faster than before. Moreover, coded targets, exterior orientation, means to determine image point correspondence for unlabeled points lead to further automation for data acquisition and processing. As a result, digital close-range photogrammetry projects can be implemented semi- or full automatically, which largely reduces the turnaround time for the applications.

When the time factor is being taken into account, on-line and off-line digital camera systems have to be mentioned. On-line systems can perform measurement in real-, or near real-time, which is very beneficial for such applications as manufacturing and assembly monitoring, or robot vision. However, accuracy, inflexibility, cost and hardware requirements are some problems associated with such systems compared with their off-line counterparts. On the other hand, off-line systems work in the traditional photogrammetric manner of separate steps of data acquisition, image mensuration and processing. The turn-

around time for off-line systems, nevertheless, is not as long as that of traditional film-based photogrammetry due to the reasons mentioned at the beginning of this section. Therefore, for digital close-range photogrammetric systems, *off-line* simply means that the final results can only be available after all the images are taken as they are not usually obtained simultaneously. Inasmuch as the image mensuration and data processing can be finished in a very short period of time (sometimes only several seconds), “*on-the-site*” result availability is the common requirement for many single-sensor off-line digital photogrammetric measurement systems.

Table 6.1 summarizes some application examples extracted from Fraser (1996; 1998) to demonstrate the potential speed of the current digital camera systems. It can be seen that the speeds for different projects were quite different due to different accuracy requirements and different complexities of the objects, thus different imaging network configurations. Although these systems universally used high-resolution digital cameras to capture the images, there would not be a significant change of speed when low-resolution digital cameras were adopted because of the similarity of operations.

Cost is another factor for clients to consider when selecting a measurement technique. Although cost is always related to accuracy, some balancing can be achieved between accuracy and cost under certain circumstances. Systems comprised of low-resolution digital cameras are more attractive when cost is the major concern for the applications. For example, a high-end digital camera itself may cost about \$10,000 or more, while with same amount of money, a digital close-range photogrammetric system with a low-resolution digital camera can be established and used for many low- to medium accuracy tasks. Here

the use of an expensive, high-end digital camera would be overkill.

Table 6.1 Speed and Accuracy of Some Digital Close-Range Photogrammetric Tasks.

Project	Descriptions	Speed and Accuracy
On-line measurement of pie crusts	to determine basic dimensional details (length, breadth and height) of 20,000 meat pies. 100,000 points.	83 pts/min* 1:110 relative accuracy (1 mm positioning accuracy)
On-line and off-line as-built survey of a helicopter (15 m long)	5080 points (2000 strip targets, 80 coded targets, 3000 non-targeted points). 160 images	17 pts/min (target points) 20~30 pts/min (non-targeted points) 1:15,000 relative accuracy
Off-line dimensional inspection of a steam generator	200 points 40 camera stations	1 pts/min 0.08 mm positioning accuracy
Off-line dimensional inspection of a door panel draw pie	400 targets 22 images	5 pts/min 0.025 mm positioning accuracy
Off-line measurement of a surface contour of the turbine blade	127 targets 14 images	2 pts/min 0.01 mm positioning accuracy

* pts/min: points per minute

Fraser (1998) divided digital close-range photogrammetric systems into three tiers according to accuracy and cost:

- the top rank are the highly automated, high accuracy, high cost (>\$100,000) VM systems for industrial photogrammetry, which come in the forms of single sensor off-line systems and real-time configuration of multiple sensors;
- the middle rank are traditional digital photogrammetric workstations which produce results of medium accuracy and have medium to high cost (\$10,000 to \$100,000). These systems typically incorporate full stereo viewing and stereo restitution capabilities, including automated processes.
- the bottom tier are low-accuracy, low-cost (<\$1000) 3D modeling systems. While these systems may have their roots in photogrammetry, their clear development focus is toward a much broader market for 3D computer modeling.

6.3 Application Areas of Low-Resolution Digital Camera Systems

The adoption of digital cameras facilitates the evolution of photogrammetry from analogue and analytical eras to the digital era. Due to the advantageous characteristics of the digital technologies, digital close-range photogrammetry is making inroads into the applications once occupied by traditional procedures and is finding more and more potential applications. Low-resolution digital camera systems are playing an important role in digital close-range photogrammetry in that they are powerful, low-cost measuring devices. Therefore, whenever cost saving is the main factor and the accuracy requirements are not very high, low-resolution digital camera systems are quite attractive. Although low-resolution and small format size of the camera limit the accuracy that can be attained by such devices, there still exist many occasions where such cameras can be used.

6.3.1 Digital Close-Range Photogrammetry

Traditional photogrammetry is a technology of measurement based on photographic images, which has long been used to map the surface of the earth, usually from aircraft and recently from satellites. Since the beginning of this decade, digital close-range photogrammetry has been widely used for non-topographic applications in industrial and engineering areas with the adaptation of the digital technologies and corresponding algorithms. It is a well proven and broadly accepted means of capturing large amounts of dimensional information with the click of a shutter. Compared to other close-range measurement technologies, such as laser trackers, 3D Coordinate Measurement Machines (CMMs), Electronic Coordinate Determination System(ECDSs), automatic theodolite

systems (ATS) etc., digital camera systems are preferred due to their practical advantages. By using digital close-range photogrammetric means, measurements can be carried out on models instead of approaching the real environment. Remeasurement is also possible when necessary, since the images are permanent records of the real scenes and objects. Rapid or even real-time image acquisition is possible and, thus, the turn-around time is largely shortened. Furthermore, the end products of digital camera systems can easily be put into most CAD, animation and rendering programs, which largely facilitates the presentation and usage of the products. As a result, they are gradually replacing the traditional film-based cameras for many measuring tasks. Therefore, they are finding wide applications and more potential applications will emerge when more and more people realize the advantages of such systems.

Measurements must meet the required accuracy, however, this does not mean they must all be to the very high accuracy. The utilization of low-resolution digital camera systems as imaging devices confines the achievable accuracy to certain levels. Nevertheless, there still exist many areas where such low-cost and low-accuracy systems are being or can be potentially applied. With powerful software (e.g., FotoG-FMS™ from the Vexcel Corporation, Photomodeler™ from the EOS Systems Inc., Photocad-Multi™ from the Desktop Photogrammetry etc.) and automation advances of digital close-range photogrammetry, users can quickly and easily generate accurate 3D information from digital images. Theoretically, anything visible on multiple photographs or images can be measured by photogrammetric means. In many cases, a low-resolution digital camera plus a notebook computer with appropriate software can compose a powerful digital close-range

photogrammetric system which can be used for many applications.

6.3.2 General Application Requirements

Many measurement applications can be described as problems of 3D model creations of real-world scenes and objects, including the human body, industrial and engineering structures, machine parts, terrain, and artifacts. The models are often used for system-, weight-, and cost calculations, as well as for engineering analysis. Due to the numerous varieties of the scenes and objects, measurement needs usually vary dramatically in accuracy requirements, level of detail, size of the project, environmental influences, etc. Compared to other close-range measuring technologies, digital camera systems can meet these needs by adopting different cameras and imaging configurations, which is attracting more and more commercial attention.

6.3.3 Existing and Possible Application Areas

Due to their advantages, low-resolution digital camera systems are being or can be applied to various measurement environments. For example, such systems can be applied for:

- industrial and engineering environments;
- archaeological and anthropological applications;
- accident reconstruction and forensics.

In addition to the above mentioned application areas, low-resolution digital camera systems can also be used for other tasks, such as small area mapping, GIS data acquisition, computer graphics, film, video and animation.

CHAPTER 7

PRACTICAL STUDIES OF LOW-RESOLUTION DIGITAL CAMERA SYSTEMS

Low-resolution digital cameras are finding more and more applications in many general business areas. However, as powerful digital imaging tools, their metric characteristics have not yet been thoroughly investigated in the photogrammetric field, mainly due to their limited image format and inferior image quality. This chapter describes several practical projects of photogrammetric investigation of three different low-resolution digital camera systems, namely, Fujix DS-100, Kodak DC-40 and Kodak DC-50 system.

7.1 Introduction

The concepts, working principles, error sources and possible applications of digital camera systems, especially the low-resolution types, were discussed in the proceeding chapters. To fully evaluate their potentials for metric applications, some practical studies are imperative in addition to theoretical investigations. A series of photogrammetric projects were designed and carried out using three different types of low-resolution digital camera systems available to the author. The main objectives of these projects were to investigate:

- the feasibility of metric applications of low-resolution digital cameras;
- the metric performances of these camera systems under different situations;
- the accuracy levels that can be achieved by these camera systems;
- effects of systematic error compensation by different data reduction methods;
- the stability and reliability of these camera systems ;
- the integration capability of different types of digital cameras for the same project.

7.2 Digital Camera Systems Studied

Most low-resolution digital cameras incorporate smaller format solid-state sensor chips, have fixed and low-quality lenses, simple optical design and little control over the image taking process, all of which certainly impose adverse influences upon the final results.

The low-resolution digital camera systems used for these studies are the Fujix DS-100, Kodak DC-50 and Kodak DC-40 system (Figure 7.1). The best image resolution from the Fujix camera is 640 x 480 pixels, and the two Kodak cameras deliver images of 756 x 504 pixels. The Kodak DC-40 is of a simple point-and-shoot type, whereas the other two are equipped with 3x zoom lenses. As for the image storage and image downloading aspects, the three cameras have distinguishing characteristics: the DC-40 has a 4 MB internal memory with a serial cable to connect the camera to a computer to download the images; the DS-100 uses a slide-in memory card for the storage medium and a special card reader cabled to the SCSI port of the host computer; the DC-50 incorporates both internal storage and a Type I/II PC card to expand its storage capability. Table 7.1 summarizes the main technical specifications for the three cameras. All three camera systems use a Digital Video Plotter (DVP) from Leica as the host computer for image storage, processing and measurement. Photogrammetric data processing methods and software are common for three systems, which discussed in next section.

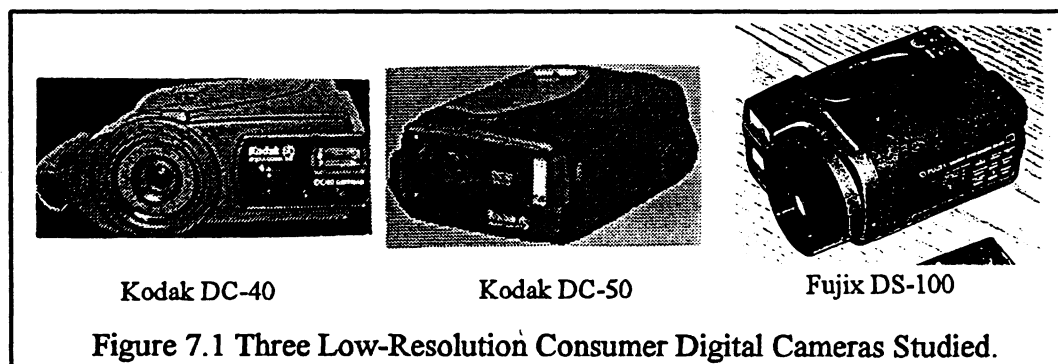


Table 7.1 Main Features of the three Low-resolution Digital Cameras Studied.

Camera	Kodak DC-40	Kodak DC-50	Fujix DS-100
Number of pixels	756 x 504	756 x 504	640 x 480
Size of pixel	9.0 μm	9.0 μm	9.7 μm
Lens type	f = 8 mm	f = 7~21 mm	f = 8~24 mm
f-stop/shutter speed	1/30~1/175 sec. , F2.8~F16, ISO 84	1/16~1/500 sec., F2.5~F24, ISO 84	1/4 ~1/750 sec., F2.8~F11, ISO 100
Storage medium	4 MB internal only: 48/96	1MB internal: 7/11/22. PC card type I/II	1MB proprietary card: 5/10/21
Interface to computers	Serial port	Serial port / PC card slot	Card reader through SCSI port

Note: 1. Number of images can be stored under the high-/standard resolution modes;

2. Number of images can be stored under the high-/standard-/economy resolution modes.

7.3 Data Processing Methods and Calibration Tests

Due to the existence of various systematic defects of both the digital camera systems and the imaging process, the acquired image data are distorted, which has an adverse influence upon the final accuracy. Therefore, effective data reduction should possess the capability to compensate for the defects and to exploit the potential accuracy to the maximum extent. Many different methods are currently being applied to model the systematic errors. Among them, self-calibrating bundle adjustment and Direct Linear Transformation (DLT) are two generally used methods and both were used for the subsequent digital image data processing, although they were originally developed for film based cameras. In addition, the Multiple-Frame Finite Element Method (MFFEM) was utilized to process the image data for one of the projects.

7.3.1 Self-Calibrating Bundle Adjustment Method I -- UNBASC2

UNBASC2 (University of New Brunswick Analytical Self-Calibration) was developed at The University of New Brunswick for both aerotriangulation and close-range photogrammetric applications by Dr. Moniwa (1977). It is based on the extended collinearity equations:

$$\begin{aligned} x + \Delta x - x_0 &= -c \frac{m_{11}(X - X_0) + m_{12}(Y - Y_0) + m_{13}(Z - Z_0)}{m_{31}(X - X_0) + m_{32}(Y - Y_0) + m_{33}(Z - Z_0)} \\ y + \Delta y - y_0 &= -c \frac{m_{21}(X - X_0) + m_{22}(Y - Y_0) + m_{23}(Z - Z_0)}{m_{31}(X - X_0) + m_{32}(Y - Y_0) + m_{33}(Z - Z_0)} \end{aligned} \quad (7.1)$$

where x , y are the image coordinates of the image points; X , Y and Z denote the object coordinates of the corresponding object points, and x_0 , y_0 and c represent the basic interior orientation parameters, i.e., the location of the principal point and the calibrated principal distance; m_{ij} are the elements of the rotation matrix between the image space and object space coordinate systems, and X_0 , Y_0 , Z_0 are the object coordinates of the perspective centre. Δx and Δy stand for the correction terms applied to the image coordinate measurements, which are functions of selected additional parameters (Aps); In UNBASC2, Δx and Δy were defined as:

$$\begin{aligned} \Delta x &= dr_x + dp_x + dq_x \\ \Delta y &= dr_y + dp_y + dq_y \end{aligned} \quad (7.2)$$

where dr_x , dr_y stand for the radial distortion correction components in x and y directions, expressed by the APs k_1 , k_2 , k_3 ; dp_x , dp_y refer to the correction terms for decentring distortion which are the functions of the APs p_1 and p_2 ; dq_x and dq_y are the affine image

deformation corrections in terms of the APs A and B . Thus, seven additional parameters, $k_1, k_2, k_3, p_1, p_2, A$ and B are included to model the image distortion, which together with the basic interior and exterior orientation parameters forms the functional model (Equation 7.1) of the UNBASC2 self-calibrating bundle adjustment. Therefore, different calibration schemes can be carried out by adopting different APs into the functional model. Table 7.2 summarizes calibration tests designed for UNBASC2 in order to study the systematic errors and the accuracy potential of the employed digital cameras.

Table 7.2 Calibration Tests with UNBASC2.

Case	APs Considered	Descriptions
UNB I	without any APs	no interior orientation
UNB II	with x_0, y_0 and c	basic interior orientation parameters
UNB III	with $x_0, y_0, c, k_1, k_2, k_3$	UNB II plus radial lens distortion compensation
UNB IV	with $x_0, y_0, c, k_1, k_2, k_3, p_1, p_2$	UNB III plus decentering lens distortion compensation
UNB V	with $x_0, y_0, c, k_1, k_2, k_3, p_1, p_2, A, B$	UNB IV plus affine deformation correction

7.3.2 Self-Calibrating Bundle Adjustment Method II -- GEBAT

GEBAT (GEneral Bundle Adjustment Triangulation) is a self-calibrating bundle adjustment approach with photo-invariant additional parameters and geodetic constrains (El-Hakim, 1979), which models the combined effects of all errors by a harmonic function rather than modeling explicitly the individual effect of some of the systematic errors as in UNBASC2. The error models are described by Equation (4.4) to (4.6). Eight coefficients (a_{00} to b_{3j}) of the harmonic function and three basic interior orientation parameters (x_0, y_0 and c) are included in the bundle adjustment for all the images due to the photo-invariant

characteristics of GEBAT. There are other versions of GEBAT (e.g. GEBAT V) which has the photo-variant capabilities, but they were not accessible to the author, thus no further calibration tests could be designed with GEBAT.

7.3.3 Direct Linear Transformation (DLT) Method

The DLT performs a direct transformation from 2D comparator coordinates into 3D object space coordinates. Due to the elimination of the intermediate step of transforming image coordinates from a comparator system to the image coordinate system, the DLT method does not need fiducial marks or initial values for the unknowns (Abdel-Aziz and Karara, 1971), which makes the DLT method especially suitable for non-metric imageries. In order to compensate for the systematic errors, an extended DLT model was developed based on the following Equation (4.2). Under this case, Δx and Δy account for the non-linear components of lens distortion and film deformation, which can be expressed as simple or sophisticated functions of a certain number of additional parameters to model radial-, decentring lens distortion and film deformation (Karara and Abdel-Aziz, 1974). The following cases were designed for some of the projects:

Table 7.3 Calibration Tests with the DLT.

Case	No. of Parameters	Descriptions
DLT I	11	11 transformation parameters l_1 to l_{11} involved
DLT II	12	l_1 to l_{11} + 1 radial distortion parameter k_1
DLT III	14	l_1 to l_{11} + 3 radial distortion parameters k_1 , k_2 and k_3
DLT IV	16	l_1 to l_{11} + k_1 , k_2 and k_3 + 2 decentring distortion parameters p_1 and p_2

7.3.4 Finite Element Method (FEM)

Modeling and compensation of systematic errors by the FEM were discussed and studied by using simulation in the Chapter 5. Theoretical findings indicate the equivalence and certain advantages of this method over other photogrammetric data reduction methods. In this chapter, the method is further verified for a real project where three low-resolution digital camera systems were calibrated by different systematic error modeling and compensation methods and comparisons were made among the methods. Table 7.4 describes the schemes designed for the FEM calibration where different numbers of elements and shape functions were adopted:

Table 7.4 Calibration Tests with the FEM.

Case	Descriptions
FEM TI	four triangular elements with linear shape functions (three nodes for each element)
FEM TII	eight triangular elements with linear shape functions (three nodes for each element)
FEM TIII	sixteen triangular elements with linear shape functions (three nodes for each element)
FEM HTI	four triangular elements with higher order shape functions (six nodes for each element)
FEM HTII	eight triangular elements with higher order shape functions (six nodes for each element)
FEM RI	four rectangular elements with linear shape functions (four nodes for each element)
FEM RII	eight rectangular elements with linear shape functions (four nodes for each element)
FEM RIII	sixteen rectangular elements with linear shape functions (four nodes for each element)
FEM HRI	four rectangular elements with higher order shape functions (eight nodes for each element)
FEM HRII	eight rectangular elements with higher order shape functions (eight nodes for each element)

7.4 Practical Projects and Results

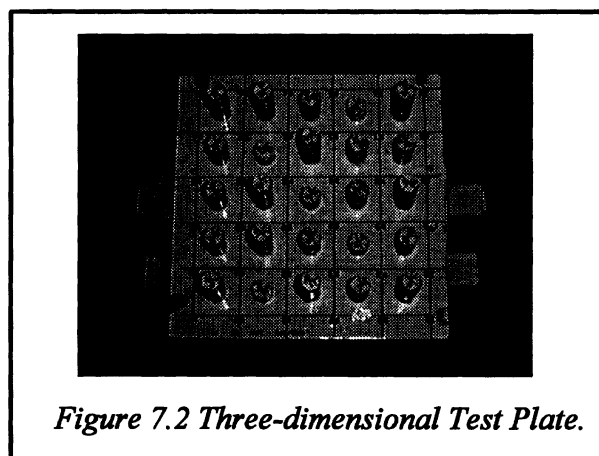
To investigate the systematic errors of low-resolution digital camera systems and the effects of systematic error modeling and compensation of different algorithms, a series of practical projects were designed and carried out.

7.4.1 Three-Dimensional (3D) Test Plate Calibration Project

This project aims to investigate the calibration effects of the three low-resolution digital camera systems available to the author. Different systematic error modeling and compensation schemes were studied and the metric performances of the camera systems evaluated and compared by using a small indoor test plate.

7.4.1.1 Test Plate

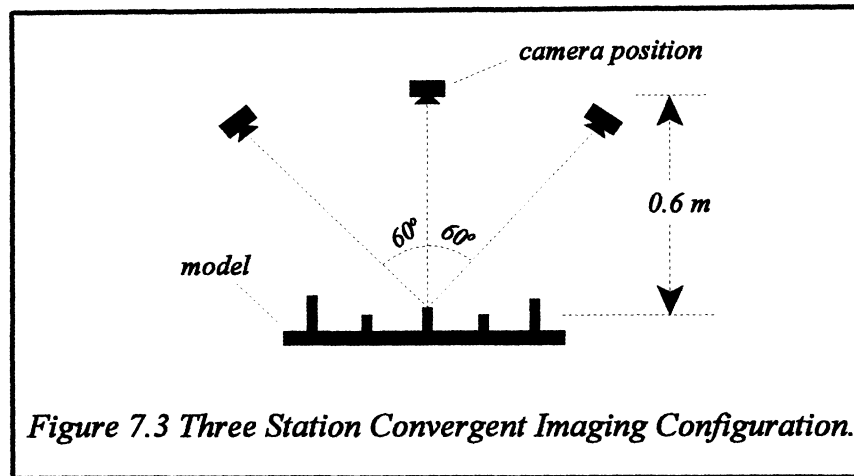
A 3D test plate with dimensions of 17 cm x 17 cm x 5 cm was used for these studies (Figure 7.2), consisting of a metal grid plate with 36 intersections engraved on the surface, and 25 bolts with different heights ranging from 12 mm to 37 mm fixed perpendicularly to the plate.



The 3D coordinates of all the target points on the plate were determined with an Electronic Coordinate Determination System (ECDS) in an arbitrarily defined object space coordinate system (El-Habrouk et al., 1996). Precisions of 0.02 mm, 0.03 mm and 0.02 mm in X, Y and Z directions in the object space were obtained. These geodetically determined values served as control and check data during the subsequent photogrammetric evaluations.

7.4.1.2 Imaging Configuration

The imaging configuration plays a critical role in a photogrammetric project. To investigate the accuracy potential of the low-resolution digital camera systems, a three-station convergent configuration was deployed for the digital image capture in this project. Because only one of each type of the cameras was available, the camera was fixed at the support frame, while the plate was rotated along its central axis into three orientations, i.e. backwards, level and forwards. This is equivalent to the situation that the model was kept still and the camera was placed at three corresponding locations providing convergence (Figure 7.3). During the imaging process, normal laboratory lighting was adopted which provided a relatively uniform illumination over the model.



7.4.1.3 Image Measurement

Images taken with the Fujix DS-100 were transferred from the memory card to the Leica Digital Video Plotter (DVP) via a Card Processor. Images taken by the Kodak DC-40 and DC-50 were downloaded to the DVP via a serial cable. To measure the image coordinates of the targets, their positions on the sensor plane were determined by first using a screen

digitization method. Then, these values were transformed into metric units based on the given pixel sizes. The image coordinate measuring precision was estimated as 0.1 pixels by large number of repetitive measurements. Due to the fact that for all the projects, the image measurement processes were implemented on the DVP, it will not be repeated during the course of the descriptions of the other projects.

7.4.1.4 Calibration Results

The UNBASC2, the GEBAT and the DLT methods were first applied to process the data of the Fujix DS-100, with the results being given in Tables 7.5.1 to 7.5.3.

Table 7.5.1 Calibration Results of the Fujix DS-100 Camera System by using UNBASC2.

Case*	Image Space (μm)		Object Space (mm)			
	σ_x	σ_y	σ_x	σ_y	σ_z	σ_{mean}
UNB I	78	61	4.67	4.46	4.77	4.63
UNB II	11	11	0.2	0.53	0.34	0.36
UNB III	10	10	0.19	0.26	0.36	0.27
UNB IV	4	3	0.16	0.1	0.08	0.11
UNB V	1	2	0.05	0.07	0.05	0.06

* Note: see Table 7.2 for the case design.

Table 7.5.2 Calibration Results of the Fujix DS-100 Camera System by using GEBAT.

Image Space (μm)		Object Space (mm)			
σ_x	σ_y	σ_x	σ_y	σ_z	σ_{mean}
11	37	1.00	1.60	1.80	1.50

Table 7.5.3 Calibration Results of the Fujix DS-100 Camera System by using DLT.

Case*	Image Space (μm)		Object Space (mm)			
	σ_x	σ_y	σ_x	σ_y	σ_z	σ_{mean}
DLT I	2.7	2.7	0.16	0.11	0.07	0.11
DLT II	1.9	1.9	0.1	0.09	0.06	0.08
DLT III	1.8	1.8	0.07	0.08	0.05	0.07
DLT IV	1.7	1.7	0.06	0.08	0.05	0.06

* Note: see Table 7.3 for the case design.

As GEBAT did not provide satisfactory results, it was not used for data processing of the other cameras' data. The results of the DLT, UNBASC2 and FEM for all the three digital camera systems are presented in Tables 7.6.1 to 7.7. Table 7.8 summarizes the resulting accuracies under the best situations for all the three digital cameras with different data reduction methods and Figure 7.4 is a graphic presentation.

Table 7.6.1 Calibration Results of three Camera Systems by using DLT.

System	Case	σ_0 (μm)	σ_x (mm)	σ_y (mm)	σ_z (mm)	σ_{mean} (mm)
Kodak DC-40	DLT I	6.1	0.19	0.27	0.37	0.27
	DLT II	5	0.18	0.29	0.27	0.25
	DLT III	5	0.17	0.25	0.27	0.23
	DLT IV	4.5	0.15	0.23	0.22	0.2
Kodak DC-50	DLT I	3.9	0.14	0.15	0.14	0.14
	DLT II	3.5	0.12	0.11	0.11	0.11
	DLT III	3.4	0.13	0.12	0.12	0.12
	DLT IV	3.5	0.11	0.11	0.11	0.11
Fujix DS-100	DLT I	3.6	0.05	0.07	0.06	0.03
	DLT II	2.4	0.03	0.04	0.04	0.04
	DLT III	2.4	0.03	0.04	0.04	0.04
	DLT IV	2.2	0.04	0.05	0.05	0.05

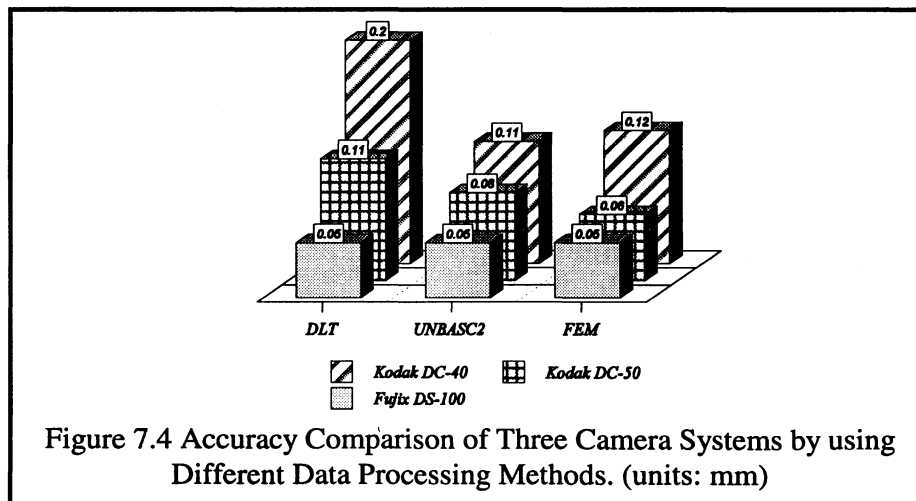


Table 7.6.2 Calibration Results of three Camera Systems by using UNBASC2.

System	Case	σ_0 (μm)	σ_x (mm)	σ_y (mm)	σ_z (mm)	σ_{mean} (mm)
Kodak DC-40	UNB I	48	3.79	1.55	2.14	2.49
	UNB II	15	0.56	0.5	0.62	0.56
	UNB III	12	0.46	0.39	0.41	0.42
	UNB IV	5	0.22	0.19	0.25	0.22
	UNB V	2	0.14	0.09	0.1	0.11
Kodak DC-50	UNB I	72	4.9	2.38	2.57	3.28
	UNB II	13	0.53	0.47	0.58	0.53
	UNB III	12	0.5	0.43	0.48	0.47
	UNB IV	4	0.16	0.18	0.15	0.16
	UNB V	2	0.11	0.06	0.07	0.08
Fujix DS-100	UNB I	70	4.67	4.46	4.77	4.63
	UNB II	11	0.2	0.53	0.34	0.36
	UNB III	10	0.19	0.26	0.36	0.27
	UNB IV	4	0.16	0.1	0.08	0.11
	UNB V	1	0.05	0.04	0.05	0.05

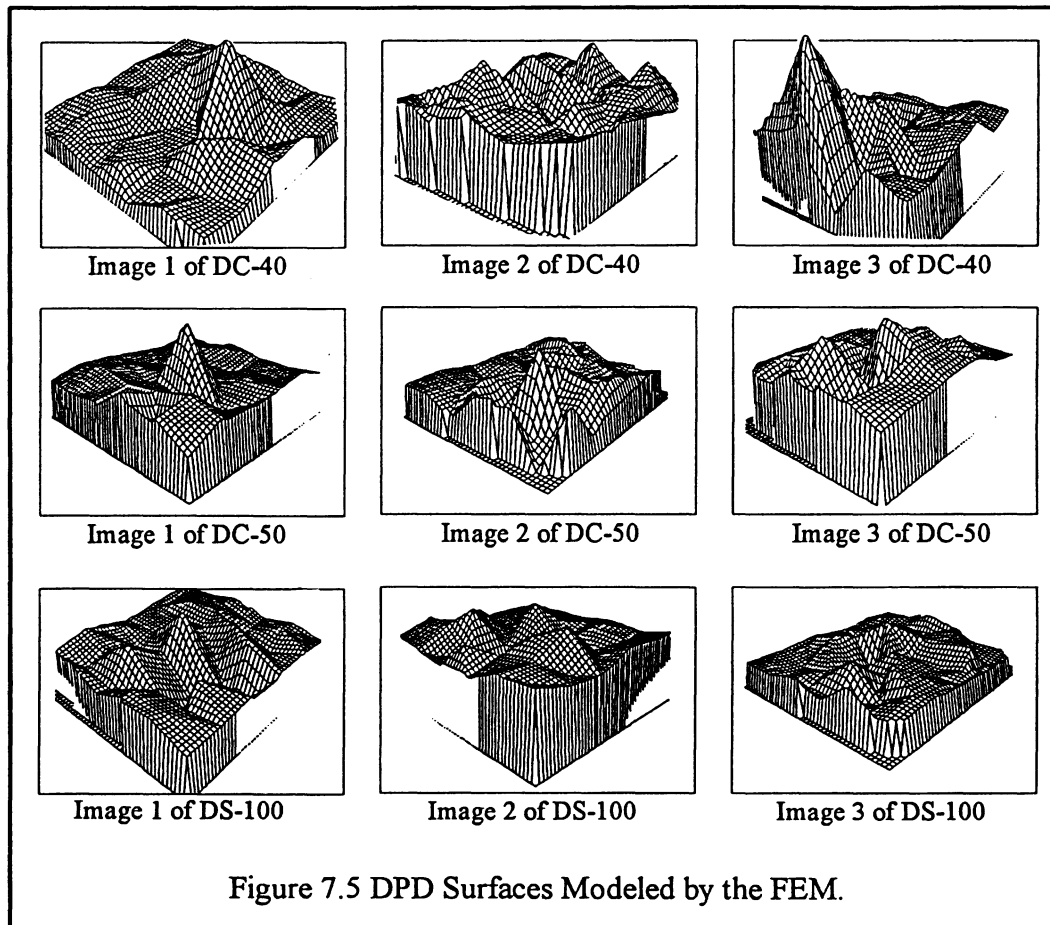
Table 7.7 Calibration Results of three Camera Systems by using FEM.

System	Case	σ_0 (μm)	σ_P (mm)	σ_X (mm)	σ_Y (mm)	σ_Z (mm)	σ_{mean} (mm)
Kodak DC-40	FEM TI	2.3	0.15	0.15	0.22	0.19	0.19
	FEM TII	2.4	0.15	0.15	0.23	0.19	0.19
	FEM TIII	2.3	0.15	0.15	0.22	0.19	0.19
	FEM HTI	2.7	0.17	0.15	0.24	0.18	0.19
	FEM HTII	2.6	0.17	0.16	0.24	0.22	0.21
	FEM RI	2.1	0.14	0.14	0.2	0.15	0.17
	FEM RII	2.3	0.15	0.15	0.22	0.18	0.18
	FEM RIII	2.2	0.14	0.14	0.19	0.17	0.17
	FEM HRI	3.7	0.24	0.17	0.32	0.23	0.25
	FEM HRII	2.4	0.15	0.14	0.22	0.18	0.18
	Full control	1.6	0.1	0.08	0.15	0.11	0.12
	Kodak DC-50	FEM TI	1.9	0.09	0.1	0.11	0.11
FEM TII		2	0.09	0.09	0.11	0.1	0.1
FEM TIII		1.9	0.09	0.09	0.1	0.09	0.09
FEM HTI		1.8	0.09	0.09	0.09	0.1	0.09
FEM HTII		2.5	0.12	0.12	0.15	0.11	0.13
FEM RI		1.6	0.08	0.09	0.08	0.1	0.09
FEM RII		1.8	0.08	0.08	0.08	0.09	0.08
FEM RIII		1.7	0.08	0.07	0.08	0.09	0.08
FEM HRI		1.9	0.09	0.09	0.11	0.1	0.1
FEM HRII		1.9	0.09	0.08	1.1	0.12	0.1
Full control		1	0.05	0.05	0.07	0.06	0.06
Fujix DS-100		FEM TI	1.4	0.05	0.05	0.08	0.07
	FEM TII	1.4	0.05	0.05	0.08	0.07	0.06
	FEM TIII	1.4	0.05	0.05	0.08	0.07	0.06
	FEM HTI	1.9	0.07	0.05	0.1	0.13	0.1
	FEM HTII	1.8	0.06	0.06	0.1	0.13	0.1
	FEM RI	1.3	0.05	0.05	0.07	0.07	0.06
	FEM RII	1.3	0.05	0.04	0.07	0.07	0.06
	FEM RIII	1.2	0.05	0.04	0.07	0.06	0.06
	FEM HRI	1.5	0.05	0.04	0.07	0.07	0.06
	FEM HRII	1.2	0.04	0.04	0.07	0.06	0.06
	Full control	1	0.04	0.03	0.06	0.05	0.05

Table 7.8 Comparison of Different Data Processing Methods.

System	DLT		UNBASC2		FEM	
	σ_0 (μm)	σ_{mean}	σ_0 (μm)	σ_{mean}	σ_0 (μm)	σ_{mean} (mm)
Kodak DC-40	4.5	0.2	2	0.11	1.6	0.12
Kodak DC-50	3.5	0.11	2	0.08	1	0.06
Fujix DS-100	1.2	0.05	1	0.05	1	0.05

Surfaces modeled by the DPDs for all the images of different camera systems are shown in the Figure 7.5.



In viewing the above results, the following conclusions can be drawn:

- As expected, GEBAT did not perform as well due to the fact that its functional model involves photo-invariant basic interior orientation parameters and additional parameters, and the low-resolution digital camera systems do not possess metric properties. In other words, the systematic errors were not properly modeled by this method. This shows that appropriate models are important for modeling the systematic defects of a digital camera system in order to make the system metrically useful.
- With the UNBASC2 and the DLT methods, the final accuracies can be improved significantly by camera calibrations. Step-by-step improvements were detected, although sometimes not obvious, which indicates the appearance of systematic errors and effectiveness of modeling and compensation.
- The basic interior orientation parameters (x_0 , y_0 and c) play the most important role in the data evaluation. The inclusion of these parameters greatly improved the results. Without them, the results are too inaccurate to meet metric application requirements.
- The assumptions of uniform pixel size and distribution are rational, as evident by the final RMSE σ_x and σ_y of the image coordinates. Although the precise pixel size could be determined during the data evaluation, accurate scale information is imperative for the object space when imaged by the cameras. As such information is not easily available, it is not realistic to include the pixel size as an unknown parameter in the photogrammetric adjustment.
- In spite of the differences in modeling and compensation for systematic errors adopted by the UNBASC2, the DLT and the FEM, the final results were quite close. The FEM showed a marginal advantage over the other two. Between UNBASC2 and the DLT, although UNBASC2 provided slightly more accurate results, DLT did present stable results while the self-calibration method is very sensitive to the imaging configuration, which was verified by testing different numbers and distributions of control and check points.
- On the FEM side, again, the rectangular elements showed their advantages over the triangular counterparts, although not significantly. However, contrary to the theoretical

findings, the increment of the number of the elements and the adaptation of higher order shape functions did not improve the final results. In addition, the modeled DPD surfaces reinforce the fact that, for the same camera system, the behaviour of the systematic errors is not fixed. Instead, they changed from scene to scene. Therefore, photo-variant modeling and compensation schemes for the systematic errors are the key to the successful precise photogrammetric applications of low-resolution digital camera systems.

- Among the three low-resolution digital camera systems, the Fujix DS-100 system presented the highest accuracy potential, next came the Kodak DC-50 system, and finally Kodak DC-40 system, under the adopted imaging configuration. Although with slightly bigger pixel size ($9.7 \mu\text{m} \times 9.7 \mu\text{m}$) and lower number of pixels (640×480) with respect to the Kodak DC-40 and DC-50 ($9.0 \mu\text{m} \times 9.0 \mu\text{m}$, 756×504 pixels), the Fujix DS-100 system provided better results than the other two for most of the test cases. This suggests that the metric performance of the digital camera systems depends not only on the pixel size and the number of the pixels of the solid-state sensors onboard the camera, but also upon the lenses and other factors which influence the image quality. The comparison between the Kodak DC-40 and DC-50 system (cameras with same CCD design but different lenses systems) also supports this conclusion.

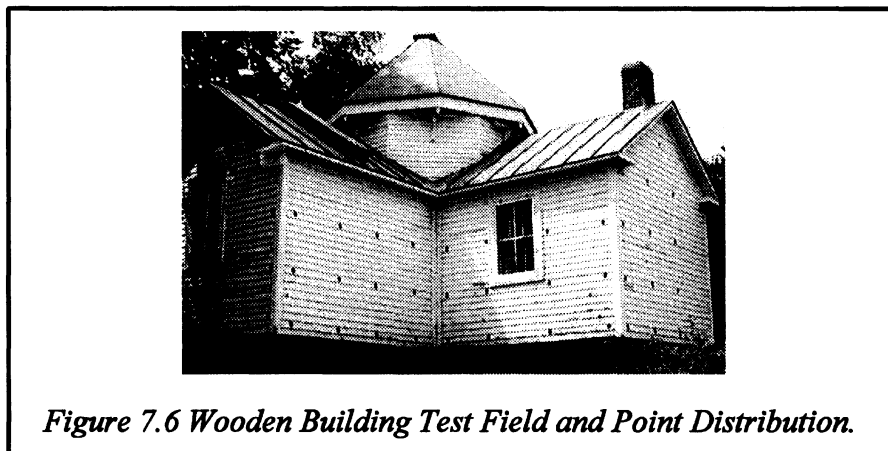
7.4.2 Architectural Dimensional Inspection

The main goals of this project are to further evaluate and to compare the metric performances of the three low-resolution digital camera systems, the accuracy potential under the adopted imaging configuration with appropriate calibration parameters, the stability and reliability of the digital camera systems, multi-exposure effects, and the integration capability of different types of digital camera systems for the same project. To fulfill these goals, an architectural test-field was set up and a five-station convergent imaging

configuration was adopted. A series of self-calibrating bundle adjustments by using the UNBASC2 method were carried out with different data processing schemes, and analyses were conducted based on the adjustment results.

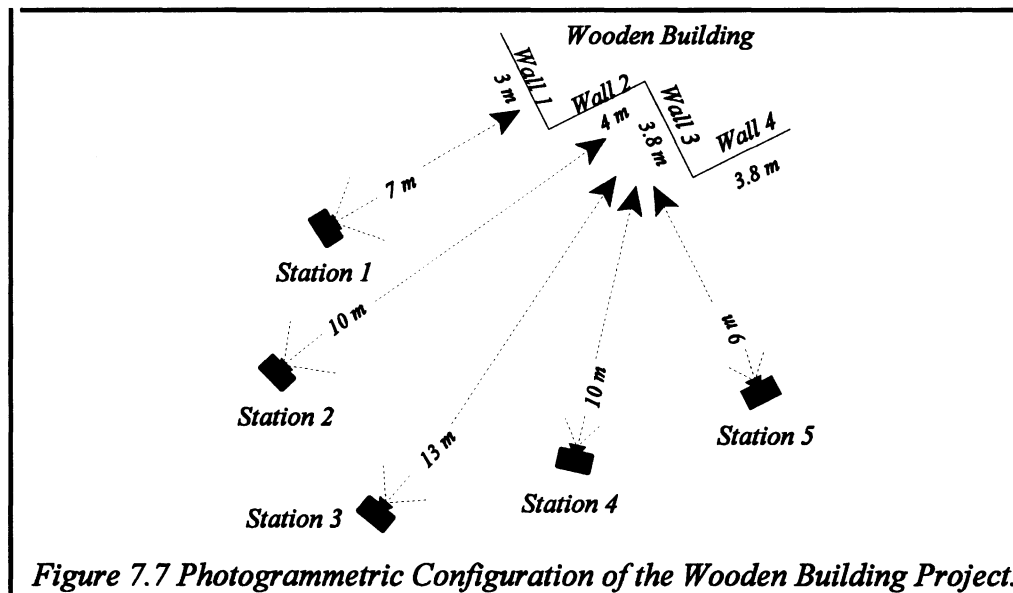
7.4.2.1 Architectural Test-field

A white wooden building on the UNB campus was selected as the test-field where the four walls of its back side provide itself as an appropriate 3D test field (Figure 7.6). Forty-nine black paper targets of seven centimetres in diameter were attached on the white walls uniformly with eight, sixteen, sixteen and nine targets on Walls 1, 2, 3 and 4, respectively. All of the targets were coordinated by precise theodolite intersection with a five-station 3D geodetic adjustment. The resulting triangulation precision were 0.7 mm, 0.6 mm and 0.1mm in X, Y and Z direction at the 95% confidence level. These geodetically determined points were used for control or check points in the subsequent photogrammetric evaluation as error-free quantities.



7.4.2.2 Photogrammetric Configuration

Considering the geometric nature of the test-field, a five-station convergent imaging configuration (Figure 7.7) was adopted to obtain appropriate convergent angles, reliable results, and to keep the measuring burden moderate. The camera-to-object distance varies from 7 m to 13 m in order to get the maximum practical imaging scales for each image and, thus, to improve the accuracy and to evaluate the distortion of the whole lens areas. Except for station 3 where all the four walls can be the imaged, the other stations can only capture either two or three walls.



To evaluate the effects of the multi-exposures, the stability and repeatability of the camera systems, especially for the two systems composed of cameras with zoom lenses, two images were taken consecutively at each of the five camera stations with each camera, i.e. ten images for each camera, and thirty for the whole project. Three photogrammetric

network configurations could be formed for each camera system, namely, Config I and Config II each uses five different images with one image from each station, whereas Config III includes ten images with two images at each station.

All the images were taken under normal daylight conditions and no special illumination was adopted. After downloading the images from the cameras or the memory cards to the DVP, some of the images were enhanced to brighten certain poorly illuminated targets before all the targets were measured on the DVP with a resulting measurement precision of 0.1 pixels estimated from the repetitive observations.

7.4.2.3 Accuracy Preanalysis

Photogrammetric point determination is essentially an optical triangulation where directions of light rays are expressed as functions of image coordinates and the basic interior orientation of the cameras. Like any other optical triangulation method, the accuracy of the photogrammetric results is mainly dependent on two factors, the intersecting geometry and the angular measurement resolution.

Equation (6.1) can be rewritten as following for accuracy preanalysis:

$$\sigma_c = \frac{q}{\sqrt{k}} d \sigma_a \quad (7.8)$$

where σ_c is the r.m.s. value of 3D object coordinates; d refers the mean camera-to-object distance; σ_a stands for the angular resolution of the camera depending on image measurement precision σ and the principal distance c ; q is a factor measuring the strength of the imaging configuration (the smaller the value, the stronger the network); k represents the mean number

of exposures at or near each camera station.

Based on the formula and the specification data of the three cameras, the precision of photogrammetric triangulation of the project is established as shown in Table 7.9, where σ is assumed as 0.1 pixels, q as 1, and d as 11 m.

Table 7.9 Accuracy Preanalysis of the Wooden Building Project.

System	Focal length (mm)	Sensor Format (mm ²)	Angular Resolution (secs. of arc)	σ_c (mm)	
				k=1	k=2
Kodak DC-40	8	6.8 x 4.5	23.2	1.24	0.64
Kodak DC-50	7 ~ 21	6.8 x 4.5	26.5 ~ 8.8	1.41 ~ 0.47	1.00 ~ 0.33
Fujix DS-100	8 ~ 24	6.2 x 4.7	25.0 ~ 8.4	1.33 ~ 0.45	0.94 ~ 0.32

It can be seen that, when used in wide angle mode, the Fujix DS-100 system and Kodak DC-50 system would give slightly worse results than the Kodak DC-40 system when other system factors are the same. This is due to either the bigger pixel size or the smaller focal length of the two cameras. However, if the DS-100 and DC-50 are zoomed into maximum focal length (telephoto mode), better results would be expected than for the DC-40 system. It is worth noting that the above figures are only based on the factors of angular resolution and intersection geometry, while systematic errors of the imaging system are deemed to be successfully compensated for.

7.4.2.4 Data Reduction Schemes

After the measurements of all the images, the photogrammetric self-calibrating bundle adjustment UNBASC2 was employed to process the image data. To effectively evaluate the metric performance of each digital camera system, the following schemes were designed for

data processing:

- **Scheme 1:** image data of the Config I was processed with different amounts of control points (test 1 to 5) to study the influence of the control upon the final results. The optimal control distribution was selected for the subsequent data processing.
- **Scheme 2:** under the selected optimal control distribution, image data of the Config I, II and III were processed and compared to evaluate the effects of the two-exposure case over the one-exposure cases.
- **Scheme 3:** Results from Config I and Config II were compared to study the repeatability and stability of the camera systems. Due to the fact that the images from the same camera station were taken consecutively in a very short interval and the camera settings and attitudes were kept approximately the same, the differences of the results between the two configurations would give rough indications of the system stability and repeatability.
- **Scheme 4:** by including different calibration parameters (basic interior orientation parameters, lens distortion parameters and affinity parameters of sensor plane) in the photogrammetric adjustment, the calibration effects were examined to study the nature of the systematic errors of the imaging systems.
- **Scheme 5:** data from different cameras were input into the same adjustment to investigate the possibility of integrating different types of cameras for the same project.

7.4.2.5 Results and Analysis

After extensive data processing based on the above schemes, the results are tabulated in Tables 7.10 to 7.15. Analysis are carried out and conclusions are derived based on the corresponding results.

Table 7.10 Influence of Different Control Configurations.

units: mm

Test	Number of control points	Kodak DC-40 System				Kodak DC-50 System				Fujix DS-100 System			
		σ_{PX}	σ_{PY}	σ_{PZ}	σ_{MA}	σ_{PX}	σ_{PY}	σ_{PZ}	σ_{MA}	σ_{PX}	σ_{PY}	σ_{PZ}	σ_{MA}
1	43	0.93	0.81	1.92	1.21	1.06	0.88	2.22	1.39	0.88	0.82	1.72	1.14
2	40	0.93	0.80	1.90	1.21	1.04	0.87	2.17	1.36	0.85	0.79	1.71	1.12
3	35	0.92	0.79	1.86	1.19	1.03	0.85	2.11	1.33	0.84	0.78	1.68	1.10
4	30	0.92	1.01	1.94	1.19	0.98	0.82	2.07	1.29	0.80	0.76	1.60	1.05
5	28	0.89	0.79	1.74	1.14	0.88	0.77	1.97	1.21	0.75	0.70	1.50	0.98

It can be seen from Table 7.10 that the precision improved for all camera configurations with a decreased number of control points. When trying to further reduce the control, the computation became divergent and the adjustment failed. This strange phenomenon was due to the loose control constraints. However it did not suggest that the fewer the control points, the better the final results.

Table 7.11. Config III vs. Config I and II (two-exposure vs. one exposure).

units: mm

System	One-exposure								Two-exposure			
	Config I				Config II				Config III			
	σ_{PX}	σ_{PY}	σ_{PZ}	σ_{MA}	σ_{PX}	σ_{PY}	σ_{PZ}	σ_{MA}	σ_{PX}	σ_{PY}	σ_{PZ}	σ_{MA}
Kodak DC-40	0.92	0.79	1.86	1.19	0.82	0.72	1.71	1.08	0.89	0.78	1.08	0.92
Kodak DC-50	1.03	0.85	2.11	1.33	0.96	0.75	2.10	1.27	1.03	0.82	2.13	1.33
Fujix DS-100	0.84	0.78	1.68	1.10	0.94	0.81	1.59	1.11	0.85	0.80	1.56	1.07

Results from Table 7.11 indicate that the two-exposure case contradicted the theoretical expectation, i.e., there were no obvious improvements in precision of the two-exposure case over the single-exposure cases. Nevertheless, compared with the single-exposure cases, the two-exposure case presented slightly better results in one case but slightly worse in the other one. The reason for this is that the photogrammetric network geometry is not strong enough.

Table 7.12 R.M.S. Differences of Object Coordinates between Config I and II.

System	σ_x (mm)	σ_y (mm)	σ_z (mm)	σ_{MA} (mm)
Kodak DC-40	1.00	1.52	1.17	1.23
Kodak DC-50	2.28	2.01	2.04	2.11
Fujix DS-100	1.70	1.25	1.20	1.38

As different camera-to-object distances were employed at each camera station to ensure the largest possible imaging scales, the autofocus functions of the two digital cameras with

zoom lenses change the focal lengths to acquire clear images, which in turn altered the interior configurations of the cameras. Results from Table 7.12 derived based on the object coordinate differences between the two sets suggest that the Kodak DC-40 system has the best stability and reliability among the three cameras, then the Fujix DS-100 system and finally, the Kodak DC-50 system. Furthermore, the average variations of the principal distances between the two configurations were estimated as 18 μ m, 37 μ m and 25 μ m for DC- 40, DC-50 and DS-100 respectively listed in Tables 7.13.1 to 7.13.3. The average principal point variations were 7, 5 and 5 pixels in x , and 4, 3, 3 pixels in y direction. In addition, the principal point offsets from the central position of the sensor chips for the three cameras were approximately 13, 12 and 8 pixels, and 9, 9 and 4 pixels in x and y directions, respectively.

Table 7.13.1 Comparison of the Interior Orientation Parameters between Config I and II. (Kodak DC-40 Digital Camera System).

Kodak DC-40 System		c (mm)	x_0 (mm)	y_0 (mm)	k_1 (10^{-3})	k_2 (10^{-4})	k_3 (10^{-5})	θ_1^* ($^{\circ}$ '")	p_{max}^* (10^{-3})	s_y	β ($^{\circ}$ '")
Config I	Image 1	8.260	3.210	2.381	2.680	-0.803	0.350	55 09 16	0.347	1.00019	0 04 14
	Image 2	8.330	3.372	2.350	4.972	-5.155	2.742	62 22 27	0.326	1.00025	0 01 22
	Image 3	8.232	3.151	2.270	4.100	1.963	0.070	71 21 53	0.770	1.00177	0 00 50
	Image 4	8.305	3.299	2.291	3.201	-1.804	0.905	71 08 44	0.378	0.99924	0 00 29
	Image 5	8.291	3.292	2.310	7.791	8.133	11.550	86 47 54	0.456	0.9994	0 02 59
Config II	Image 1	8.283	3.281	2.355	2.390	0.109	-0.320	88 07 15	0.193	1.00009	0 02 04
	Image 2	8.292	3.329	2.336	2.271	0.807	-0.820	86 59 43	0.267	1.00005	0 00 49
	Image 3	8.200	3.302	2.318	4.937	-4.960	1.571	66 59 26	0.460	1.00077	0 01 26
	Image 4	8.301	3.340	2.344	2.883	-1.223	0.691	70 04 45	0.209	0.99986	0 00 07
	Image 5	8.288	3.310	2.330	1.706	2.992	-4.010	78 05 30	0.456	0.9998	0 05 25

Note: θ_1 and p_{max} are p_1 and p_2 (decentering lens distortion parameters) related parameters.

Table 7.13.2 Comparison of the Interior Orientation Parameters between Config I and II.
(Kodak DC-50 Digital Camera System).

Kodak DC-50 System		c (mm)	x ₀ (mm)	y ₀ (mm)	k ₁ (10 ⁻³)	k ₂ (10 ⁻⁴)	k ₃ (10 ⁻⁵)	θ ₁ (°′′)	P _{max} (10 ⁻³)	s _y	β (°′′)
Config I	Image 1	7.148	3.256	2.343	3.354	-0.350	-0.249	20 34 00	0.211	1.000026	0 03 00
	Image 2	7.100	3.230	2.360	4.203	-3.736	3.255	01 03 58	0.302	0.999692	0 01 59
	Image 3	7.080	3.317	2.410	4.834	-4.767	4.088	12 21 29	0.206	1.000797	0 03 22
	Image 4	7.184	3.270	2.301	3.720	-2.346	1.974	58 07 33	0.023	0.998503	0 01 08
	Image 5	8.224	3.303	2.258	1.765	1.510	-1.717	06 12 18	0.330	0.999633	0 06 38
Config II	Image 1	7.134	3.231	2.363	4.314	-1.854	0.818	18 10 02	0.330	1.001503	0 05 51
	Image 2	7.146	3.275	2.381	3.327	0.389	-0.782	00 15 22	0.297	0.999502	0 00 47
	Image 3	7.142	3.380	2.354	7.736	-15.250	17.960	52 40 04	0.396	1.00168	0 01 54
	Image 4	7.150	3.350	2.299	3.279	-0.055	-0.271	69 20 34	0.309	0.99883	0 00 38
	Image 5	8.254	3.264	2.271	4.980	7.288	-8.886	20 24 07	0.240	0.999805	0 02 48

Table 7.13.3 Comparison of the Interior Orientation Parameters between Config I and II.
(Fujix DS-100 Digital Camera System).

Fujix DS-100 System		c (mm)	x ₀ (mm)	y ₀ (mm)	k ₁ (10 ⁻³)	k ₂ (10 ⁻⁴)	k ₃ (10 ⁻⁵)	θ ₁ (°′′)	P _{max} (10 ⁻³)	s _y	β (°′′)
Config I	Image 1	8.001	3.122	2.412	4.392	-2.188	0.595	66 50 45	0.489	0.97676	0 04 04
	Image 2	7.965	3.153	2.399	3.182	0.441	-1.073	84 20 52	0.302	0.97713	0 02 22
	Image 3	8.602	3.265	2.449	4.189	-4.657	2.750	78 58 06	0.781	0.97629	0 01 35
	Image 4	8.016	3.187	2.368	4.565	-2.989	1.432	85 59 12	0.400	0.97600	0 02 12
	Image 5	8.028	3.200	2.330	3.275	-0.844	1.642	86 10 58	0.399	0.97739	0 03 19
Config II	Image 1	7.983	3.108	2.401	2.992	0.493	-0.922	75 05 31	0.338	0.99720	0 04 05
	Image 2	7.956	3.071	2.379	3.259	0.467	-0.908	66 54 56	0.120	0.97788	0 01 59
	Image 3	8.671	3.202	2.351	3.248	-3.099	2.375	80 53 51	0.465	0.97668	0 01 59
	Image 4	8.000	3.239	2.379	3.938	-1.157	0.125	80 58 47	0.540	0.97677	0 00 48
	Image 5	8.023	3.176	2.305	4.181	-4.702	6.483	70 14 20	0.268	0.97704	0 03 23

In the calibration aspect (Tables 7.14.1 to 7.14.3), no system performed well without any calibration parameters, with the Fujix DS-100 system having the least severe situation. The inclusion of the basic interior orientation parameters (x_0 , y_0 and c) greatly improved the triangulation precision for all the camera systems, and the Kodak DC-50 system achieved the largest improvement, while the metric results from the other two systems were still rather poor. The inclusion of decentring distortion or affine transformation parameters greatly improved the precision for Kodak DC-40 system, which suggests that the camera is suffering from decentring lens distortions and sensor affine deformation, whereas the DC-50 and the DS-100 system did not conform to this rule. It can be seen that the calibration of the three digital camera systems was quite successful after all the calibration parameters were included, in other words, most of the systematic errors were effectively compensated for by the self-calibrating bundle adjustment. However, the discrepancies between the σ_{XP} , σ_{YP} , σ_{ZP} and σ_X , σ_Y , σ_Z indicate that there still exist certain residual systematic errors that cannot be successfully modeled with the current functional models. In addition, for all the three digital camera systems tested, the accuracies in the vertical direction were almost two-fold worse than for the X and Y directions, which is due to the imaging configuration rather than intrinsic problems of the cameras.

Table 7.14.1 Calibration Results for the Kodak DC-40 Digital Camera System.

Test	Description	σ_0 (μm)	σ_X (mm)	σ_Y (mm)	σ_Z (mm)	σ_{PX} (mm)	σ_{PY} (mm)	σ_{PZ} (mm)
T1	no additional parameters	141	N/R	N/R	N/R	N/R	N/R	N/R
T2	x_0, y_0, c	20	9.40	8.87	6.62	7.36	8.25	5.72
T3	x_0, y_0, c, p_1, p_2	4	5.51	6.06	5.09	3.62	3.42	4.27
T4	x_0, y_0, c, A, B	4	6.06	7.40	3.45	3.58	3.35	4.32
T5	$x_0, y_0, c, k_1, k_2, k_3, A, B$	1	0.85	1.41	1.58	0.94	0.86	1.92
T6	$x_0, y_0, c, k_1, k_2, k_3, p_1, p_2$	1	0.78	1.34	1.51	0.91	0.83	1.85
T7	$x_0, y_0, c, k_1, k_2, k_3, p_1, p_2, A, B$	1	0.74	1.47	1.50	0.89	0.79	1.81

Table 7.14.2 Calibration Results for the Kodak DC-50 Digital Camera System.

Test	Description	σ_o (μm)	σ_x (mm)	σ_y (mm)	σ_z (mm)	σ_{rx} (mm)	σ_{ry} (mm)	σ_{rz} (mm)
T1	no additional parameters	52	176.30	218.67	50.11	26.60	110.22	177.32
T2	x_0, y_0, c	4	7.43	5.49	6.30	4.14	3.83	5.52
T3	x_0, y_0, c, p_1, p_2	4	6.39	5.86	5.18	3.86	3.57	4.56
T4	x_0, y_0, c, A, B	3	6.96	6.92	3.37	3.82	3.47	4.69
T5	$x_0, y_0, c, k_1, k_2, k_3, A, B$	1	0.97	1.59	2.21	1.04	0.84	2.21
T6	$x_0, y_0, c, k_1, k_2, k_3, p_1, p_2$	1	0.84	1.38	2.40	1.11	0.88	2.23
T7	$x_0, y_0, c, k_1, k_2, k_3, p_1, p_2, A, B$	1	1.01	1.58	2.40	1.03	0.82	2.13

Table 7.14.3 Calibration Results for the Fujix DS-100 Digital Camera System.

Test	Description	σ_o	σ_x	σ_y	σ_z	σ_{rx}	σ_{ry}	σ_{rz}
T1	no additional parameters	41	45.31	68.73	30.91	18.88	57.15	93.99
T2	x_0, y_0, c	10	17.45	11.98	19.54	8.80	9.08	14.94
T3	x_0, y_0, c, p_1, p_2	6	13.28	12.43	7.88	5.84	4.90	6.40
T4	x_0, y_0, c, A, B	31	66.13	95.97	18.59	14.23	55.21	63.08
T5	$x_0, y_0, c, k_1, k_2, k_3, A, B$	1	2.05	1.38	1.95	0.92	0.86	1.65
T6	$x_0, y_0, c, k_1, k_2, k_3, p_1, p_2$	5	12.23	13.36	7.42	4.83	4.24	5.45
T7	$x_0, y_0, c, k_1, k_2, k_3, p_1, p_2, A, B$	1	0.90	1.47	2.02	0.86	0.80	1.56

Results from Table 7.15 of the multi-camera integration test indicate the possibility of using different digital cameras for the same project. The average alterations of the basic interior orientation parameters between the single-camera and multi-camera cases were 1 pixel for the principal point offsets and $7\mu m$ for the principal distance, which obviously did not significantly influence the photogrammetric precision.

In viewing the above analysis, we can see that among the three digital cameras, the Kodak DC-40 presented better accuracy, stability and repeatability when the other two were used in the wide-angle mode. Under the best calibration cases, the relative accuracies corresponding to the largest test-field dimension were estimated as *1:6000*, *1:4500* and

1:5100 in object space for DC-40, DC-50 and DS-100, respectively, for the adopted imaging configuration. Although the zoom function is very helpful in close-range photogrammetry, it certainly adversely influences the final accuracy even when calibration parameters were included during the data processing. However, between the two digital cameras with zoom lenses, the Fujix DS-100 (\$3000) performed better from a metric standpoint. However, with the much lower street price (\$600) and marginally lower accuracy, the Kodak DC-50 is preferred from the cost-to-performance aspect.

Table 7.15 Integration Test of Multi-Cameras

units: mm

		Single-camera Block			Multi-camera Block		
		c	x_0	y_0	Δc	Δx_0	Δy_0
Kodak DC-40	Image 1	8.278	3.284	2.355	-0.004	0.009	-0.008
	Image 2	8.292	3.325	2.336	-0.001	0.003	-0.003
	Image 3	8.200	3.301	2.318	0.022	-0.012	-0.009
	Image 4	8.300	3.338	2.344	-0.001	-0.003	0.004
	Image 5	8.288	3.309	2.330	0.001	0.016	-0.002
Kodak DC-50	Image 1	7.134	3.231	2.363	-0.001	-0.006	0.000
	Image 2	7.146	3.275	2.381	-0.007	-0.004	0.005
	Image 3	7.142	3.377	2.354	-0.014	0.011	0.013
	Image 4	7.150	3.350	2.299	0.005	0.000	-0.007
	Image 5	8.254	3.264	2.271	0.010	-0.005	0.042
Fujix DS-100	Image 1	7.983	3.108	2.401	-0.007	-0.007	0.004
	Image 2	7.956	3.071	2.379	0.015	0.001	-0.002
	Image 3	8.671	3.202	2.351	0.001	0.008	-0.003
	Image 4	8.000	3.239	2.379	-0.002	0.003	0.001
	Image 5	8.023	3.176	2.305	0.010	0.022	0.025

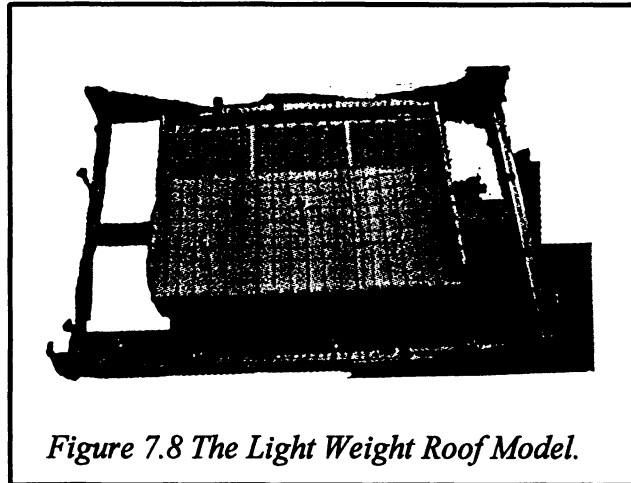
7.4.3 Lightweight Structure Deformation Monitoring

This project is designed to study and compare the performance of a digital camera system with that of a non-metric film based camera system for structural deformation monitoring, a typical application example of close range photogrammetry.

7.4.3.1 Model Preparation

A structural model of a light weight roof was prepared for the project, consisting of a wooden box, 94 cm long and 63 cm wide, the height along the longer walls was 15 cm, and 26 cm along the shorter ones (Figure 7.8) (Faig et al., 1996). A wire net of 11 x 17 wires was spanned from opposite walls, simulating hanging and standing cables of a roof. Adjacent wires were separated by 5 cm in both directions, forming 187 intersections used for deformation monitoring of the roof surface. In order to provide the best definition and identification of the above intersection points, both size and color of the wires had to be optimized. Wires with diameter of 8.5 μm were most suitable for the selected image scales. The black color for the wires provided the best contrast to the white background of the structure. Deformation of the structure was simulated by changing the tension of the standing wires, which in turn affected the hanging wires.

In addition to the 187 structure points, 18 control points with different heights were deployed around the model, with 3 of them being located inside the model to improve the geometry of the photogrammetric network. 3D coordinates of the control points in an arbitrary local coordinate system were determined by an ECDS with precisions of 0.030 mm, 0.025 mm and 0.020 mm in X, Y and Z directions, respectively.



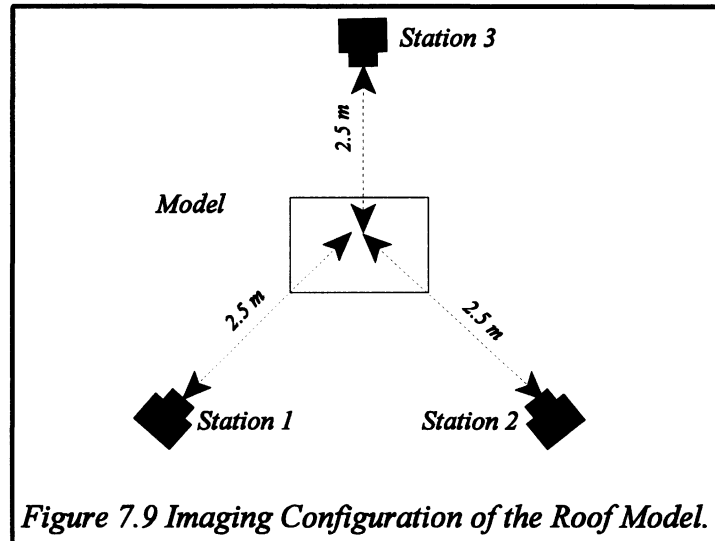
7.4.3.2 Cameras Utilized

The digital camera used for this project was the Fujix DS-100 whose technical specifications were listed in the previous sections (Table 7.1). A film-based camera Olympus OM10 is employed as well for purpose of comparison. The Olympus OM10 camera is a standard SLR camera with 36 mm x 24 mm image format, equipped with a lens of 28 mm focal length with the f-stop ranging from 2.8 to 22, an automatic exposure time adaptor and four artificial fiducial marks.

7.4.3.3 Photogrammetric Configuration and Image Acquisition

A three-station convergent photogrammetric network (Figure 7.9) was established to monitor the deformation of the structure with 100 percent overlap for any pair of the convergent images. Images were taken at each of three stations before and after deformation with both cameras from the same station with approximately the same orientation. Due to the differences in the image formats for the two cameras (i.e. area of the emulsion for the film camera and dimension of the CCD chip for the digital camera), and differences in the

focal lengths, for the same camera-to-object distance, the image scales are different for the softcopy and hardcopy images. The camera-to-object distance was selected to be 2.5 m which resulted in an image scale of 1:100 for the film camera, and 1:125 for the digital camera.



During the imaging process, for the Olympus OM10 camera, $f/22$ was used as aperture, which represented the smallest diaphragm opening of 1.3 mm in order to maximize the depth of field. The regular illumination of the laboratory dictated an exposure time of 1 second. For the Fujix DS-100, on the other hand, the lenses was zoomed to obtain the large practical image scales. The maximum f-stop of 11 and the maximum exposure time of 1/4 second were used.

In addition to one hardcopy set and one set of softcopy images taken directly with the Olympus OM10 and the Fujix DS-100 respectively, a third set of images was obtained by scanning the hard copy images. A Nikon scanner for slides was used for this task. The

scanning resolution was 59 DPMM (Dots Per Millimetre) and the final resolution for the output images was 101.7 PMM (Pixels Per Millimetre), resulting in a $9.8 \mu\text{m} \times 9.8 \mu\text{m}$ pixel size. The scanned images had a format of 1.325 cm x 1.000 cm and an image scale of 1:160 with a hypothetical focal length of 16 mm.

7.4.3.4 Image Mensuration

Image coordinates of the six hardcopy images were measured by using the analytical plotter Wild BC2 at the University of Moncton, N.B., Canada. The mean measuring precision was estimated as $4\mu\text{m}$. The six softcopy images and six scanned images were measured on the DVP with the comparable measuring precision of the analytical plotter.

7.4.3.5 Results and Analysis

After image coordinate determination of three sets of different images, UNBASC2 was used to evaluate the image data. For the comparison of the results, the pertinent accuracy information from the photogrammetric bundle adjustments is summarized in Tables 7.16.1 and 7.16.2. Figure 7.10 illustrates the deformation behavior of the roof model determined by the digital camera.

It can be seen from the results that sub-millimetre accuracies were achieved in object space with all three different types of images. The digital camera clearly matches the non-metric one in accuracy, which indicates that off-the-shelf digital cameras plus certain computer hardware and software can provide photogrammetric accuracies that are equivalent to the those obtained with the film based camera systems. In fact, the test results show a slightly higher accuracy for the digital camera system, which is remarkable because of the

smaller image scale compared to the hardcopy images. In addition, the scanned imagery can also be used for certain metric applications in order to make use of the advantages of digital photogrammetry when digital cameras are not available.

Table 7.16.1 RMS Values of the Image Coordinates

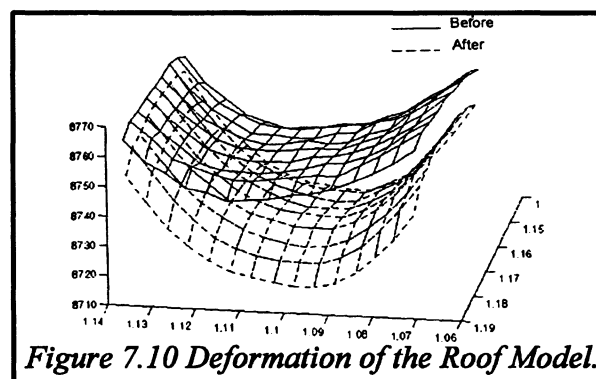
units:μm

Image Type	Before Deformation			After Deformation		
	σ_x	σ_y	σ_0	σ_x	σ_y	σ_0
Hardcopy	3.5	2.5	3.0	3.0	3.4	3.2
Softcopy	1.2	1.5	1.3	1.5	1.7	1.6
Scanned	3.6	3.1	2.8	3.2	3.3	3.2

Table 7.16.2 RMS Values of the Object Space Coordinates based on the Check Points

units:mm

Image Type	Before Deformation					After Deformation				
	σ_x	σ_y	σ_z	σ_{mean}	Rel. accuracy	σ_x	σ_y	σ_z	σ_{mean}	Rel. accuracy
Hardcopy	0.38	0.18	0.29	0.28	1:4000	0.4	0.2	0.3	0.31	1:3700
Softcopy	0.16	0.06	0.20	0.14	1:8000	0.2	0.1	0.1	0.17	1:7000
Scanned	0.53	0.31	0.54	0.46	1:2500	0.4	0.7	0.3	0.51	1:2200



In concluding this chapter, the metric performances of three low-resolution digital camera systems were studied through a series photogrammetric projects focusing on different

camera systems can be applied metrically in such situations that require low- or medium accuracy. Their metric performances largely depend on the imaging sensor, lenses quality, image processing and other factors of the systems. However, modeling and compensation of the systematic errors through a calibration are the keys factors to be considered when applying such camera systems for measurement tasks.

CHAPTER 8

CONCLUSIONS AND RECOMMENDATIONS

Digital cameras are making inroads into various areas once occupied by film-based cameras, because of the advantages of direct digital image data outputs. At present, most digital cameras available on the market are the inexpensive, low-resolution type which are designed more for massive general imaging usage than for photogrammetric tasks. However, as low-cost and promising imaging tools for measurement systems, their metric characteristics have hardly been studied.

In this dissertation, a series of photogrammetric investigations was conducted for low-resolution digital camera systems, from both the theoretical and practical aspects. Working principles, error sources and calibration of such systems were discussed in detail. Different systematic error modeling and compensation algorithms were studied and compared under simulation and practical situations. Accuracy potentials of three typical low-resolution digital camera systems were investigated by using several test projects. Applications and possible applications of low-resolution digital cameras for metrology tasks were also explored.

Low-resolution digital camera systems are non-metric types viewed from a photogrammetric standpoint, which suffer from geometric and radiometric imperfectness. Geometric defects deviate the image points from their theoretical locations, while radiometric deficiencies mainly make the digital numbers of the corresponding pixels incorrect. In order to use these camera systems for measurement applications, the geometric

and radiometric errors of the camera systems have to be modeled and compensated to a certain extent depending on the accuracy requirements of the final products.

A system calibration is necessary when accurate measurement results are expected to be drawn from the images, and it can effectively determine and further compensate for the systems' systematic errors. Various calibration methods exist which differ in the calibration procedures, the equipment requirements, and the mathematic models to describe the behavior of the systematic errors of the systems. Each method has its own strengths and shortcomings. In photogrammetry, a camera system calibration is mainly focused on the geometric part. Many analytical calibration methods, mainly the self-calibration methods, developed for calibrating film-based cameras methods are being widely used for the calibration of digital camera systems.

Finite element methods (FEM), are widely used in structural analysis, but their applications to camera system calibrations have only attracted limited attention in photogrammetry since the proposal of this idea in 1982. A modified FEM camera calibration model, namely the MFFEM (Multiple-Frame FEM) was presented based on the original model, and it was verified through simulation and a practical case. Influences of various factors (different level random errors in image coordinate observations, shape functions, form and number of the elements, imaging configuration) upon the accuracy of the final results were studied and compared with other commonly used methods. The MFFEM can effectively model and compensate for the radial lens distortion and sensor plane unflatness through the adoption of the differential principal distances for different image points. When many control points are available, this method did not show a significant accuracy

improvement. However, in cases where the number of the control points is very limited, the MFFEM displayed its advantages over other methods in that it still presented reliable results.

A software package UNBDCSC (UNB Digital Camera System Calibration) was developed and used for data processing by using the MATLAB programming environment, which can also be applied for calibrating film-based cameras. The MFFEM function is the main characteristic of the package, whereby different forms and numbers of the elements, low and high order shape functions can be easily adapted.

Photogrammetry is essentially an optical triangulation method. The final accuracy depends on a number of factors, concerning the camera used, imaging configuration, systematic error modeling and compensation as well as object attributes. In addition to theoretical studies, practical verifications are imperative to effectively evaluate the metric performances and accuracy potentials of low-resolution digital camera systems. To fulfill this, several projects were designed and implemented for three low-resolution digital camera systems. The results showed that a relative accuracy of about 1:5000 in object space can be routinely achieved by these camera systems under practical situations. However, 1:10,000 accuracy would also be attainable when the image mensuration precision can be improved. Theoretically, the accuracy limit for such camera systems is 1:20,000, with all the involved factors (imaging configuration, targeting, illumination and calibration) being optimized.

Under the same imaging configuration, the performances of the three low-resolution digital camera systems were not the same due to structural differences of the camera, manufacturing qualities and other system differences. Their behaviors also changed with the projects. While these cameras have similar numbers of CCD sensor elements, the lens

qualities and characteristics influence the metric performances of the camera systems. Generally speaking, among the three camera systems, the Fujix DS-100 system displayed the best accuracy potential (1:8000 relative accuracy), which is especially true when the camera-to-object distances from all camera stations are not very different. On the other hand, the Kodak DC-40 system presented the highest camera interior geometric stability due to the adoption of lenses with fixed focal length. The results suggest that while the digital cameras with zooming function are very useful for some applications, their interior orientations changed with the zooming of the lenses, which is barely modeled by the camera calibration, even with the on-the-job methods.

In spite of their design limitations and, thus, limited attainable accuracies, low-resolution digital cameras are powerful imaging devices for measuring systems, especially when the accuracy requirements are not very stringent and the cost is the main concern. Such camera systems can be potentially used for many metric applications, ranging from industry, engineering, archaeology and anthropology to accident reconstruction and forensics.

The availability of more digital cameras, sophisticated image measurement software and other accessories imposed limitations upon the studies described in this dissertation. Therefore, there are several aspects that deserve more work in the future. Firstly, the software package used in this dissertation was designed for a single experienced user and requires significant refinement for more general cases. A GUI (Graphic User Interface) needs to be developed for easy operation, for example the selection of different algorithms for systematic error modeling and compensation, different number and size of elements, different shape functions in the FEM module, graphic display, which should be easily carried

out by simply clicking on the corresponding icons on the user menu. Secondly, more studies are worth conducting with the FEM by using a reseau grid placed in front of the sensor plane. Since the grid points are uniformly distributed and their relative locations are known to a very high accuracy, the effects of the lens distortion, sensor deformation and other perturbations of the digital camera system could be well determined by comparing the practical locations on the images with the theoretical expectations and, thus, the effectiveness of the FEM models can be further verified and studied. Furthermore, the radiometric calibration can be implemented with the help of certain special devices, in order to check whether higher accuracies could be obtained. If radiometric calibration is proved to be helpful, the combination of geometric and radiometric calibration would be a very good topic for further studies. Finally, low-resolution digital camera systems need to be compared with their high-end counterparts under the same conditions to determine the differences of their metric performances.

REFERENCES

- Abdel-Aziz, Y. I. (1975). "Film distortion in non-metric cameras." *Photogrammetric Engineering and Remote Sensing*, Vol. 41, No. 3, pp. 613-615.
- Abdel-Aziz, Y. I. and H. M. Karara (1971). "Direct linear transformation from comparator coordinates into object space coordinates in close-range photogrammetry." *Proceedings of the Symposium on Close-Range Photogrammetry*, Urbana, Illinois, pp.1-18.
- Baran, N. M. (1988). *Finite Element Analysis on Microcomputers*. McGraw-Hill Book Company, New York.
- Baxes, G. A. (1994). *Digital Image Processing: Principles and Applications*. John Wiley & Sons, Inc., pp. 37-68.
- Berger, J. (1988). "Segmenting sci/industrial imaging: a camera manufacturer's view." *Advanced Imaging: Solutions for the Electronic Imaging Professional*, Vol. 13, No. 2, pp. 91-92.
- Beyer, H. A. (1992a). "Geometric and radiometric analysis of a CCD based close-range photogrammetry system." Dissertation No. 9701, Institute of Geodesy and Photogrammetry, ETH-Zürich, 180 pages.
- Beyer, H. A. (1992b). "Advances in characterization and calibration of digital imaging system." *International Archives of Photogrammetry and Remote Sensing*, Washington, D.C., Vol. 29, Part B5, pp. 545-555.
- Beyer, H. A. (1995). "Digital photogrammetry in industrial applications." *International Archives of Photogrammetry and Remote Sensing*, Vol. 30, Part 5W1, pp. 373-378.
- Bösemann, W., R. Godding and W. Richmann (1990). "Photogrammetric investigation of CCD cameras." *SPIE Proceeding: Close Range Photogrammetry Meets Machine Vision*, Vol. 1395, pp. 119-126.
- Brown, D. C. (1966). "Decentring distortion of lenses." *Photogrammetric Engineering*, Vol. 32, No. 3, pp. 444-462.
- Brown, D. C. (1971). "Close-range camera calibration ." *Photogrammetric Engineering*, Vol. 38, No. 8, pp. 855-866.
- Brown, D. C. (1976). "The bundle adjustment – progress and prospects." *International*

Archives of Photogrammetry and Remote Sensing, Vol. 21, Part 3, Helsinki, 33 pages.

Bujakiewicz, A. (1976). "The correction of lens distortion with polynomials." *The Canadian Surveyor*. Vol. 30, No. 2, pp. 67-76.

Burner, A. W., W. L. Snow, M. R. Shortis, and W. K. Goad (1990). "Laboratory calibration and characterization of video cameras." *SPIE Proceedings of Close-Range Photogrammetry Meets Machine Vision*, Zurich, Switzerland, Vol. 1395, pp. 664-671.

Burner, A. W. (1995). "Zoom lens calibration for wind tunnel measurements." *Videometrics IV*, SPIE Proceedings, Philadelphia, P.A., USA, Vol. 2598, Ed. S.F. El-Hakim, pp. 19-31.

Chen, Y. and A. F. Schenk (1992). "A rigorous calibration method for digital cameras." *International Archives of Photogrammetry and Remote Sensing*, Washington, D. C., USA, Vol. 29, Part B1, pp. 199-205.

Curry, S., S. Baumrind, J. M. Anderson (1986). "Calibration of an array camera." *Photogrammetric Engineering and Remote Sensing*, Vol. 52, No. 5, pp. 627-636.

Curtin, D.P. (1998). *Digital Photography – An On-line Book*. <http://www.shortcourses.com/>.

Desai, C. S. and J. F. Abel (1972). *Introduction to the Finite Element Method: A Numerical Method for Engineering Analysis*. Van Nostrand Reinhold Company, New York.

Donnelly, B. E. (1988). "Film flatness in 35mm cameras." M.Surv Thesis, The University of Newcastle, New South Wales, No. 2308, 116 pages.

Eastman Kodak Company (1997). "Kodak digital imaging sensors are 'eyes' enabling N A S A ' s M a r s R o v e r t o ' s e e ' . " <http://www.kodak.com/aboutKodak/corpInfo/pressReleases/pr19970626-04.shtml>.

Ebner, H., B. Hofmann-Wellenhof, P. Reiss and F. Steidler (1980). "HIFI – A minicomputer program and package for height interpolation by finite elements." *International Archives of Photogrammetry and Remote Sensing*, Part B4, Hamburg, Germany, pp. 202-215.

Edmundson, K. L., K. Novak and G. He (1991). "Analytical calibration of a stereo-vision system." *Technical Papers ACSM-ASPRS Annual Convention*, Baltimore, USA, Vol. 5, pp. 86-92.

- El-Habrouk, H., X. P. Li, and W. Faig (1996). "Determination of geometric characteristics of a digital camera by self-calibration." *International Archives of Photogrammetry and Remote Sensing*, Vienna, Austria, Vol. 31, Part B1, pp. 60-64.
- El-Hakim, S. F. (1979). "Potential and limitations of photogrammetry for precise surveying." Ph.D. dissertation, Department of Surveying Engineering, University of New Brunswick, Fredericton, N. B., Canada.
- El-Hakim, S. F., A. W. Burner and R. R. Real (1989). "Video technology and real-time photogrammetry." *Non-Topographic Photogrammetry*, 2nd Ed., H.M.Karara (Editor-in-Chief), American Society for Photogrammetry and Remote Sensing, pp. 279-304.
- Faig, W. (1971). "Calibration of close-range photogrammetric cameras." Proceedings of ASP Symposium on Close-range Photogrammetry, University of Illinois, pp. 111-131.
- Faig, W. (1976a). "Aerotriangulation." Department of Surveying Engineering Lecture Notes, No. 40, University of New Brunswick, Fredericton, N.B., Canada.
- Faig, W. (1976b). "Photogrammetric potential of non-metric cameras." *Photogrammetric Engineering and Remote Sensing*, Vol.42, No.1, pp. 47-49.
- Faig, W. (1984). "Aerial triangulation and adjustment." Monograph 10, School of Surveying, University of New South Wales, Kensington, NSW, Australia, 51 pages.
- Faig, W. (1989). "Non-metric and semi-metric cameras: data reduction." *Non-Topographic Photogrammetry*, 2nd Ed., H.M.Karara (Editor-in-Chief), American Society for Photogrammetry and Remote Sensing, pp. 71-79.
- Faig, W., H. El-Habrouk, X. P. Li and M. Hosny (1996). "A comparison of the performances of digital and conventional non-metric cameras for engineering applications." *International Archives of Photogrammetry and Remote Sensing*, Vienna, Austria, Vol. 31, Part B5, pp.147-151.
- Faig, W. and T. Y. Shih (1988). "Functional review of additional parameters." *Proceedings of ACSM/ASPRS Annual Convention*, St. Louis, Vol. 3, pp. 158-168.
- Faig, W., T. Y. Shih and X. S. Liu (1990). "A non-metric stereo system and its calibration." *Proceedings of ACSM/ASPRS Annual Convention*, Denver, Colorado, USA, Vol. 5, pp. 18-25.
- Faig, W. and X. P. Li (1997). "An accuracy study of a low-cost digital camera". *Proceedings of Geomatics in the Era of Radasat*. Ottawa, Canada.

- Fraser, C. S. (1992). "Photogrammetric measurement to one part in a million." *Photogrammetric Engineering and Remote Sensing*, Vol. 58, No. 3, pp. 305-310.
- Fraser, C. S. (1996). "Industrial measurement applications." In *Close Range Photogrammetry and Machine Vision*, Atkinson K. B. (Ed.), pp. 329-361.
- Fraser, C. S. (1997a). "Digital camera self-calibration." *ISPRS Journal of Photogrammetry and remote sensing*, Vol. 52, No. 4, pp. 149-159.
- Fraser, C. S. (1997b). "Innovations in automation for vision metrology systems." *Photogrammetric Record*, Vol.15, No. 90, pp. 901-911.
- Fraser, C. S. (1998). "Some thoughts on the emergence of digital close-range photogrammetry." *Photogrammetric Record*, Vol. 16, No. 9, pp. 37-50.
- Fraser, C. S. and J. A. Mallison (1992). "Dimensional characterization of a large aircraft structure by photogrammetry." *Photogrammetric Engineering and Remote Sensing*, Vol. 58, No. 5, pp. 539-543.
- Fraser, C. S. and M. R. Shortis (1992). "Variation of distortion within the photographic field." *Photogrammetric Engineering and Remote Sensing*, Vol. 58, No. 6, pp. 851-855.
- Fraser, C. S. and M. R. Shortis (1995). "Metric exploitation of still video imagery." *Photogrammetric Record*, Vol. 15, No. 85, pp. 107-122.
- Fraser, C. S., M. R. Shortis and G. Ganci (1995). "Multi-sensor system calibration." *Videometrics IV*, SPIE Proceedings, Vol. 2598, Ed. S.F. El-Hakim, Philadelphia, P.A., USA, pp. 2-18.
- Fryer, J. G. (1986). "Distortion in a zoom lens." *Australian Journal of Geodesy, Photogrammetry, and Surveying and Remote Sensing*, No. 44, pp. 49-59.
- Fryer, J. G. (1989). "Camera calibration in non-topographic photogrammetry." *Non-Topographic Photogrammetry*, 2nd Ed., H.M.Karara (Editor-in-Chief), American Society for Photogrammetry and Remote Sensing, pp. 59-69.
- Fryer, J. G. (1992). "Recent developments in camera calibration close-range applications." *International Archives of Photogrammetry and Remote Sensing*, Vol. 29, Part B5, Washington, D.C., U.S.A , pp. 594-599.
- Fryer, J. G. (1996). "Camera calibration." *Close-range Photogrammetry and Machine Vision*. K. B. Atkinson (Editor), Whittles Publishing, Scotland, UK, pp. 156-179.

- Fryer, J. G. and D. C. Brown (1986). "Lens distortion for close-range photogrammetry." *Photogrammetric Engineering and Remote Sensing*, Vol. 52, No. 1, pp. 51-58.
- Godding, R. and D. Woytowicz (1995). "A new digital high resolution recording system." *International Archives of Photogrammetry and Remote Sensing*, Vol. 30, Part 5W1, *From Pixels to Sequences--Sensors, Algorithms and Systems*, pp. 31-35.
- Grafarend, E. (1974). "Optimisation of geodetic networks." *Bollettino di Geodesia e Scienze Affini*, Vol. 33, No. 4, pp. 351-406.
- Heipke, C., M. Stephani, G. Strunz and R. Lenz (1992). "Photogrammetric calibration and point determination using a digital CCD camera." *International Archives of Photogrammetry and Remote Sensing*, Washington, D.C., USA, Vol. 29, Part B5, pp. 556-560.
- Johanning G. J. (1996). "Videometry in the entertainment industry." Unpublished paper, Geodetic Services, Inc., 7 pages.
- Karara, H. M. and Y. I. Abdel-Aziz (1974). "Accuracy aspects of non-metric imageries." *Photogrammetric Engineering*, Vol. 40, No. 9, pp.1107-1117.
- Kenefick, J. F., M. S. Gyer and B. F. Harp (1972). "Analytical self-calibration." *Photogrammetric Engineering*, Vol. 38, No. 11, pp. 1117-1126.
- Kochi, N., H. Ohtani, S. Nakamura, T. Uchiyama, M. Chida, H. Sato and T. Noma (1995). "Development of a metric CCD camera and its application." *International Archives of Photogrammetry and Remote Sensing*, Vol. 30, Part 5W1, Intercom mission Workshop "From Pixels to Sequences", pp. 254-258.
- Lake, D. (1995a). "Imaging sensors: why do they cost what they cost?" *Advanced Imaging: Solution for the Electronic Imaging Professional*, Vol. 10, No. 6, pp. 18-22.
- Lake, D. (1995b). "Why CMOS imagers are the rage: a revolution in the making." *Advanced Imaging: Solution for the Electronic Imaging Professional*, Vol. 10, No. 10, pp. 12-18.
- Lee, C. K. and W. Faig (1996). "Vibration monitoring with video camera." *International Archives of Photogrammetry and Remote Sensing*, Vienna, Austria, Vol. 31, Part B5, pp. 152-159.
- Lenz, R. (1989). "Image data acquisition with CCD cameras." *Proceedings of the Congress on Optical 3-D Measurement Techniques*, pp. 22-34.

- Li, X. P. (1990). "Deformation monitoring and analysis by photogrammetry." Master Thesis, Wuhan Technical University of Surveying and Mapping, Hubei, China.
- Li, X. P. and W. Faig (1996). "On digital camera calibration." *Geoinformatics '96 Wuhan: Progress in GPS, DPS, RS, GIS and Their Integration*, Wuhan, China, pp. 251-258.
- Li, X. P and W. Faig (1997). "Digital camera calibration: a summary of current methods." *Geomatics Info Magazine*, Vol. 11, No.12, pp. 40-41.
- Li, X. P and W. Faig (1998). "Photogrammetric snapshots on a shoe-string: a survey on low-resolution digital cameras." *Geomatics Info Magazine*, Vol.12, No.1, pp. 67-70.
- Lichti, D. D. (1996). "Constrained finite element self-calibration". M.Sc Thesis. The University of Calgary.
- Lichti, D. D. and M. A. Chapman (1995). "CCD camera calibration using the finite element method." *SPIE Proceedings of Videometrics IV*, Vol.2598, Ed. S.F.El-Hakim, 22-26 October, Philadelphia, PA, USA, pp. 34-43.
- Lichti, D. D. and M. A. Chapman (1997). "Constrained FEM self-calibration." *Photogrammetric Engineering and Remote Sensing*, Vol. 63, No. 9, pp. 1111-1119.
- Mason, S. (1995). "Conceptual model of the convergent multistation network configuration task." *Photogrammetric Record*, Vol. 15, No. 86, pp. 277-299.
- McCaughan D. V. and B. R. Holeman (1979). "Applications of CCDs to imaging." *Charge-coupled Devices and System*, M. J. Howes/D.V.Morgan (Eds.), John Wiley & Sons, Inc., Chichester, pp. 241-295.
- Mcglone, J. C., E. M. Mikhail and F. C. Paderes, Jr. (1989). "Analytical data reduction schemes in non-topographic photogrammetry." *Non-Topographic Photogrammetry*, 2nd Ed., H. M. Karara (Editor-in-Chief), American Society for Photogrammetry and Remote Sensing, pp. 37-57.
- Melen, T. and J. G. Balchen. (1994). "Modeling and calibration of video cameras." *International Archives of Photogrammetry and Remote Sensing*, Vol. 30, Part 3, *ISPRS Comm. III Symposium on Spatial Information from Digital Photogrammetry and Computer Vision*, Munich, Germany, pp. 569-584.
- Moffitt, F. H. and E. M. Mikhail (1980). *Photogrammetry*. 3rd Edition, Harper and Row, Publishers, New York.
- Moniwa, H. (1977). "Analytical photogrammetric system with self-calibration and its

- applications." Ph.D. dissertation, Department of Surveying Engineering, University of New Brunswick, Fredericton, N.B., Canada.
- Munjy, R.A.H. (1982). "The application of the finite element approach in photogrammetry." Ph.D. dissertation, Department of Civil Engineering, University of Washington, Seattle, Washington, USA.
- Munjy, R. A. H. (1986a). "Self-calibration using the finite element approach." *Photogrammetric Engineering and Remote Sensing*, Vol. 52, No. 3, pp. 411-418.
- Munjy, R. A. H. (1986b). "Calibrating non-metric cameras using the finite-element method." *Photogrammetric Engineering and Remote Sensing*, Vol. 52, No. 8, pp.1201-1205.
- Murai, S., R. Matsuoka and T. Okuda (1984). "A study of analytical calibration for non-metric camera and accuracy of three dimensional measurement." *International Archives of Photogrammetry and remote Sensing*, Vol. 25, Part A5, pp. 570-579.
- Paquette, L., R. Stampfler, W. A. Davis and T. M. Caelli (1990). "A new camera calibration method for robotic vision." SPIE Proceedings, Vol. 1395, *Close-Range Photogrammetry Meets Machine Vision*, pp. 656-663.
- Peipe, J. (1995). "Photogrammetric investigation of a 3000 x 2000 pixel high resolution still video camera." *International Archives of Photogrammetry and Remote Sensing*, Vol. 30, Part 5W1, ISPRS Intercom mission Workshop. pp. 36-39.
- Peipe, J. and C.-T. Schneider (1995). "High resolution still video camera for industrial photogrammetry." *Photogrammetric Record*, Vol. 15, No. 85, pp. 135-139.
- Peterson, A. E., N. G. Durdle, V. J. Raso and D. L. Hill (1993). "Calibration of video cameras for scoliosis mapping." *Geomatica*, Vol. 47, No. 1, pp.29-38.
- Rosenberg, P. (1971). "Resolution, detectability and recognizability." *Photogrammetric Engineering*, Vol. 37, No. 12, pp. 1255-1258.
- Shih, T. Y. (1989). "Critical evaluation of stereophotogrammetric methodology with emphasis on close-range applications." Ph.D. dissertation, Department of Surveying Engineering, University of New Brunswick, Fredericton, N.B., Canada.
- Shortis, M. R. and H. A. Beyer (1996). "Sensor technology for digital photogrammetry and machine vision." *Close-range Photogrammetry and Machine Vision*. K. B. Atkinson (Editor), Whittles Publishing, Scotland, UK, pp.106-155.
- Shortis, M. R., W. L. Snow and W. K. Goad (1995). "Comparative geometric tests of

- individual and science CCD cameras using plumb line and test range calibrations.” *International Archives of Photogrammetry and Remote Sensing*, Vol. 30, Part 5W1, *From Pixels to Sequences*, pp. 53-59.
- Stefanidis, A., P. Agouris and A. F. Schenk (1990). “Evaluation of the performance of a digital camera.” *Proceedings of ACSM-ASPRS Annual Convention*, Denver, Colorado, USA, Vol. 5, pp. 109-118.
- Strang, G. and G. J. Fix (1973). *An Analysis of the Finite Element Method*. Prentice Hall Inc., Englewood Cliff, New Jersey.
- Szostak-Chrzanowski, Anna (1988). “An iterative modelling of ground subsidence using non-linear elastic finite element analysis.” *5th International (FIG) Symposium on Deformation Measurement and 5th Canadian Symposium on Mining Surveying and Rock Deformation Measurement*, Fredericton, N. B., Canada, pp. 580-592.
- Trinder, J. C. (1989). “Precision of digital target location.” *Photogrammetric Engineering and Remote Sensing*, Vol. 55, No. 6, pp. 883-886.
- Ural, O. (1973). *Finite Element Method: Basic Concepts and Applications*. Intext Educational Publishers, New York.
- Vösselman, G. and W. Förstner (1988). “The precision of a digital camera.” *International Archives of Photogrammetry and Remote Sensing*, Kyoto, Japan, Vol. 27, Part B1, pp. 148-157.
- Warner, W. S., R. W. Graham and R. E. Read (1996). *Small Format Aerial Photography*. Whittles Publishing, Latheronwheel, pp.121.
- Wiley, A. G. and K. W. Wong (1990). “Metric aspects of zoom vision.” SPIE Proceedings, Vol. 1395, *Close-Range Photogrammetry Meets Machine Vision*, pp. 112-118.
- Wiley, A. G. and K. W. Wong (1995). “Geometric calibration of zoom lenses for computer vision metrology.” *Photogrammetric Engineering and Remote Sensing*, Vol. 61, No.1, pp. 69-74.
- Wolf, P.R. (1974). *Elements of Photogrammetry*. McGraw-Hill, Inc.
- Wong, K. W., M. Lew and Y. Ke (1990). “Experience with two vision systems.” SPIE Proceeding, Vol. 1395, *Close Range Photogrammetry Meets machine Vision*, pp. 3-7.
- Ziemann, H. (1971). “Sources of image deformation.” *Photogrammetric Engineering and Remote Sensing*, Vol. 37, No.12, pp. 1259-1265.

Zienkiewicz, O. C. (1989). *The Finite Element Method. 4th Ed. , Vol. 1: Basic Formulation and Linear Problems*, McGraw Hill Book Company Limited, London, UK.

APPENDIX I. A SURVEY OF LOW-RESOLUTION DIGITAL CAMERAS

In the context of this dissertation, low-resolution digital cameras loosely refer to digital cameras which deliver images with less than one million pixels. Most low-resolution digital cameras incorporate smaller format solid-state sensor chips, use fixed and low-quality lenses, simple optical design and have little control over the image taking process, which certainly imposes adverse influences upon the final results (Li and Faig, 1997).

I.1 Geometric Resolution

The geometric resolution of an image is of major concern to photogrammetrists. Different makes of digital cameras offer different resolutions. Most of the digital cameras in the low-resolution range capture images at geometric resolution of 640 x 480 pixels with some entry-level ones having 324 x 240 pixels or 493 x 373 pixels. Some are delivering slightly higher resolution of 756 x 564 pixels, 768 x 576 pixels, 832 x 608 pixels, 1024 x 768 pixels and, even, 1000 x 800 pixels. Many digital cameras have the capability of “resolution-selection”. Some of them can capture images with different resolutions while others only use different levels of compression while the resolution is in fact kept unchanged. Furthermore, some cameras (e.g. Kodak DC-120) claim to deliver high-resolution images with more pixels than the original number of the CCD elements. Of course, this is just a process of interpolation adding more pixels artificially, which provides no improvement on the image quality.

I.2 Lens System

Both the quality and focal length of the camera lens has a direct impact on the resulting images. About sixty percent of low-resolution digital cameras under investigation use less

expensive fixed-focal length (generally equivalent to a 50-mm lens on a 35-mm film camera) and focus-free lenses to ensure low cost. Fifteen percent of them incorporate dual-focal length lenses and twenty-five percent of high-end low-resolution digital cameras are equipped with motorized zoom lenses (3x to 12x). Some advanced models can accept a wide variety of standard lenses used by ordinary cameras and a few cameras (e.g. Minolta Dimage V) have removable lenses tethered to the camera body by a cord which allows you to position the lens in places where the whole camera body does not fit. Zoom lenses are quite attractive for practical applications, as they can enlarge the image scale without having to change lenses or to physically approach the objects under investigation, which is beneficial in some industrial and engineering environments. Nevertheless, the zoom lenses also pose a vexing problem to the photogrammetrists who have to deal with the complicated variation of the camera's internal configuration when frequently zooming in and out.

I.3 Light Sensitivity

Light sensitivity is usually expressed as film speed for a film-based camera or an ISO (International Standardization Organization) number. As for a solid-state sensor-based camera, the ISO number is also used to describe the sensitivity of the sensor. The higher the number, the more sensitive the imager (solid-state sensor) is to light. Typically, ISO numbers range from 84 to 1600 for most low-resolution digital cameras. Although high ISO numbers can significantly enhance low-light capabilities, the sharpness of the images will be decreased as larger sensor elements have to be adopted to increase the sensitivity. Therefore, a tradeoff has to be made for the sensor designers (Curtin, 1998).

I.4 Storage

With digital cameras, image data are stored on either solid-state memory chips or rotating magnetic disks, and both are erasable and reusable. Many early versions of digital cameras have only the fixed internal storage capability (usually 1MB to 4MB). Other cameras are only equipped with removable memory cards. Some recent models have both functions. There are different memory cards (e.g. PC cards, CompactFlash cards, Miniature cards, SmartMedia cards and MultiMedia cards) being used by different digital cameras. Among them, the PC card (initially called PCMCIA card) type is the most commonly used, as it can be inserted directly into the PC card slot. However, some cameras use proprietary memory cards where either a special card reader, or a special adapter, or a software driver is used to transfer images. While most memory cards have a storage capability of 2MB to 8MB, some have reached 100MB for Type I/II, and 520MB for Type III PC Cards. It is worth to note that some latest cameras (e.g. Sony Digital Movica) can use 3.5-inch floppy disks as the storage medium in order to standardize storage formats. In general, the number of the images that can be stored in a digital camera depends upon the capability of the storage media, resolution of the images and data compression methods and capabilities.

I.5 Interface and Software

After the imaging, the images have to be transferred to a computer from the cameras or memory cards for further processing. Here the interface and some special software play important roles. SCSI (Small Computer System Interface), serial or parallel ports are the

commonly used interfaces, with SCSI being the fastest way, and serial ports the slowest. Many digital cameras come with a “free” cable and software. By simply connecting the camera to the serial/parallel ports of the computer and running the software, the images can be transferred easily, but slowly. For the cameras using removable memory cards (the latest trend), either standard PC slots are used or compatible card readers have to be connected to the computer. In addition, cameras such as the Nikon CoolPix 100 can be directly inserted into the PCMCIA. Furthermore, the Sony DSC-F1 achieves the transfer of images without a direct physical connection between the camera and computer by using infrared technology.

I.6 Control

Compared to some of the high-resolution counterparts which in fact are SLR cameras, many low-resolution digital cameras are just of the point-and-shoot type only with built-in automatic control, i.e., auto-focus, auto-exposure, auto-white balance. These functions are favourable for entry-level users, but with less control, the image quality is quite limited. However, some cameras allow the users to change part or all of the imaging settings (f-stop, shutter speed, white-balance, flash modes, etc.) either through the computer or via on-board control buttons. Furthermore, a few advanced low-resolution digital cameras have auto- and manual control selections for more creative control. With fixed resolution, control over the imaging is desirable for photogrammetrists to accommodate different imaging conditions and to ensure optimum image quality (sharpness, depth-of-field etc.).

I.7 Viewfinder and Other Features

Optical viewfinders without automatic parallax correction are being used by many cameras in this range, which cannot guarantee WYSIWYG (what you see is what you get), especially at close distance. Therefore, TTL (through the lens) viewfinders are utilized for more accurate image framing. Some cameras are equipped with LCD (Liquid Crystal Display) which can be used as viewfinders and image playback screens to review your shots while the camera cap is put on. However, the LCDs are battery-consuming devices, and standard TTL viewfinders are more appealing as framing aids. Other aspects, such as built-in flash, built-in microphone, sequential image recording, annotation capability, ease-of-use, etc. are also preferred by users at reasonable price ranges.

Table I.1 Common Low-resolution Digital Cameras and Their Main Features.

Name	Resolution ¹	Lens Type ²	f-stop/Shutter Speed	Storage	Price ³	Interface	Others
Apple QuickTake 100	640 x 480	f=50mm fixed focal length	1/30~1/175 sec. F2.8~F16, ISO84	1-MB RAM:16/32 ⁴	B	Serial cable	
Apple QuickTake 150	640 x 480	f=50mm fixed focal length	1/30~1/175 F2.8~F16, ISO 84	1-MB RAM:16/32	B	Serial cable	
Apple QuickTake 200	640 x 480	f=38mm fixed focal length	1/4~1/5000 sec. F2.2~F8.0	2MB Wafer-thin SmartMedia Card: 20/30	B	Serial connection PC card slot	1.8" LCD screen No built-in flash; Manual compensation JPEG format
Agfa ePhoto 307	640 x 480	f=43mm(6mm) fixed focal length	1/8~1/10,000 sec ISO125	2MB internal only: 36/72	A	Serial cable	JPEG format
Canon RC-250	320 x 240	f=60mm fixed focal length	1/30~1/500 sec. F2.8~F22 ISO100	Memory card	B	Video capture card or \$2500 SCSI 2 video diskette drive	
Casio QV-10	320 x 240	f=60 mm fixed focal length	1/8~1/4000 sec. F2/F8 manual switchable	2MB RAM : 96	A	Serial cable	1.8" LCD screen; manual compensation; JPEG format

(Table I.1 continued)

Name	Resolution ¹	Lens Type ²	f-stop/Shutter Speed	Storage	Price ³	Interface	Others
Canon PowerShot 350	640 x 480	f=42mm (6mm) fixed focal length	1/4~1/1,000 sec F2.8	2MB Compact Flash Card:11/23/47 ⁵	B	Serial cable / PC slot	1.8" LCD screen; manual compensation; JPEG format
Casio QV-10A	320 x 240	f=60 mm fixed focal length	1/8~1/4000 sec F2.8/F8 manual change	2MB RAM: 96	A	Serial cable	1.8" LCD screen; no built-in flash; JPEG format
Casio QV-30	320 x 240	f= (4.0/9.0 mm) dual focal lengths	1/8~1/4000sec. F2.8/ F8 manual change.	2MB RAM: 96	A	Serial cable	2.5"LCD screen; JPEG format
Casio QV-100	640 x 480	f=40.5mm. fixed focal length	1/8~1/4000 sec. F2.8/ F8 manual change. ISO:100/1600	4MB RAM: 64/192	A	Serial cable	1.8" LCD screen; JPEG format
Casio QV-120	640 x 480			2MB internal RAM only	A		1.8" LCD screen
Casio QV-300	640 x 480	f=47/106mm (4.9/11mm) dual focal lengths		4MB internal RAM only: 64/192 .	B	Serial cable	2.5" LCD screen; no built-in flash; JPEG format
Chinon ES-1000	501x 370	f=6.5mm	1/30~1/4000 sec. F4~F11	1MB internal RAM Proprietary/Type II PC Memory Card	A		

(Table I.1 continued)

Name	Resolution ¹	Lens Type ²	f-stop/Shutter Speed	Storage	Price ³	Interface	Others
Chinon ES-3000	640 x 480	f=38~114mm (7-21mm) 3x zoom lens	1/16~1/500 sec. F2.5~F24 ISO 200	1MB internal RAM: 5/10/40 PCMCIA card I/II	B	Serial cable	
Compro D-Cam	640 x 480					Parallel cable	
Connectix QuickCam	640 x 480						
Dycam 3	496 x 365			8/56	B		
Dycam 4	496 x 365			8/24	B		
Dycam 4XL	496 x 365			36/100	B		
Dycam 10-C	640 x 480	f=38mm~114mm 3x zoom lens	1/16~1/500 sec. F2.6~F16	1MB internal RAM: 5/10/40 4MB PCMCIA card: 21/43/172	B	Serial cable PC card slot	
EPix EPixPro	768 x 494			PCMCIA III card			
Epson PhotoPC	640 x 480	f=43 (6mm) fixed focal length	1/30~1/10,000 sec F5.6 ISO130	1MB internal RAM:16/32 4MB card(\$250):80/160	A	Serial cable Card reader	

(Table I.1 continued)

Name	Resolution ¹	Lens Type ²	f-stop/Shutter Speed	Storage	Price ³	Interface	Others
Epson PhotoPC 500	640 x 480	f=43 (6mm) fixed focal length	1/30~1/10,000 sec. F2.8/F8.0 (2 steps) ISO130	Internal RAM: 30/60 2 MB memory card: 65/130	A	Serial cable Card reader	7.4 micron square pixels; optional 1.8" LCD
Epson PhotoPC600	1024 x 768				B		LCD screen
FujiFilm DS-7	640 x 480	f=38mm (5.7mm) fixed focal length	1/4~1/5,000 sec. F2.2/8.0 ISO100	No internal 2 MB SmartMedia card: 30/60	A	RS-232C serial cable + PC card adapter	1.8" LCD screen JPEG format; no build-in flash
FujiFilm DS-100	640 x 480	f=40~120mm (8 ~24 mm) 3x zoom lens	1/4~1/750 sec. F2.8~F11 ISO100	No internal 1MB proprietary card: 5/10/21	D	Card driver (\$2500)	ADCT compression; manual exposure compensation
FujiFilm DS-220	640 x 480	f=36/72 mm (5.5/11mm) dual-focal lengths	1/4~1/1000 sec. F3.5~F11 ISO120/240	2MB Type I PCMCIA card: 10/20/40	C	Serial cable Card reader	Optional LCD screen; JPEG format
HP PhotoSmart	640 x 480	f=43 (6mm) fixed focal length	F2.8	2MB miniature card: 4/16/32	A		Also sold as Konica Q-EZ
Kodak DC 20	493 x 373	f=47 mm fixed focal length	1/30~1/4000 sec. F4~F11 ISO800/1600	1MB RAM internal: 8/16	A	Serial cable	No built-in flash; Kodak format

(Table I.1 continued)

Name	Resolution ¹	Lens Type ²	f-stop/Shutter Speed	Storage	Price ³	Interface	Others
Kodak DC 25	493 x 373	f=47 mm fixed focal length	1/30~1/4000 sec. F4~F11 ISO800/1600	2-MB RAM internal: 14/29. Optional 2, 4, 15 MB CompactFlash Picture Card	A	Serial cable	1.6" LCD Screen; Kodak format
Kodak DC 40	756 x 504	f=42 mm (8mm) fixed focal length	1/30~1/175 sec. F2.8~F16 ISO84	4-MB internal RAM only:48/96	A	Serial cable	Kodak format
Kodak DC 50	756 x 504	f=37~111 mm (7~21mm) 3x zoom lens	1/16~1/500sec. F2.5~F24 ISO84	1-MB RAM: 7/11/22 5MB PCMCIA I/II card:63	A	Serial cable + PCMCIA slot	manual exposure compensation Kodak format
Konica Q-EZ	640 x 480	f=43mm (6mm) fixed focal length	F2.8	2MB miniature card: 4/16/32	A		also sold as HP PhotoSmart
Konica Q-mini	640 x 480	f=43mm (6mm) fixed focal length		2-MB internal RAM: 11/23/47 Compact flash card	B		1.8" LCD screen; JPEG format
Logitech FotoMan Pixtura	768 x 512	f=42mm fixed focal length	1/30~1/175sec. F2.8~F16 ISO84				
Matsushita Coolshot	640 x 480			Compact flash card			

(Table I.1 continued)

Name	Resolution ¹	Lens Type ²	f-stop/Shutter Speed	Storage	Price ³	Interface	Others
Minolta Dimage V	640 x 480	f=4.8 ~13 mm. 2.7x zoom lens (removable lens tethered to computer by a 1 m long cord)	1/30~1/10000sec. F5~F5.6 ISO100	2 MB SSFDC Card: 16/40	B	Serial cable; PC card adapter	1.8" LCD screen; JPEG / EXIF format; manual compensation
Nikon Coolpix 100	512 x 480	f=52mm (6.2mm) fixed focal length	1/45~1/10000sec. ISO100	1MB internal RAM:21/42	A	Plug into the PCII/III slot directly	JPEG format
Nikon Coolpix 300	640 x 480			PCMCIA II card	B		
Olympus VC-1100	768 x 480	zoom lens		PCMCIA card			
Olympus D-200L	640 x 480	f=36 mm (5mm) fixed focal length	F2.8	2MB internal RAM only: 20/80	B	Serial cable	LCD screen; JPEG format
Olympus D-220L	640 x 480	f=36 mm (5mm) fixed focal length	F2.8	2MB SSFDC card			
Olympus D-300L	1024 x 768	f=36 mm (5mm) fixed focal length	F2.8	6MB internal RAM: 30/120	B	Serial cable	LCD screen; JPEG format
Olympus D-500L	1024 x 768			2MB Smart media card	B		LCD screen

(Table I.1 continued)

Name	Resolution ¹	Lens Type ²	f-stop/Shutter Speed	Storage	Price ³	Interface	Others
Panasonic CoolShot	640 x 480	f=50mm (5.2mm) fixed focal length		2MB Compact flash card:24/96	A		Optional LCD screen; JPEG format
Panasonic KXL-600A	640 x 480	f=50mm (5.2 mm) fixed focal length	1/15~1/4000 Sec. ISO100	2MB memory card: 24/96	A	Card reader	Optional LCD screen; JPEG format
Panasonic Palmcam	640 x 480	f=55mm (5.7mm) fixed focal length		2MB internal RAM: 16/32/94	A		1.8" LCD screen; no built-in flash; JPEG format
Pentax EI-C90		fixed focal length					LCD screen
Ricoh RDC-1	768 x 576	f=7.1~21.3 mm, 3x zoom-lens	F 2.8	1MB internal RAM Optional 8MB PCMCIA II card: 81/162	B	Serial cables /PC card adapter	Optional LCD screen; Full motion and sound; DSC format in conformance with JPEG

(Table I.1 continued)

Name	Resolution ¹	Lens Type ²	f-stop/Shutter Speed	Storage	Price ³	Interface	Others
Ricoh RDC-2	768 x 576	f=35/55mm (3.7/5.6mm). dual-focal length .	F2.0 1/8~1/1000 sec	2MB internal memory : 19 /38 Optional PCMCIA I/II card	B	Serial cables /PC card adapter	Optional LCD screen; Remote control IR sensor; DSC format in conformance with JPEG format
Ricoh RDC-2E	768 x 576	f=35/55mm (3.7/5.6mm). dual-focal lengths	1/8~1/2000 sec.	2MB internal memory: 10/20/41 Optional PCMCIA I/II cards	B	Serial cables	LCD screen; DSC format in conformance with JPEG format
Ricoh RDC-300	640 x 480	f=38mm (4 mm) fixed focal length	1/5~1/8000 sec. F3.8	4MB internal memory: 25/50/100	A	Serial cables	1.8" LCD screen; JPEG format
Samsung SSC-410N		3x zoom lens					LCD screen
Sanyo DSC-V1	640 x 480				B	SCSI out	2" LCD screen
Sharp VE-LC1	640 x 480		1/50~1/4000 sec	MiniDisc	B		
Sony DK-1	768 x 576	f=38~460 mm 12x Zoom lens		2MB card:28		card/SCSI connector	auto/manual control

(Table I.1 continued)

Name	Resolution ¹	Lens Type ²	f-stop/Shutter Speed	Storage	Price ³	Interface	Others
Sony DKC-ID1	768 x 576	f= 38~460 mm 12x zoom lens	1/15~1/4000 sec. ISO100	2MB Type II PCMCIA card	C	SCSI-2 Interface Card reader	JPEG format; Auto/Manual selectable focus and shutter-speed control
Sony DSC-F1	640 x 480	f=35 mm fixed focal length	1/30~1/500sec. 1/7.5~1/1000sec. Manual Override	4MB RAM: 30/58/108	B	infrared wireless connectivity to a PC + serial cable	1.8" LCD screen; continuous recording; JPEG format
Sony MVC-FD5	640 x 480	f=47 mm fixed focal length	1/60~1/4000sec F4.8/F2.0 ISO100	3.5" floppy diskette:20/40	A		JPEG format
Sony MVC-FD7	640 x 480	f= 40~400 mm 10x zoom lens	1/60~1/4000sec F4.8/F1.8 ISO100	3.5" floppy diskette:20/40	B		2.5" LCD screen; JPEG format
Vivitar ViviCam 2000	480 x 320			2MB internal RAM	A		
Vivitar ViviCam 3000	1000 x 800	f=50mm (18mm) fixed focal length	1~1/2000 sec. F4	1MB RAM: 4/15 Optional 2 MB PCMCIA II card : 50/100	A	RS-232 cable	Wavelet compression; Vivitar format

(Table I.1 continued)

Name	Resolution ¹	Lens Type ²	f-stop/Shutter Speed	Storage	Price ³	Interface	Others
Yashica KC 600	640 x 480	f=47mm(6.5mm) fixed focal length	1/8~1/4000 F4.0/F5 ISO 100	2MB Compact flash card: 8/21/65	B		1.8" LCD screen; JPEG format

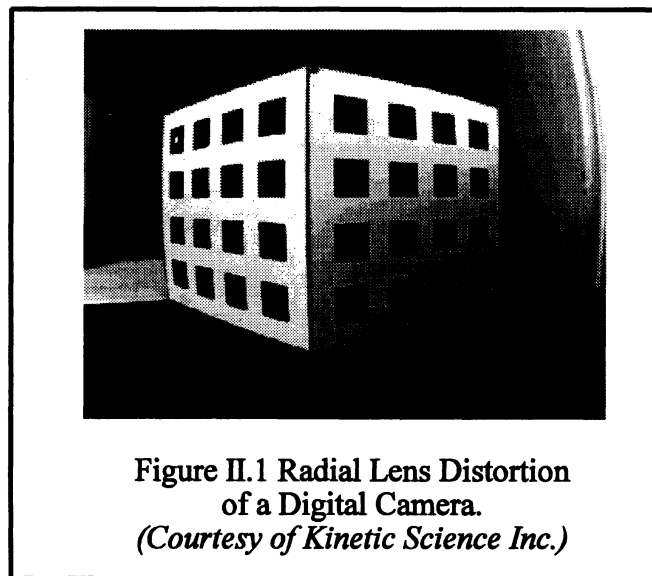
Notes:

1. Pixels with the best mode;
2. Focal length equivalent to 35mm film cameras. The numbers in the brackets are the true focal lengths.
3. When more than one price are available, the lowest one is listed here. A: less than US\$ 500, B: US\$ 500 - 1,000, C: US\$ 1,000 - 2,000, D: more than 2,000\$.
4. High-resolution / standard-resolution.
5. High-resolution / standard-resolution / economy-resolution.

APPENDIX II. LENS DISTORTION OF DIGITAL CAMERAS

II.1 Radial Lens Distortion

As its name indicates, radial lens distortion affects the position of image points on straight lines radially out from the principal point of best symmetry (usually very close to the principal point), which is mainly caused by imperfect grinding of the lenses. Radial lens distortion is also known as symmetric distortion, since it is a function only of the radial distance and is the same at any angle around the principal point (Mcglone et al., 1989). The term positive or pin-cushion and negative or barrel describe whether an image point is distorted closer to or away from the principal point. Figure II.1 clearly shows a radially distorted image from a digital camera.



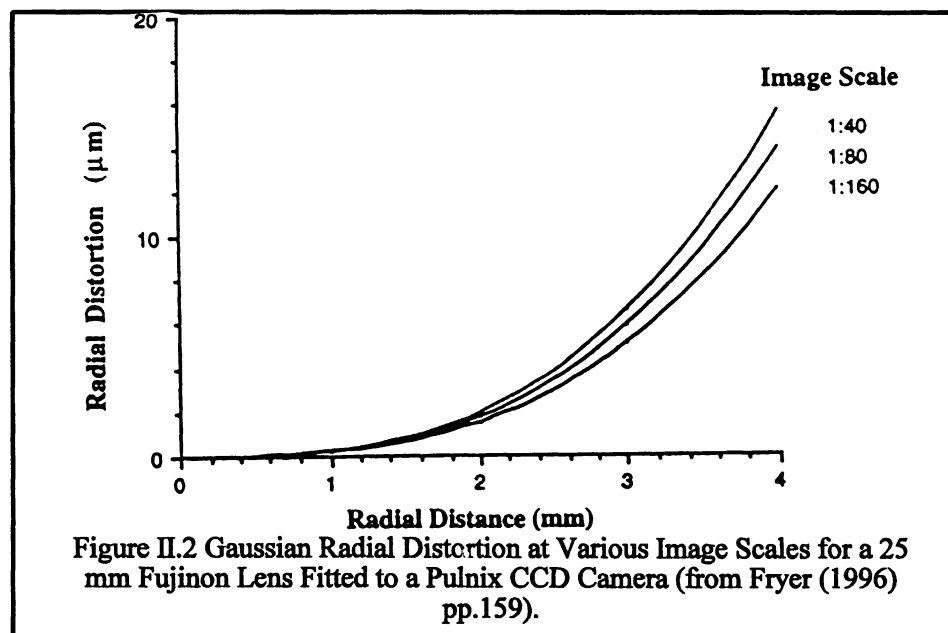
The mathematical expressions for both radial and decentering lens distortions can be derived from the Seidel aberrations, named after the famous 19th century German

mathematician. The polynomial series is universally used to quantify distortion (Bujakiewicz, 1976; Karara and Abdel-Aziz, 1974). Only the low-order terms are included in the expression for most low-resolution digital cameras. Usually, the Gaussian polynomial form of radial lens distortion δr employs the following equation when the principal distance is carried as an unknown during data reduction:

$$\delta r = k_1 r^3 + k_3 r^5 + k_5 r^7 + \dots \quad (\text{II.1})$$

where k_i are the coefficients of radial distortion when the lens is focussed to infinity; r is the radial distance from the principal point of best symmetry, $r = \sqrt{\bar{x}^2 + \bar{y}^2}$ and $\bar{x} = x - x_0$, $\bar{y} = y - y_0$. x , y , x_0 and y_0 are image coordinates of the image point considered, and of the principal point, respectively.

Distortion is usually plotted in micrometers as a function of radial distance in millimetres. Figure II.2 provides an example illustration of radial lens distortion.



While radial lens distortions of a metric aerial camera are usually limited to less than 10 μm (1 to 2 μm for the latest lenses), a standard camera (such as a low-resolution digital camera) usually has radial distortions of 100 to 1000 μm (Warner et al., 1996, pp.65).

Studies show that the effect of radial distortion is almost an order of magnitude larger than that of decentring distortion (Karara and Abdel-Aziz, 1974; Murai et al., 1984). The k_1 term of radial distortion is always the most significant, with k_2 and k_3 usually not being relevant for lenses in typical small format cameras (Fryer, 1992).

It is also known that radial distortion varies with focussing of the lens and also within the photographic depth of field. The former will be discussed in detail in Section II.3. The latter phenomenon is relevant for very close range photogrammetry (at camera-to-object-distances of less than 30 focal lengths) but, even in these cases, it is only significant if there is considerable variation in depth for the target points on the object (Fryer, 1996).

II.2 Decentring Lens Distortion

As discussed previously, most digital cameras incorporate compound lenses. The centers of curvature of all the spherical surfaces should ideally be collinear with the optical axis of the entire system. Practically however, not all lens elements can be perfectly aligned at the time of manufacturing and decentring lens distortion will, thus, be caused by the misalignment.

Decentring distortion is more complicated than its radial counterpart because it consists of a radial asymmetric and a tangential component. Brown (1966) presented the Brown-Conrady model (an extension of the Conrady model), which became the most popular

mathematical model to describe decentring lens distortion. Under this case, the x and y components can be approximately expressed as:

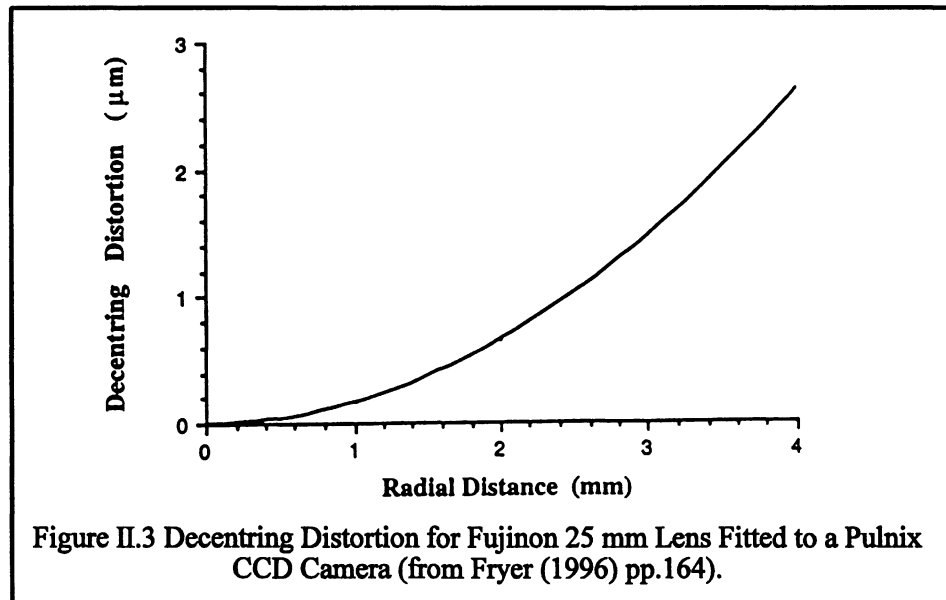
$$\begin{aligned}\delta_{dx} &= p_1(r^2 + 2\bar{x}^2) + 2p_2\bar{x}\bar{y} \\ \delta_{dy} &= 2p_1\bar{x}\bar{y} + p_2(r^2 + 2\bar{y}^2)\end{aligned}\quad (\text{II.2})$$

where p_i are the polynomial coefficients and the other terms have the same meanings as before. Usually, the profile function $p(r)$ is defined as:

$$p(r) = r^2 \sqrt{p_1^2 + p_2^2} \quad (\text{II.3})$$

Based on this, decentring distortion can be represented graphically as shown in Figure II.3.

It is worth noting that the decentring distortion also varies with focussing and depth of field.



II.3 Variation of Radial Lens Distortion

According to Brown (1971), Fryer and Brown (1986), if radial lens distortions are

calibrated for two distinct focal settings (preferably infinite focusing for one of them), the radial lens distortion for any other setting can be computed from these values.

Let s_1 and s_2 refer to two arbitrary distances between the two object planes and the camera for which the radial distortion functions δ_{rs_1} , δ_{rs_2} are known from calibration as:

$$\begin{aligned}\delta_{rs_1} &= k_{1s_1} r^3 + k_{2s_1} r^5 + k_{3s_1} r^7 + \dots \\ \delta_{rs_2} &= k_{1s_2} r^3 + k_{2s_2} r^5 + k_{3s_2} r^7 + \dots\end{aligned}\quad (\text{II.4})$$

Then, the radial distortion of the object plane at distance s for which the lens is focused, can be computed as :

$$\delta_{rs} = \alpha_s \delta_{rs_1} + (1 - \alpha_s) \delta_{rs_2} \quad (\text{II.5})$$

thus,

$$\delta_{rs} = k_{1s} r^3 + k_{2s} r^5 + k_{3s} r^7 + \dots \quad (\text{II.6})$$

where

$$\begin{aligned}k_{1s} &= \alpha_s k_{1s_1} + (1 - \alpha_s) k_{1s_2} \\ k_{2s} &= \alpha_s k_{2s_1} + (1 - \alpha_s) k_{2s_2} \\ k_{3s} &= \alpha_s k_{3s_1} + (1 - \alpha_s) k_{3s_2} \\ \alpha_s &= \frac{s_2 - s}{s_2 - s_1} \frac{s_1 - f}{s - f}\end{aligned}\quad (\text{II.7})$$

If the variation of distortion for points distributed throughout the whole photographic field is considered, a further extension has to be done. Let $\delta_{rss'}$ denote the distortion corresponding to points under consideration at a distance s' when the lens is focused at a distance s , we have:

$$\delta_{rs'} = \frac{1}{\gamma_{ss'}} \delta_{rs'} = \gamma_{ss'}^2 k_{1s'} r^3 + \gamma_{ss'}^4 k_{2s'} r^5 + \gamma_{ss'}^6 k_{3s'} r^7 + \dots \quad (\text{II.8})$$

where

$$\gamma_{ss'} = \frac{s-f}{s'} \frac{s'}{s} \quad (\text{II.9})$$

By using these formulae the radial distortion for any camera-to-object distance can be computed and the observed image points can, thereby, be accurately reduced to their theoretical positions.

II.4 Variation of Decentering Lens Distortion

If a lens has been calibrated for decentering distortion at infinite focus, with the distortion parameters being p_1 , p_2 and $p(r)$ (profile function) and the principal distance c is also known for that focus setting, then according to Fryer and Brown (1986), the decentering distortion corresponding to a focusing distance s (with principal distance c_s) can be described as follow:

$$\begin{aligned} p_{1s} &= \frac{c}{c_s} p_1 = \left(1 - \frac{c}{s}\right) p_1 \\ p_{2s} &= \frac{c}{c_s} p_2 = \left(1 - \frac{c}{s}\right) p_2 \\ p_{rs} &= \sqrt{p_{1s}^2 + p_{2s}^2} = \frac{c}{c_s} p_r = \left(1 - \frac{c}{s}\right) p_r \end{aligned} \quad (\text{II.10})$$

Thus, the x and y components at the image point (x, y) are represented by:

$$\begin{aligned} \delta d_{x_s} &= \left(1 - \frac{c}{s}\right) [p_1 (r^2 + 2\bar{x}^2) + 2p_2 \bar{x}\bar{y}] \\ \delta d_{y_s} &= \left(1 - \frac{c}{s}\right) [p_2 (r^2 + 2\bar{y}^2) + 2p_1 \bar{x}\bar{y}] \end{aligned} \quad (\text{II.11})$$

As with symmetric radial distortion, a further extension is needed to account for the

variability of decentring distortion within the photographic field, which can be implemented by simply applying a scaling factor $\gamma_{ss'}$ to Equation (II.11) where $\gamma_{ss'}$ is given by Equation (II.9).

APPENDIX III DEFINITIONS OF COMMON TERMS OF GEOMETRIC CAMERA CALIBRATION

There are many terms related to camera structure and camera calibrations and sometimes they are misunderstood and, thus, misused. Several main terms linked to camera calibration have to be clarified here.

Principal distance: a physical property which refers to the perpendicular distance from the rear perspective center of the lens system to the image plane. Although often used synonymously with focal length, they are not the same, especially in close range applications with focusable lenses, except when the lens is focused at infinity. The principal distance is one of the important elements defining the inner orientation of a camera system.

Calibrated principal distance/camera constant: a mathematical quantity with the dimension of a length, which is determined by adding a small change to the principal distance such as to cause the radial lens distortion to be zero at a selected radial distance. It is often selected to produce a balanced positive and negative radial lens distortion. Within the used radial distance, such changes of principal distance and with it the radial lens distortion amounts will not affect the results of coordinates of object points (Fryer, 1996).

Photogrammetric principal point (PPP): the foot of the perpendicular from the rear perspective center to the image plane. Distances on the image are measured from this point and used in the collinearity equations (Burner et al., 1990), which means it is this point that is used in the photogrammetric adjustment.

Principal point of autocollimation (PPA): the location of a point on the image plane formed by the direct axial ray passing through the center of the lens system when the image

plane is positioned precisely perpendicular to the optical axis. Some European definitions refer to this point as PPA (Moriwa, 1977), and often PPA and PPP are exchangeably used in some photogrammetric literatures.

Principal point of (the best) symmetry (PPS): the point on the image plane about which all radial components of lens distortion are symmetrical, with the 'best' implying that it is selected to reduce the asymmetry of the distortion to a minimum if a perfect one does not exist. It is the PPS that should be used as the proper reference for radial distortion computation. For an ideal camera system in which no distortion is present and the image plane is correctly aligned with respect to the optical axis, both PPA and PPS coincide with PPP.

APPENDIX IV. PARTIAL DERIVATIVES OF THE MODIFIED COLLINEARITY EQUATIONS

If the modified collinearity equations are rewritten as:

$$\begin{aligned} f_x &= x - x_0 + c \frac{U}{W} \\ f_y &= y - y_0 + c \frac{V}{W} \end{aligned} \quad (\text{IV.1})$$

where

$$\begin{bmatrix} U \\ V \\ W \end{bmatrix} = \begin{bmatrix} m_{11} & m_{12} & m_{13} \\ m_{21} & m_{22} & m_{23} \\ m_{31} & m_{32} & m_{33} \end{bmatrix} \begin{bmatrix} X - X_s \\ Y - Y_s \\ Z - Z_s \end{bmatrix} \quad (\text{IV.2})$$

then the partial derivatives of the equations with respect to the interior orientation parameters, exterior orientation parameters and object space coordinates are given as follows:

$$\frac{\partial f_x}{\partial X_s} = \frac{c}{W} \left[-m_{11} + \frac{U}{W} m_{31} \right] \quad (\text{IV.3})$$

$$\frac{\partial f_x}{\partial Y_s} = \frac{c}{W} \left[-m_{12} + \frac{U}{W} m_{32} \right] \quad (\text{IV.4})$$

$$\frac{\partial f_x}{\partial Z_s} = \frac{c}{W} \left[-m_{13} + \frac{U}{W} m_{33} \right] \quad (\text{IV.5})$$

$$\frac{\partial f_x}{\partial \omega} = \frac{c}{W} \{ m_{12}(Z - Z_s) - m_{13}(Y - Y_s) - \frac{U}{W} [m_{32}(Z - Z_s) - m_{33}(Y - Y_s)] \} \quad (\text{IV.6})$$

$$\frac{\partial f_x}{\partial \phi} = \frac{c}{W} \{ -\cos \kappa W - \frac{U}{W} [\cos \kappa U - \sin \kappa V] \} \quad (\text{IV.7})$$

$$\frac{\partial f_x}{\partial \kappa} = \frac{cV}{W} \quad (\text{IV.8})$$

$$\frac{\partial f_x}{\partial x_0} = -1 \quad (\text{IV.9})$$

$$\frac{\partial f_x}{\partial y_0} = 0 \quad (\text{IV.10})$$

$$\frac{\partial f_x}{\partial c} = \frac{U}{W} \quad (\text{IV.11})$$

$$\frac{\partial f_x}{\partial X} = -\frac{\partial f_x}{\partial X_s} \quad (\text{IV.12})$$

$$\frac{\partial f_x}{\partial Y} = -\frac{\partial f_x}{\partial Y_s} \quad (\text{IV.13})$$

$$\frac{\partial f_x}{\partial Z} = -\frac{\partial f_x}{\partial Z_s} \quad (\text{IV.14})$$

and

$$\frac{\partial f_y}{\partial X_s} = \frac{c}{W} \left[-m_{21} + \frac{V}{W} m_{31} \right] \quad (\text{IV.15})$$

$$\frac{\partial f_y}{\partial Y_s} = \frac{c}{W} \left[-m_{22} + \frac{V}{W} m_{32} \right] \quad (\text{IV.16})$$

$$\frac{\partial f_y}{\partial Z_s} = \frac{c}{W} \left[-m_{23} + \frac{V}{W} m_{33} \right] \quad (\text{IV.17})$$

$$\frac{\partial f_y}{\partial \omega} = \frac{c}{W} \{ m_{22}(Z - Z_s) - m_{23}(Y - Y_s) - \frac{V}{W} [m_{32}(Z - Z_s) - m_{33}(Y - Y_s)] \} \quad (\text{IV.18})$$

$$\frac{\partial f_y}{\partial \phi} = \frac{c}{W} \{ \sin \kappa W - \frac{V}{W} [\cos \kappa U - \sin \kappa V] \} \quad (\text{IV.19})$$

$$\frac{\partial f_y}{\partial \kappa} = -\frac{cU}{W} \quad (\text{IV.20})$$

$$\frac{\partial f_y}{\partial x_0} = 0 \quad (\text{IV.21})$$

$$\frac{\partial f_y}{\partial y_0} = -1 \quad (\text{IV.22})$$

$$\frac{\partial f_y}{\partial c} = \frac{V}{W} \quad (\text{IV.23})$$

$$\frac{\partial f_y}{\partial X} = -\frac{\partial f_y}{\partial X_s} \quad (\text{IV.24})$$

$$\frac{\partial f_y}{\partial Y} = - \frac{\partial f_y}{\partial Y_s} \quad (\text{IV.25})$$

$$\frac{\partial f_y}{\partial Z} = - \frac{\partial f_y}{\partial Z_s} \quad (\text{IV.26})$$

VITA

Candidate's full name: Xiaopeng Li

Place and date of birth: Shou Xian, Anhui, P. R. China
June 29, 1965

Permanent address: Theatrical Company of Shou Xian, 232200
Shou Xian, Anhui, P. R. China

Schools attended: Shou Xian Western City Primary School
Shou Xian, Anhui, P. R. China
1971 ~ 1976
Shou Xian Second High School
Shou Xian, Anhui, P. R. China
1976 ~ 1979
Shou Xian First High School
Shou Xian, Anhui, P. R. China
1979 ~ 1981

Universities attended: Wuhan Technical University of Surveying and
Mapping
Wuhan, Hubei, P. R. China
1981 ~ 1985
B.Sc.E. (1985)
Wuhan Technical University of Surveying and
Mapping
Wuhan, Hubei, P. R. China
1987 ~ 1990
M.Sc.E. (1990)
University of New Brunswick
Fredericton, N.B. Canada
1994 ~ 1999
Ph.D. candidate

Publications:

Li, X.P. (1985). "Wuhan Yangtze River bridge deformation monitoring." *Proceedings of the Second Symposium of Undergraduate Students of Hubei*, Wuhan, Hubei, China.

Li, X.P. (1990). "Deformation monitoring and analysis by photogrammetry." Master Thesis, Wuhan Technical University of Surveying and Mapping, Hubei, China.

Li, X.P. (1991). "Landslide monitoring by terrestrial photogrammetric method." *Proceedings*

of Wuhan Urban Construction Conference, Wuhan, Hubei, China.

Li, X.P. (1995). "Non-contact three-dimensional precise positioning system based on electronic theodolites." *Engineering of Surveying and Mapping*, Vol. 4, No.1, pp. 31-37.

El-Habrouk, H., Li, X.P. and Faig, W. (1996). "Determination of geometric characteristics of a digital camera by self-calibration." *International Archives of Photogrammetry and Remote Sensing*, Vienna, Austria, Vol. XXXI, Part B1, pp.60-64.

Faig, W., El-Habrouk, H., Li, X.P. and Hosny, M. (1996). "A comparison of the performances of digital and conventional non-metric cameras for engineering applications." *International Archives of Photogrammetry and Remote Sensing*, Vienna, Austria, Vol. XXXI, Part B5, pp.147-151.

Li, X.P. and Derenyi, E. (1996). "The photogrammetry and remote sensing education at the University of New Brunswick." *Geoinformatics '96 Wuhan: Progress in GPS, DPS, RS, GIS and Their Integration*, Wuhan China, pp. 244-250.

Li, X.P. and Faig, W. (1996). "On digital camera calibration." *Geoinformatics '96 Wuhan: Progress in GPS, DPS, RS, GIS and Their Integration*, Wuhan China, pp. 251-258.

Li, X.P. and Faig, W. (1997). "An accuracy study of a low-cost digital camera." *Geomatics in the Era of Radarsat*, Ottawa.

Li, X.P. and Faig, W. (1997). "Digital camera calibration: a summary of current methods." *Geomatics Info Magazine*, Vol.11, No.12, pp.40-41.

Li, X.P. and Faig, W. (1998). "A survey on low-resolution digital cameras: photogrammetric snapshots on a shoe-string." (1998). *Geomatics Info Magazine*, Vol.12, No.1, pp.67-70.

Li, X.P. and Faig, W. (1999). "Low-resolution consumer digital cameras, suitable photogrammetric tools?" *Photogrammetric Engineering and Remote Sensing*, Vol. 65, No. 4, pp. 427-429.